

INFORMATION TO USERS

This manuscript has been reproduced from the microfilm master. UMI films the text directly from the original or copy submitted. Thus, some thesis and dissertation copies are in typewriter face, while others may be from any type of computer printer.

The quality of this reproduction is dependent upon the quality of the copy submitted. Broken or indistinct print, colored or poor quality illustrations and photographs, print bleedthrough, substandard margins, and improper alignment can adversely affect reproduction.

In the unlikely event that the author did not send UMI a complete manuscript and there are missing pages, these will be noted. Also, if unauthorized copyright material had to be removed, a note will indicate the deletion.

Oversize materials (e.g., maps, drawings, charts) are reproduced by sectioning the original, beginning at the upper left-hand corner and continuing from left to right in equal sections with small overlaps.

ProQuest Information and Learning
300 North Zeeb Road, Ann Arbor, MI 48106-1346 USA
800-521-0600

UMI[®]

University of Alberta

KIR Enrichment at the Inhibitory Natural Killer Cell Immunological Synapse

by

Leah Jean Standeven



A thesis submitted to the Faculty of Graduate Studies and Research in partial fulfillment of the requirements for the degree of *Master of Science*

in

Immunology

Department of *Medical Microbiology and Immunology*

Edmonton, Alberta

Spring 2005



Library and
Archives Canada

Bibliothèque et
Archives Canada

0-494-08152-X

Published Heritage
Branch

Direction du
Patrimoine de l'édition

395 Wellington Street
Ottawa ON K1A 0N4
Canada

395, rue Wellington
Ottawa ON K1A 0N4
Canada

Your file *Votre référence*

ISBN:

Our file *Notre référence*

ISBN:

NOTICE:

The author has granted a non-exclusive license allowing Library and Archives Canada to reproduce, publish, archive, preserve, conserve, communicate to the public by telecommunication or on the Internet, loan, distribute and sell theses worldwide, for commercial or non-commercial purposes, in microform, paper, electronic and/or any other formats.

The author retains copyright ownership and moral rights in this thesis. Neither the thesis nor substantial extracts from it may be printed or otherwise reproduced without the author's permission.

AVIS:

L'auteur a accordé une licence non exclusive permettant à la Bibliothèque et Archives Canada de reproduire, publier, archiver, sauvegarder, conserver, transmettre au public par télécommunication ou par l'Internet, prêter, distribuer et vendre des thèses partout dans le monde, à des fins commerciales ou autres, sur support microforme, papier, électronique et/ou autres formats.

L'auteur conserve la propriété du droit d'auteur et des droits moraux qui protègent cette thèse. Ni la thèse ni des extraits substantiels de celle-ci ne doivent être imprimés ou autrement reproduits sans son autorisation.

In compliance with the Canadian Privacy Act some supporting forms may have been removed from this thesis.

Conformément à la loi canadienne sur la protection de la vie privée, quelques formulaires secondaires ont été enlevés de cette thèse.

While these forms may be included in the document page count, their removal does not represent any loss of content from the thesis.

Bien que ces formulaires aient inclus dans la pagination, il n'y aura aucun contenu manquant.


Canada

For Peter Standeven

September 29, 1954 - April 15, 2003

Abstract

Under normal conditions the constitutive killing activity of NK cell is kept in check by inhibitory killer cell immunoglobulin-like receptors (KIRs) that bind classical MHC-I molecules. Although KIRs are known to exhibit ligand-induced enrichment at the inhibitory NK cell immunological synapse, the processes that regulate KIR clustering have yet to be fully elucidated. We have found that the actin cytoskeleton plays a role in the stability of conjugates with either sensitive or resistant target cells and, importantly, regulates the rate at which KIR clusters. Our results also implicate the cytoplasmic tail of KIR in facilitating efficient clustering.

Table of Contents

CHAPTER I	1
INTRODUCTION	1
1.1 Natural Killer (NK) cells	1
1.2 Human MHC-I molecules.....	1
1.3 Target cell recognition.....	2
1.4 The actin cytoskeleton	4
1.5 The cytoskeleton and delivery of the lethal hit.....	8
1.6 Extracellular signals and the regulation of cytoskeletal dynamics.....	10
1.7 Lymphocyte function-associated molecule I (LFA-1).....	12
1.8 NK cell activating receptors	13
1.9 NK cell inhibitory receptors that bind MHC-I molecules	14
1.10 Membrane-proximal signaling pathways of NK cell activating receptors	19
1.11 Mechanism of KIR-mediated inhibition.....	21
1.12 The immunological synapse	24
1.13 The helper T cell immunological synapse.....	25
1.14 The cytotoxic T cell immunological synapse	28
1.15 The NK cell immunological synapse.....	30
1.16 KIR at the NK cell immunological synapse	32
1.17 Investigating the processes that regulate KIR clustering.....	34
CHAPTER II	36
MATERIALS AND METHODS	36
2.1 Cell Lines.....	36
2.2 Antibodies and Reagents	40

2.3 Immunofluorescence (cell surface) Staining	41
2.4 Cytolysis Assay.....	41
2.5 Two-Color Flow Cytometry Conjugate Assay	43
2.6 Confocal Imaging of Living Cells	44
2.7 Determining the Frequency of KIR-EGFP Clustering	45
2.8 Generating Snapshots of the Effector:Target Interface	46
2.9 Quantifying KIR-EGFP Enrichment at the Effector:Target Interface.....	46
2.10 Statistics.....	47
CHAPTER III	48
RESULTS - PART A	48
3.1 KIR2DL1 chimeras with EGFP	48
3.2 Generating NK92/KIR2DL1 TR-GFP	48
3.3 KIR2DL1-GFP and not KIR2DL1 TR-GFP is capable of mediating inhibition.....	52
3.4 KIR2DL1-GFP and KIR2DL1 TR-GFP exhibit ligand-induced clustering.....	54
3.5 KIR2DL1 TR-GFP exhibits a defective clustering phenotype.....	54
3.6 KIR2DL1-GFP and KIR2DL1 TR-GFP exhibit varying intensities of enrichment at the inhibitory NK cell immune synapse	59
3.7 The mean total intensity sum of KIR2DL1-GFP and KIR2DL1 TR-GFP are statistically different	62
3.8 KIR2DL1(K346*) is impaired in its ability to drive 221-Cw6-GFP clustering.....	64
CHAPTER IV	68
RESULTS - PART B	68
4.1 YTS /KIR2DL1-GFP cytolysis of target cells is inhibited by azide	68
4.2 YTS/KIR2DL1-GFP conjugate formation with target cells is inhibited by azide.....	70
4.3 KIR2DL1-GFP clustering in YTS is decreased in the presence of azide.....	72

4.4 YTS /KIR2DL1 -GFP cytolysis of target cells is Src family kinase dependent.....	74
4.5 YTS/KIR2DL1-GFP conjugate formation with target cells is Src family kinase dependent.....	76
4.6 KIR2DL1-GFP clustering in YTS is independent of Src family kinase signaling.....	76
4.7 NK92/KIR2DL1-GFP cytolysis of target cells requires an intact actin cytoskeleton	79
4.8 NK92/KIR2DL1 conjugate formation requires an intact cytoskeleton	81
4.9 KIR2DL1-GFP clustering in NK92 and YTS requires an intact cytoskeleton.....	81
4.10 The actin cytoskeleton regulates the rate at which KIR2DL1-GFP and Cw6-GFP cluster.....	84
4.11 The dose response to actin disruption for cytolysis by YTS cells.....	86
4.12 The dose response to actin disruption for conjugate formation by YTS cells.....	88
4.13 The dose response to actin disruption for clustering by KIR-EGFP in YTS cells .	88
4.14 The effect of cytochalasin D on KIR clustering is not through inhibition of LFA-1 mediated adhesion.....	92
CHAPTER V	98
DISCUSSION	98
REFERENCED LITERATURE	115
APPENDIX 1	136
APPENDIX 2	137

List of Tables

Table 1: Properties of the target cell lines used to investigate the processes that regulate KIR2DL1 clustering in YTS and NK92, two human NK-like cell line.....	37
Table 2: Properties of the immortalized YTS cell lines used to study the processes that regulate KIR2DL1 clustering.....	38
Table 3: Properties of the immortalized NK92 cell lines used to study the processes that regulate KIR2DL1 clustering.....	39
Table 4: The mean total intensity sum of KIR2DL1-GFP and KIR2DL1 TR-GFP are significantly difference ($p < 0.05$)	63

List of Figures

Figure 1: NK cells recognize loss of self MHC-I molecules for induction of cytotoxic effecotor function.....	3
Figure 2: Actin exists in a monomeric (G-actin) form or in a polymeric (F-actin) form.....	5
Figure 3: The actin cytoskeleton is a highly dynamic structure	7
Figure 4: Delivery of the lethal hit by cytotoxic lymphocytes	9
Figure 5: Coupling of Rho family GTPases to upstream signals by Vav and subsequent activation of downstream effectos (protein kinases).....	11
Figure 6: Human NK cell activating receptors associate with signal-transducing adaptor proteins via a positively charged residue in their transmembrane domain.....	15
Figure 7: Human NK cell inhibitory receptors that bind MHC-I molecules.	16
Figure 8: The protein tyrosine kinase Syk is central to the development of NK cell cytotoxicity	20
Figure 9: Mechanism of KIR-mediated inhibition.....	22
Figure 10: The helper T cell immunological synapse.....	26
Figure 11: The cytotoxic T cell immunological synapse.....	29
Figure 12: Sustained accumulation of signaling molecules and cell-surface receptors at the inhibitory and activating NK cell immunological synapses	31
Figure 13: Activating signals are rapidly disrupted at the inhibitory NK cell immunological synapse.....	33
Figure 14: KIR2DL1 chimeras with EGFP	49
Figure 15: Cell surface expression profiles of NK92/KIR2DL1-GFP and NK92/KIR2DL1 TR-GFP	51
Figure 16: KIR2DL1-GFP inhibits NK92 cytolysis of 221-Cw4 target cells	53
Figure 17: Ligand-induced KIR-EGFP recruitment to the NK cell immune synapse.....	55
Figure 18: KIR2DL1 TR-EGFP is impaired in its ability to cluster.....	57
Figure 19: The defect in KIR2DL1 TR-GFP clustering is apparent at later time points after cell mixing	58

Figure 20: Varying intensities of KIR-EGFP enrichment at the inhibitory NK cell immune synapse.....	60
Figure 21: KIR2DL1-GFP and KIR2DL1 TR-GFP exhibit varying patterns of enrichment at the interface with 221-Cw4 target cells	61
Figure 22: KIR2DL1(K346*) is another KIR2DL1 truncation mutant	65
Figure 23: KIR2DL1(K346*) is impaired in its ability to drive 221-Cw6-GFP clustering.....	67
Figure 24: YTS cytolysis of sensitive target cells is inhibited by azide in a dose-dependent manner	69
Figure 25: YTS conjugate formation with sensitive target cells is inhibited by azide in a dose-dependent manner	71
Figure 26: KIR2DL1-GFP clustering is decreased in the presence of 50mM azide	73
Figure 27: YTS cytolysis of sensitive target cells is dependent on Src family kinases...	75
Figure 28: YTS conjugate formation with sensitive target cells is dependent on Src family kinases	77
Figure 29: KIR2DL1-GFP clustering is independent of Src family kinase signaling	78
Figure 30: NK92 cytolysis of sensitive target cells requires an intact cytoskeleton	80
Figure 31: NK92 conjugate formation with target cells requires an intact cytoskeleton.	82
Figure 32: KIR2DL1-GFP clustering in NK92 requires an intact cytoskeleton.....	83
Figure 33: KIR2DL1-GFP clustering in YTS requires an intact cytoskeleton.....	85
Figure 34: The dose response to actin disruption for cytolysis by YTS cells.....	87
Figure 35: The dose response to actin disruption for cytolysis by YTS cells can be titrated	89
Figure 36: The dose response to actin disruption for conjugate formation by YTS cells	90
Figure 37: The dose response to actin disruption for clustering by KIR-EGFP in YTS cells.....	91
Figure 38: The TS1/22.1.1.13 anti-LFA-1 antibody constitutively stains YTS/KIR2DL1-GFP	93
Figure 39: YTS adhesion to target cells is dependent on activated LFA-1	95

Figure 40: KIR2DL1-GFP clustering is independent of activated LFA-1	96
Figure 41: The anti-KIR antibody HP3E4 blocks KIR2DL1-GFP clustering in YTS	97
Figure 42: KIR2DL1-GFP mutants	99
Figure 43: Proposed model for KIR clustering at the inhibitory NK cell immunological synapse.....	113

List of Abbreviations

ACK	activated cdc-42 kinase
ADP	adenosine diphosphate
APC	antigen-presenting cell
Arp 2/3	actin-related protein 2/3
ATP	adenosine triphosphate
BADTA	bis (acetoxymethyl) 2,2':6',2"- terpyridine- 6,6"- dicarboxylate
CD	cluster designation
CD2AP	CD2-associated protein
c-SMAC	central SMAC
Cw3-GFP	HLA-Cw3 fused to EGFP
Cw6-GFP	HLA-Cw6 fused to EGFP
DIC	differential interference contrast
DMSO	dimethyl sulfoxide
EBV	Epstein Barr virus
ECMV	encephalomyocarditis virus
EDTA	ethylene diamine tetraacetic acid
EGFP	enhanced green fluorescent protein
ELM	Eukaryotic Linear Motif
ERK	extracellular regulated kinase
ERM	ezrin-radixin-moesin
FACs	fluorescence-activated cell sorting
FBS	fetal bovine serum

GDP	guanosine diphosphate
GEF	guanine nucleotide exchange factor
GTPase	guanosine triphosphatase
GTP	guanosine triphosphate
HLA	human leukocyte antigen
ICAM	intercellular adhesion molecule
IFN-γ	interferon- γ
IL	interleukin
ILT2	Ig-like transcript 2
IRES	internal ribosome entry site
ITAM	immune tyrosine-based activating motif
ITIM	immunoreceptor tyrosine-based inhibition motif
KIR	killer cell immunoglobulin-like receptor
KIR-EGFP	KIR2DL1 chimeras with EGFP
LAT	linker for activated T cells
LFA	lymphocyte function-associated molecule
LIMK1	LIM-kinase I
LSM	laser scanning microscope
M	mean
MAPK	mitogen-activated protein kinase
MEK	mitogen-activated or extracellular signal-regulated protein kinase
MHC-I	major histocompatibility class I

MIP	maximum intensity projection
MTOC	microtubule-organizing center
NK	natural killer
PAK1	p21-activated kinase 1
PBS	phosphate buffered saline
PET	polyethyene terephthalate
PKC-θ	protein kinase C θ
PI3K	phosphoinositide 3-kinase
PIP2	phosphatidylinositol (4,5)-bisphosphate
PIP3	phosphatidyl inositol-3,4,5-triphosphate
PLC-γ	phospholipase C γ
p-SMAC	peripheral SMAC
PP2	4-amino-5-(4-chlorophenyl)-7-(<i>t</i> -butyl)pyrazolo[3,4-d]pyrimidine
PTK	protein tyrosine kinase
RNAi	RNA interference
ROCK	p160 Rho-associated coiled-coil-containing protein kinase
RT-PCR	real-time polymerase chain reaction
SC2	Schneider cell 2
SD	standard deviation
SH2	Src homology 2
SH3	Src homology 3
SHP-1	Src homology protein 1

SLP-76	SH2 domain-containing leucocyte protein of 76 kDa
SMAC	supramolecular activation cluster
TCR	T cell receptor
TNF	tumor necrosis factor
WASP	Wiskott Aldrich syndrome protein

CHAPTER I

Introduction

1.1 Natural Killer (NK) cells

Human Natural Killer (NK) cells are a subpopulation of lymphocytes that comprise approximately 15% of peripheral blood lymphocytes and are found in peripheral tissues such as the liver, placenta, and peritoneal cavity (1). Upon activation, NK cells secrete certain cytokines, including interferon- γ (IFN- γ) and tumor necrosis factor (TNF) (2). In addition, NK cells are a type cytotoxic lymphocyte that is capable of mediating direct lysis of tumorigenic cells and virally infected cells. However, unlike cytotoxic T cells (another type of cytotoxic lymphocyte), NK cells are capable of directly lysing virally infected and tumorigenic cells without prior sensitization (1). Cytotoxic T cell activation requires prior sensitization via their T cell receptors (TCRs), whereas NK cells are constitutively active and are capable of releasing pre-formed cytotoxic granules upon target cell contact. Central to NK recognition and lysis of target cells is the ability of NK cells to detect the absence of self-major histocompatibility complex Class I (MHC-I) molecules (3).

1.2 Human MHC-I molecules

MHC-I molecules are glycoproteins that are expressed on the surface of virtually all cells, with the exception of red blood cells and cells of the central nervous system, In structural terms, MHC-I molecules are comprised of a transmembrane protein non-

covalently attached to the molecule of β 2-microglobulin. MHC-I molecules function to present antigenic peptides to cytotoxic lymphocytes. The genes of MHC-I exhibit a huge degree of diversity of alleles and thus are considered to be extremely polymorphic. Humans have three types of classical MHC-I molecules (MHC-I molecules) and these are referred to as human leukocyte antigen (HLA)-A, HLA-B, and HLA-C. In humans, there are a number of non-classical MHC-I molecules. Non-classical MHC-I molecules exhibit structural homology to the classical MHC-I molecules but generally have limited polymorphism, low cell surface expression, and more restricted tissue distribution (4, 5). HLA-E is an example of a non-classical MHC-I molecule and requires binding of peptides derived from the signal sequences of classical MHC-I molecules in order to be expressed on the cell surface (5, 6). MHC-I molecules function to present peptide antigen to cytotoxic T cells, which possess the molecular machinery necessary for cytolysis of a target cell.

1.3 Target cell recognition

Cytotoxic T cells are effector cells of the adaptive immune system and require peptide antigen complexed with MHC-I molecules to identify an infected cell. Given that cytotoxic T cells are efficient killers, many pathogens and cancers have evolved immune evasion strategies to avoid cytotoxic T cells by decreasing the cell surface expression of MHC-I molecules. In response to this selective pressure, NK cells, which are effector cells of the innate immune system, have evolved the ability to recognize virus-infected and tumorigenic cells that have down-regulated cell surface expression of MHC-I molecules (Figure 1). NK cells express a variety of activating receptors that enable them

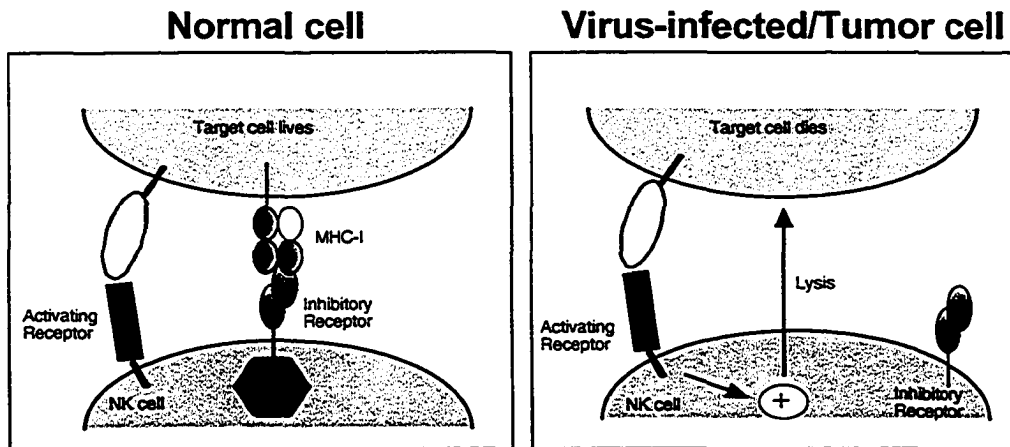


Figure 1: NK cells recognize loss of self MHC-I molecules for induction of cytotoxic effector function. Whether or not an NK cell recognizes and lyses a potential target cell depends on the balance between positive and negative signals that arise from cell surface activating and inhibitory receptors. Although NK cells express a variety of activating receptors that enable them to lyse virtually all cells, under normal conditions the constitutive killing activity of NK cell is kept in check by cell surface inhibitory receptors that bind classical and non-classical MHC-I molecules. This target cell recognition system allows NK cells to recognize virus-infected and tumorigenic cells that have down-regulated cell surface expression of MHC-I molecules in order to avoid cytotoxic T cells.

to lyse virtually all cells. However, under normal conditions the constitutive killing activity of NK cell is kept in check by cell surface inhibitory receptors that bind classical and non-classical MHC-I molecules. This current hypothesis for regulation of NK cells, which states that NK cells recognize loss of self MHC-I molecules for induction of cytotoxic effector function, is referred to as the "missing self" hypothesis (3, 7).

1.4 The actin cytoskeleton

In eukaryotic cells, the cytoskeleton is composed primarily of actin microfilaments (thin, thread-like fibers approximately 5-9 nm in size), microtubules (large, cylindrical tube-like fibers approximately 25 nm in size), and intermediate filaments (approximately 10 nm in size). Microtubules are polymers of α - and β -tubulin subunits and originate from the microtubule-organizing center (MTOC). Actin microfilaments are polymers of actin (F-actin) that assemble via non-covalent interactions between the monomeric subunits (G-actin) (8) (Figure 2). Briefly, a G-actin molecule binds adenosine triphosphate (ATP), which is hydrolyzed to adenosine diphosphate (ADP) following incorporation of the molecule into the growing polymer (F-actin). G-actin is mainly attached to the rapidly growing (barbed or plus) end of the filament and the opposite end, which by comparison grows rather slowly, is referred to as the pointed (or minus) end (8, 9). Actin microfilaments together with a large number of actin-binding proteins and other associated proteins comprise the actin cytoskeleton (8). The portion of the actin cytoskeleton that lies just beneath the plasma membrane is referred to as the cortical actin cytoskeleton.

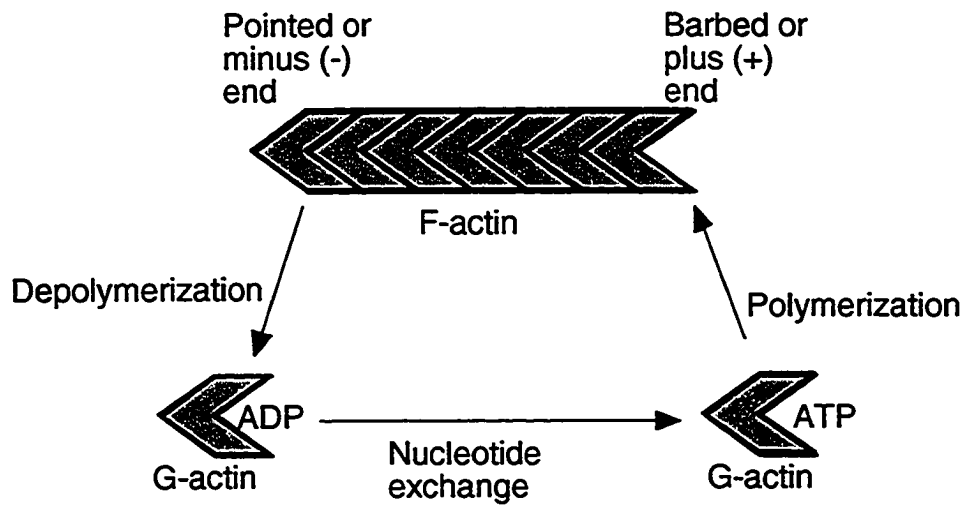


Figure 2: Actin exists in a monomeric (G-actin) form or in a polymeric (F-actin) form. G-actin molecules binds ATP, which is hydrolyzed to ADP following incorporation of the molecule into the growing polymer (F-actin). G-actin is mainly attached to the rapidly growing (barbed or plus) end of the filament and the opposite end, which by comparison grows rather slowly, is referred to as the pointed (or minus) end. Adapted from Samstag *et al.* 2003 and Welch *et al.* 1997.

The actin cytoskeleton is a highly dynamic structure requiring processes such as generation of new actin filaments (nucleation), enhanced polymerization of pre-existing filaments (elongation), and recycling of actin filaments into monomeric subunits (depolymerization) (reviewed in (9)) (Figure 3). Furthermore, branching, bundling, and crosslinking of actin filaments results in higher ordered F-actin structures thereby resulting in a dense network of cytoskeletal actin. The ability of the actin cytoskeleton to undergo dynamic rearrangement requires an ever-present pool of ATP-G-actin monomers. High amounts of unpolymerized actin are maintained in unstimulated cells as a result of mono-binding proteins (profilin and thymosin- β 4) that prevent incorporation of monomeric actin into actin filaments. High amounts of unpolymerized actin are also maintained as a result of capping proteins (capping protein or gelsolin) that bind to the ends of actin filaments to prevent the attachment of further actin monomers. Free barbed ends (required for polymerization) occur by nucleation of new actin filaments, by uncapping of barbed ends in existing actin filaments through release of capping proteins, or by severing of noncovalent bonds between actin monomers within filamentous actin, resulting in shorter filaments with free barbed ends. Association of the Wiskott Aldrich syndrome protein (WASP) with actin monomers and the actin-related protein 2/3 (Arp2/3) complex initiates actin nucleation. Displacement of capping proteins from actin filaments is mediated by polyphosphoinositides, such as phosphatidylinositol (4,5) biphosphate (PIP₂) and phosphatidyl inositol-3,4,5-triphosphate (PIP₃). The actin-binding protein cofilin is unique in that it can mediate actin polymerization or depolymerization, depending on the activation state of Arp2/3 complexes. In the presence of Arp2/3 activating signals, severing by the actin-binding protein cofilin

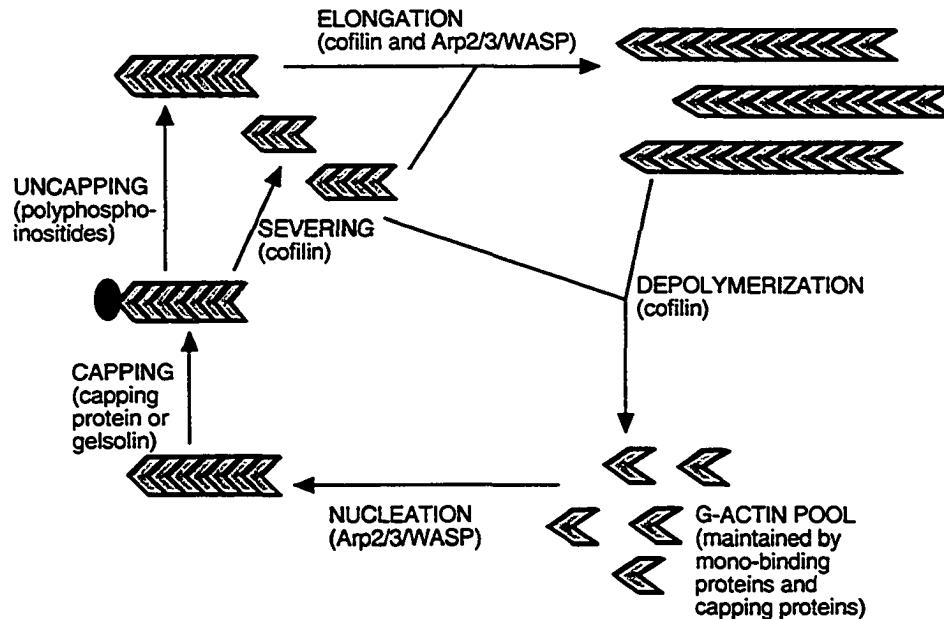


Figure 3: The actin cytoskeleton is a highly dynamic structure. The actin cytoskeleton is a highly dynamic structure requiring processes such as generation of new actin filaments (nucleation), enhanced polymerization of pre-existing filaments (elongation), and recycling of actin filaments into monomeric subunits (depolymerization). High amounts of unpolymerized actin are maintained in unstimulated cells as a result of mono-binding proteins (profilin and thymosin- β 4) and capping proteins (capping protein or gelsolin). Free barbed ends (required for polymerization) occur by nucleation of new actin filaments, by uncapping of barbed ends in existing actin filaments through release of capping proteins, or by severing of non-covalent bonds between actin monomers within filamentous actin, resulting in shorter filaments with free barbed ends. Association of the WASP with actin monomers and the Arp2/3 complex initiates actin nucleation. Displacement of capping proteins from actin filaments is mediated by PIP2 and PIP3. In the presence of Arp2/3 activating signals severing by the actin-binding protein cofilin produces free barbed ends, which can favor actin polymerization. In the absence of Arp2/3 activating signals, cofilin increases actin depolymerization by the formation of unpolymerizable heterodimers and the enhancement of the off-rate of actin monomers from the pointed end or both ends of actin filaments. Adapted from Samstag *et al.* 2003.

produces free barbed ends, which can favor actin polymerization. However, in the absence of Arp2/3 activating signals, cofilin increases actin depolymerization by the formation of unpolymerizable heterodimers and the enhancement of the off-rate of actin monomers from the pointed end or both ends of actin filaments. The actin-binding capacity of cofilin is negatively regulated by phosphorylation by the serine kinase LIM-kinase (LIMK). Although cofilin is phosphorylated mainly in resting lymphocytes, this actin-binding protein is dephosphorylated upon stimulation.

1.5 The cytoskeleton and delivery of the lethal hit

Both cytotoxic T cells and NK cells employ a similar sequence of events for delivery of cytolytic granules (lethal hit) that is dependent on both actin microfilaments and microtubules (10-12). Directed degranulation of a cytotoxic cell is a multistep process that begins with effector cell conjugate formation with a target cell (Figure 4). Adhesion is followed by engagement of activating receptors and adhesion molecules, which initiates intracellular signaling through tyrosine kinases and the generation of secondary messengers (namely inositol phosphate hydrolysis and increased intracellular calcium levels). These signaling cascades result first in the local polarization of the cortical actin cytoskeleton and second in the repositioning of the MTOC such that it lies beneath the area of contact with the target cell. Reorganization of the MTOC then aligns the secretory apparatus, including the Golgi apparatus, towards the target cell and this allows for direct release of lytic granules (via exocytosis) at the site of target cell contact. The contents of the lytic granules, including perforin and granzymes, trigger the target cell to die by apoptosis.

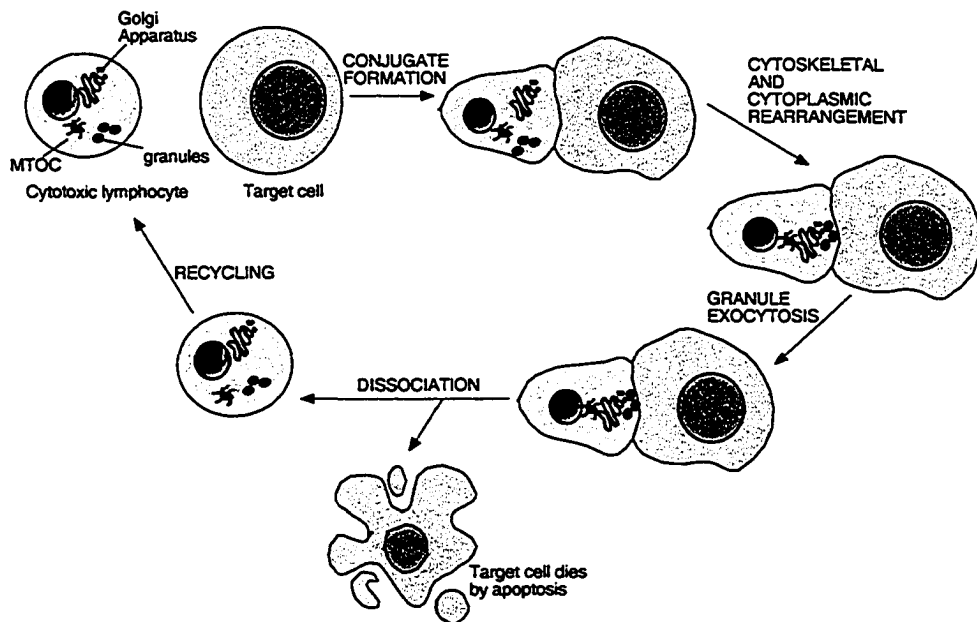


Figure 4: Delivery of the lethal hit by cytotoxic lymphocytes. Directed degranulation of a cytotoxic cell begins with tight conjugate formation between an effector cell (cytotoxic lymphocyte) and a target cell. Tight adhesion is followed by engagement of activating receptors and adhesion molecules, which initiates intracellular signaling that results first in the local polarization of the cortical actin cytoskeleton and second in the repositioning of the MTOC. Reorganization of the MTOC aligns the secretory apparatus, including the Golgi apparatus, towards the target cell and this allows for direct release of lytic granules (via exocytosis) at the site of target cell contact. The effector cell dissociates and is free to encounter other potential target cells. The contents of the lytic granules, including perforin and granzymes, trigger the target cell to die by apoptosis. Adapted from Immunology, Kuby, 4th and 5th Editions.

1.6 Extracellular signals and the regulation of cytoskeletal dynamics

Extracellular signals regulate actin dynamics through the Rho family of small guanosine triphosphatases (GTPases) (reviewed in (13)). The Rho family of small GTPases consists of several proteins including Rac, Rho, and Cdc42, which interact with downstream effectors upon binding to guanosine triphosphate (GTP). Guanine nucleotide exchange factors (GEFs) are multidomain proteins that activate Rho family GTPases by converting them from an inactive guanosine diphosphate (GDP)-bound state to an active GTP-bound form. Vav is a well-characterized GEF that activates Rho family GTP-binding proteins. In mammalian cells, the Vav family of GEFs consists of three structurally similar members known as Vav1, Vav2, and Vav3 (13). Importantly, the GEF activity of Vav is greatly enhanced upon its phosphorylation by tyrosine kinases (13). As a result, Vav has the ability to couple protein tyrosine kinase-dependent regulation to a G-protein-mediated control (13).

In lymphocytes, actin cytoskeletal rearrangements and granule exocytosis are controlled in part through the activation of Rac1, RhoA, and Cdc42 (all members of the Rho family of small GTPases) (13) (Figure 5). Multiple effectors exist for activated Rac, Rho, and Cdc42 and several of these targets are protein kinases (13). In the case of Rac, the sequential recruitment and activation of Rac1→p21-activated kinase 1→mitogen-activated or extracellular signal-regulated protein kinase 1/2→extracellular regulated kinase 1/2 (Rac1→PAK1→MEK1/2→ERK1/2) drives cytotoxic function in NK cells through granule mobilization (14). In the case of Rho, the RhoA/p160 Rho-associated coiled-coil-containing protein kinase/LIMK (RhoA/ROCK/LIMK) pathway has been found to be required for inhibition of actin polymerization and lipid raft polarization to

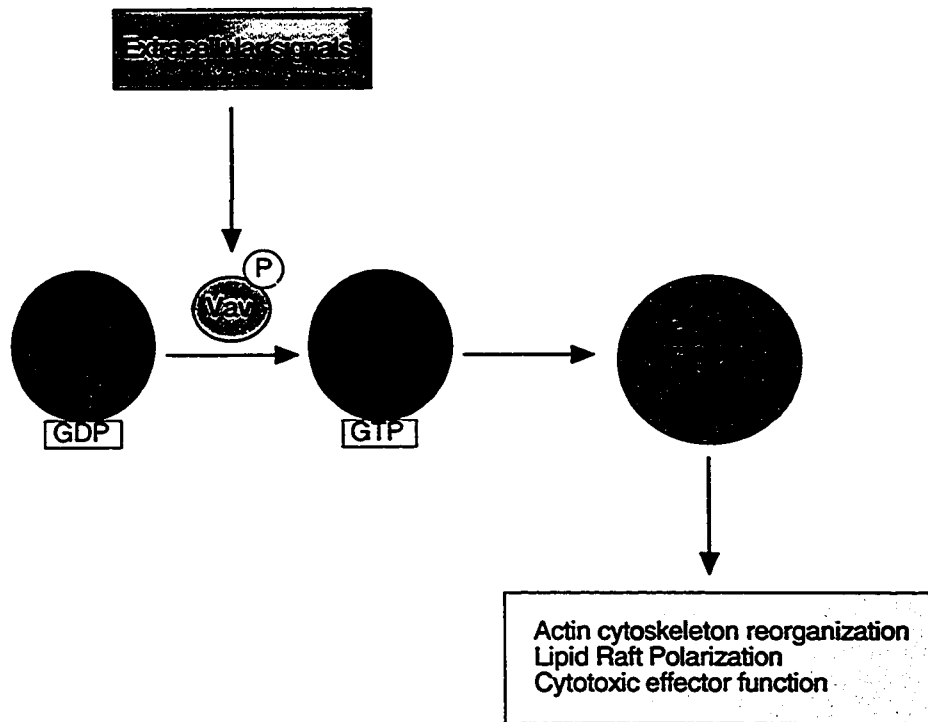


Figure 5: Coupling of Rho family GTPases to upstream signals by Vav and subsequent activation of downstream effector molecules (protein kinases). The GEF Vav activates Rho family GTPases by converting them from an inactive GDP-bound state to an active GTP-bound form. Given that the activity of Vav is greatly enhanced upon its phosphorylation by tyrosine kinases, Vav has the ability to couple protein tyrosine kinase-dependent regulation to a G-protein-mediated control. Members of the Rho family of small GTPases include Rac, Rho, and Cdc42, which interact with downstream effectors upon binding to GTP. Multiple effectors exist for activated Rac, Rho, and Cdc42 and several of these targets are protein kinases (PACK, ROCK, ACK). In lymphocytes, actin cytoskeletal rearrangements and granule exocytosis are controlled in part through the activation of Cdc42, Rac, and RhoA. For example, Cdc42 regulates T cell polarization, RhoA is required for inhibition of actin polymerization, lipid raft polarization and subsequent delivery of the lethal hit, and Rac1 activation drives cytotoxic effector function through granule mobilization. Adapted from Khurana *et al.* 2003.

the site of target contact and the subsequent delivery of the lethal hit (15). Of note, Vav1 acts as a GEF for Rac1 subfamily member, whereas Vav2 acts as a GEF for the RhoA subfamily member (13). The Cdc42 Rho family member targets the tyrosine kinase activated cdc-42 kinase (ACK) and Cdc42 has been shown to regulate T cell polarization (13).

1.7 Lymphocyte function-associated molecule I (LFA-1)

There are a number of cell surface adhesion molecules that mediate cytotoxic lymphocyte conjugate formation with target cells, including the $\beta 2$ integrin known as lymphocyte function-associated molecule I (LFA-1). LFA-1 is a heterodimeric transmembrane receptor composed of an α subunit (CD11a) and a $\beta 2$ subunit (CD18). The ligands for human LFA-1 include Intercellular Adhesion Molecule (ICAM)-1, ICAM-2, and ICAM-3.

The contribution of LFA-1 to T cell conjugate formation with antigen presenting cells has been well studied. In T cells, LFA-1 is regulated by changes in affinity and avidity. LFA-1 exists in either an inactive (or low affinity) state or an active (or high affinity) state (16-18). In addition, engagement of the antigen-specific T cell receptor initiates "inside out" signaling that rapidly and transiently increases LFA-1 avidity (19). The actin cytoskeleton plays a key role in this "inside out" signaling (20). In resting cells, the cytoplasmic tails of the CD11a and CD18 subunits mediate attachment of LFA-1 to the actin cytoskeleton. Upon activation, LFA-1 dissociates from the actin cytoskeleton, clusters by lateral diffusion at the effector-target interface, and then renews its attachment to the actin cytoskeleton, the net result of which is an increased avidity

state for LFA-1 (20-22). Further to this, work by Stewart *et al.* suggests that following agonist exposure leading to Ca^{2+} mobilization, LFA-1 is released from cytoskeletal restraints by the Ca^{2+} -induced activation of a calpain-like enzyme (21).

LFA-1 adhesion is involved in NK cell conjugate formation with, and cytolysis of, target cells (23). However it has been difficult to define the minimal requirements for NK cell adhesion and cytolysis and to determine the contribution of individual receptors, such as LFA-1, to these cellular processes. To address this issue, a target cell system has been developed whereby ligands of human NK cells have been expressed in *Drosophila* Schneider cell 2 (SC2) cells (24). Experiments using these SC2 cells suggest that NK cells use LFA-1 to bind directly to target cells and that co-engagement of the NK cell surface receptors CD2 and 2B4 contributes to adhesion via LFA-1. The SC2 target cell system has also been used to study the contribution of LFA-1 to activation signals required for NK cell cytolysis (25). Data from these experiments suggests that LFA-1 alone is sufficient to initiate early activation signals in NK cells and that the "inside-out" signaling that regulates LFA-1 binding in T cells is not required (25). There is precedence for this finding that LFA-1 directly mediates adhesion and transduces activating signals for cytolysis. In murine neutrophils, LFA-1 engagement can induce degranulation via the Syk tyrosine kinase (26). However, with human cells, LFA-1 is not usually sufficient and other activating receptors are required for activation.

1.8 NK cell activating receptors

NK cells express a variety of activating receptors, which recognize diverse ligands on target cells, including NKG2D and the natural cytotoxicity receptors (NCRs)

NKp46, NKp30, and NKp44 (27-31) (Figure 6). In general, NK cell activating receptors consist of a short cytoplasmic tail that does not contain any sequence motifs typically involved in activation of signaling cascades. In order to initiate cytolysis of target cells, these activating NK cell receptors must associate with signal-transducing adaptor molecules via a positively charged residue in their transmembrane domain. NKG2D associates with the DAP10 adaptor protein that contains a YxxM motif (32). NKp46 associates with CD3 ζ and Fc ϵ R1 γ adaptor proteins that contain one and three immune tyrosine-based activating motifs (ITAMs), respectively, in their cytoplasmic tails (33, 34). NKp30 associates with CD3 ζ adaptor proteins. NKp44 associates with the ITAM-bearing DAP12 signal-transducing molecule that contains a single ITAM in the cytoplasmic portion (35). Engagement of these activating NK cell receptors leads to phosphorylation of key tyrosine residues in the cytoplasmic portion of the adaptor proteins that in turn recruits other effector kinases necessary for the propagation of the activating signals.

1.9 NK cell inhibitory receptors that bind MHC-I molecules

The constitutive killing activity of NK cells is regulated by several inhibitory receptors that bind MHC-I molecules. In humans, these receptors include the lectin-like CD94/NKG2 receptors and the inhibitory killer cell immunoglobulin-like receptors (KIRs) (36) (Figure 7). Although CD94/NKG2A and KIR both bind MHC-I molecules, they have very different structures.

CD94/NKG2A inhibitory receptors are heterodimers in which a 26-kD CD94 protein is covalently linked to a 43-kD NKG2A protein (37). The type II transmembrane

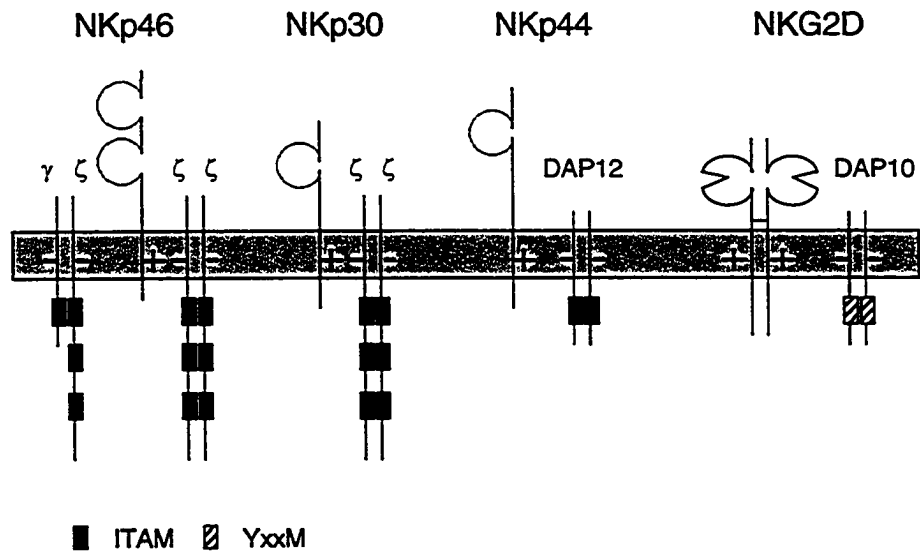


Figure 6: Human NK cell activating receptors associate with signal-transducing adaptor proteins via a positively charged residue in their transmembrane domain. NK cells express a variety of activating receptors, including NKG2D, NKp46, NKp30, and NKp44. In general, NK cell activating receptors consist of a short cytoplasmic tail that does not contain any sequence motifs typically involved in activation of signaling cascades. Therefore, these activating receptors must associate with signal-transducing adaptor molecules via a positively charged residue in their transmembrane domain. NKG2D associates with the DAP10 adaptor protein that contains a YxxM motif. NKp46 associates with CD3 ζ and Fc ϵ RI γ adaptor proteins that contain one and three ITAMs, respectively. NKp30 associates with CD3 ζ adaptor proteins. NKp44 associates with the ITAM-bearing DAP12 signal-transducing molecule that contains a single ITAM. Engagement of these activating NK cell receptors leads to phosphorylation of key tyrosine residues in the YxxM motif or the ITAMs that in turn recruits other effector kinases necessary for the propagation of the activating signals. Adapted from Moretta *et al.* 2001.

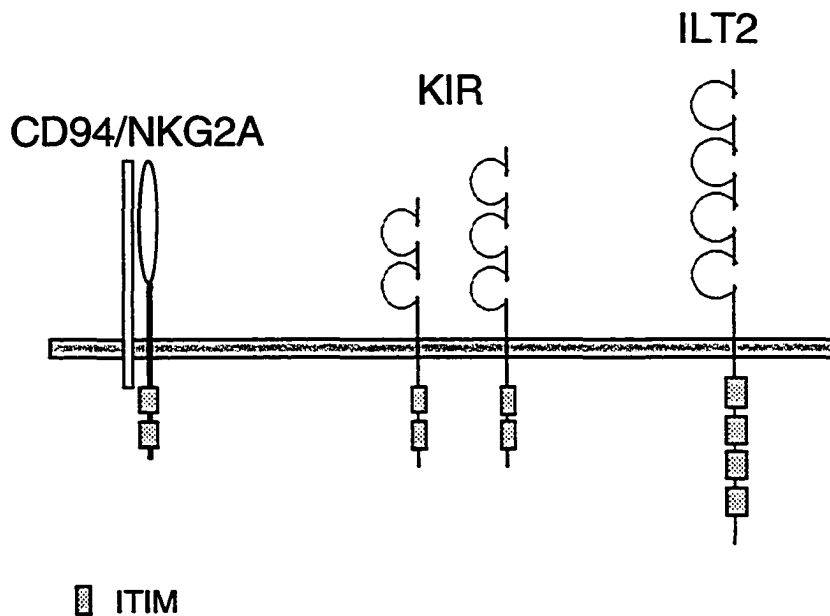


Figure 7: Human NK cell inhibitory receptors that bind MHC-I molecules. The constitutive killing activity of NK cells is regulated by several inhibitory receptors that bind MHC-I molecules. In humans, these receptors include the lectin-like CD94/NKG2 receptors and the KIRs. CD94/NKG2A inhibitory receptors are heterodimers of the type II transmembrane glycoproteins CD94 (a C-type lectin) and NKG2A. The cytoplasmic tail of NKG2A contains two copies of the ITIM. KIRs are type I transmembrane proteins belonging to the immunoglobulin-like receptor superfamily. KIRs have long cytoplasmic tails that contain two copies of the ITIM. A second example of an inhibitory receptor belonging to the immunoglobulin-like receptor superfamily is the Ig-like transcript 2 (ILT2) receptor. ILT2 receptor contains four ITIMs in its cytoplasmic tail. Phosphorylation of conserved tyrosine residues in the ITIMs is required for inhibitory receptor function.

glycoprotein CD94 is a C-type lectin and is required for cell surface expression of NKG2A. The type II transmembrane glycoprotein NKG2A is responsible for inhibitory signaling and for ligand binding specificity. The cytoplasmic tail of NKG2A contains two copies of the immunoreceptor tyrosine-based inhibition motif (ITIM), which has been defined as I/VxYxxL (38). Phosphorylation of conserved tyrosine residues in the ITIM of NKG2A is required for its inhibitory function (39). The extracellular domain of NKG2A binds to HLA-E, a non-classical MHC-I molecule that requires binding of peptides derived from the signal sequences of classical MHC-I molecules in order to be expressed on the cell surface (5, 6).

KIRs are type I transmembrane proteins belonging to the immunoglobulin-like receptor superfamily. Unlike the nonpolymorphic CD94/NKG2A, KIRs exhibit a high degree of structural diversity. KIR nomenclature has a structural basis and three criteria have been used to classify them: the number of extracellular immunoglobulin-like domains, the length of cytoplasmic tail, and the specific gene locus (40, 41). KIRs contain two or three extracellular immunoglobulin-like domains and are referred to as KIR2D or KIR3D, respectively (40). Inhibitory KIRs have a long cytoplasmic tail and are denoted as KIR2DL or KIR3DL, respectively. The long cytoplasmic tails of KIR2DL and KIR3DL contain two copies of the ITIM region. Similar to CD94/NKG2A, phosphorylation of conserved tyrosine residues in the ITIM of KIR is also required for its inhibitory function (42). KIR genes are highly polymorphic and individual haplotypes vary in both the number of genes and the specific alleles (41). Therefore the nomenclature for KIR also includes a numeric identifier for the gene locus encoding the protein. For example there are three KIR2DL loci and they are identified as KIR2DL1,

KIR2DL2, and KIR2DL3, respectively. An asterisk is used as a separator before a numerical allele designation and thus an example of a complete inhibitory KIR name is KIR2DL1*002 (40).

Human inhibitory KIRs bind to HLA-A, HLA-B, and HLA-C classical MHC-I molecules. Of note, KIR2DL1 binds to HLA-C. The extracellular region of KIR2DL1, consisting of two immunoglobulin-like domains, mediates the ligand-binding specificity. An acute angle between the two immunoglobulin-like domains of KIR2DL1 forms an elbow that interacts with HLA-C (43). Many KIR2D molecules are also able to bind zinc through a zinc-binding motif (HEGVH) located in the amino-terminal immunoglobulin-like domain (44, 45). This zinc-binding motif, which corresponds to the canonical zinc binding motif of HEXXH, is important for KIR inhibitory function but is not required for binding to HLA-C (44, 46, 47).

In addition to inhibitory KIR, an example of another inhibitory receptor belonging to the immunoglobulin-like receptor superfamily is the Ig-like transcript 2 (ILT2) receptor (Figure 7). The ILT2 receptor contains four ITIMs in its cytoplasmic tail, has four extracellular immunoglobulin-like domains, and is expressed on B cells, monocytes, dendritic cells and on minor subsets of NK cells and T cells (48, 49). ILT2 receptor binds both classical and non-classical MHC-I molecules by recognition with a nonpolymorphic region in the $\alpha 3$ domain of MHC-I proteins (50, 51). Based on these observations, it has been suggested that the function of ILT2 receptor in NK cells is to act as a MHC-I inhibitory receptor with broad specificity.

1.10 Membrane-proximal signaling pathways of NK cell activating receptors

NK cell conjugate formation with sensitive target cells has long been known to induce inositol phosphate (phosphoinositide) release and increased intracellular free calcium (52, 53). A more membrane-proximal signaling event is the activation of Src family kinases, such as Lck, Fyn, and Lyn, that is closely followed by phosphorylation of specific tyrosine residues in the adaptor molecule associated with the NK cell activating receptor (54). This in turn leads to the recruitment and activation of other effector kinases (54). Phosphorylation of DAP-10 is believed to result in the recruitment of the p85 subunit of PI3K (55). In contrast, phosphorylation of DAP-12, CD3 ζ or Fc ϵ RI γ leads to the recruitment and activation of Syk family kinases, ZAP-70 and Syk (54, 56) (Figure 8). The protein tyrosine kinase Syk is central to the development of NK cell cytotoxicity as demonstrated by combined biochemical, pharmacologic, and genetic approaches (57). Activated Syk kinases will in turn phosphorylate multiple molecules that are essential for propagating the activating signal cascade, including PI3K, phospholipase C γ (PLC- γ), SH2 domain-containing leukocyte protein of 76 kDa (SLP-76), WASP, linker for activated T cells (LAT), protein kinase C- θ (PKC- θ), and Vav (54). The existence of multiple molecular substrates for Syk kinases allows for the simultaneous initiation of separate signaling pathways required to drive cytotoxic function in NK cells. These pathways and effector functions include gene transcription required for cytokine production (SLP-76, PLC- γ , PKC- θ , and LAT), granule polarization and release (PI3K), and cytoskeleton remodeling (WASP and Vav) (54). An additional event in the generation of cellular cytotoxicity by NK cells is the Src and Syk family kinase-dependent polarization of lipid rafts (plasma membrane

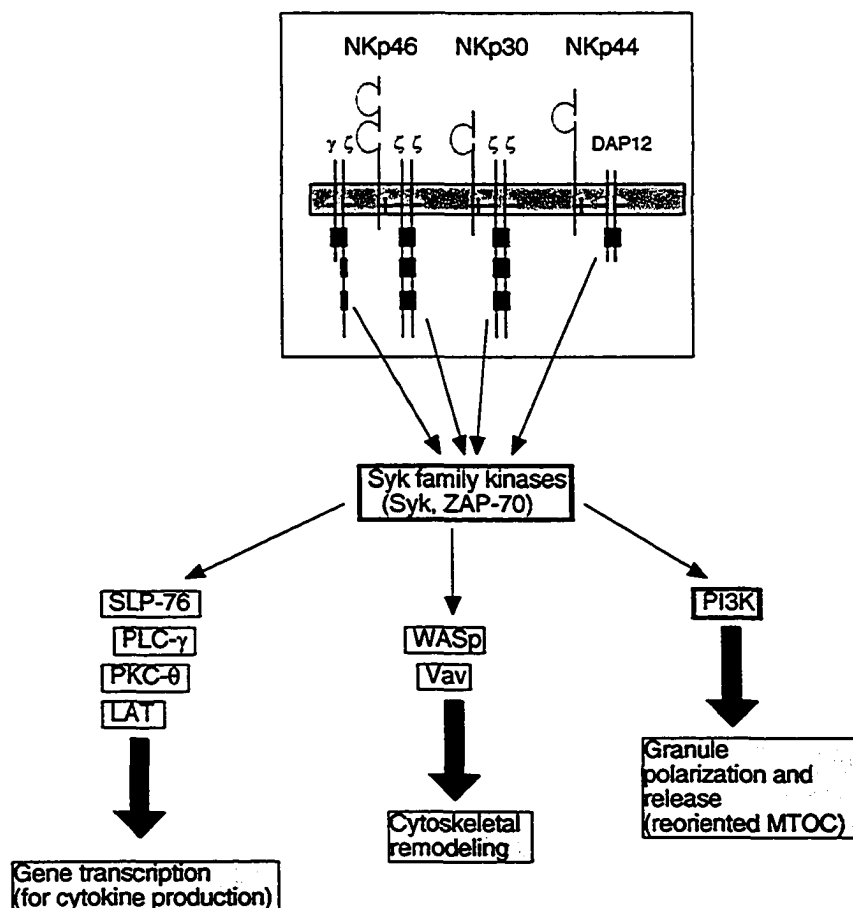


Figure 8: The protein tyrosine kinase Syk is central to the development of NK cell cytotoxicity. Phosphorylation of specific tyrosine residues in the adaptor molecule associated with the NK cell activating receptor leads to the recruitment and activation of other effector kinases. For example, phosphorylation of DAP-12, CD3 ζ or Fc ϵ RI γ leads to the recruitment and activation of Syk family kinases, ZAP-70 and Syk. The existence of multiple molecular substrates for Syk family kinases allows for the simultaneous initiation of the separate signaling pathways that are required to drive cytotoxic effector function in NK cells. These pathways and effector functions include gene transcription required for cytokine production (SLP-76, PLC- γ , PKC- θ , and LAT), granule polarization and release (PI3K), and cytoskeleton remodeling (WASP and Vav). Adapted from Lanier *et al.*2003 and Vyas *et al.*2002.

microdomains containing sphingolipids and cholesterol) to the site of target cell recognition (58).

1.11 Mechanism of KIR-mediated inhibition

Inhibitory receptors are believed to act "*in cis*" meaning that they must be in close proximity to activating receptors in order to block activating signals (reviewed in (59)). Engagement of KIR by MHC-I molecules (ligands) inhibits NK cell effector function by directly altering membrane proximal signaling events (60). Critical signaling events for cytotoxicity, namely inositol phosphate hydrolysis (release) and increased intracellular calcium levels, are inhibited following recognition of sensitive target cells (bearing MHC-I molecules) (60). Engagement of inhibitory receptors also disrupts adhesion to resistant target cells, the purpose of which may be to increase the availability of NK cells for the detection of sensitive target cells that will trigger NK cell cytotoxic effector function (23). Finally, engagement of KIR by MHC-I molecules on target cells has been found to block polarization of lipid rafts, suggesting that influence on raft redistribution may also influence the development of NK cell cytotoxic effector function (58).

The earliest membrane-proximal signaling event to take place during KIR-mediated inhibition is the phosphorylation of the conserved tyrosine residues in the cytoplasmic tail of KIR (Figure 9). This phosphorylation is paramount to the ability of the inhibitory receptors to antagonize the signals emanating from activating receptors (42). The signaling and cell surface molecules involved in this process of KIR phosphorylation have yet to be definitely identified. One proposed mechanism is that ITIM phosphorylation is dependent on the tyrosine kinases that are recruited and

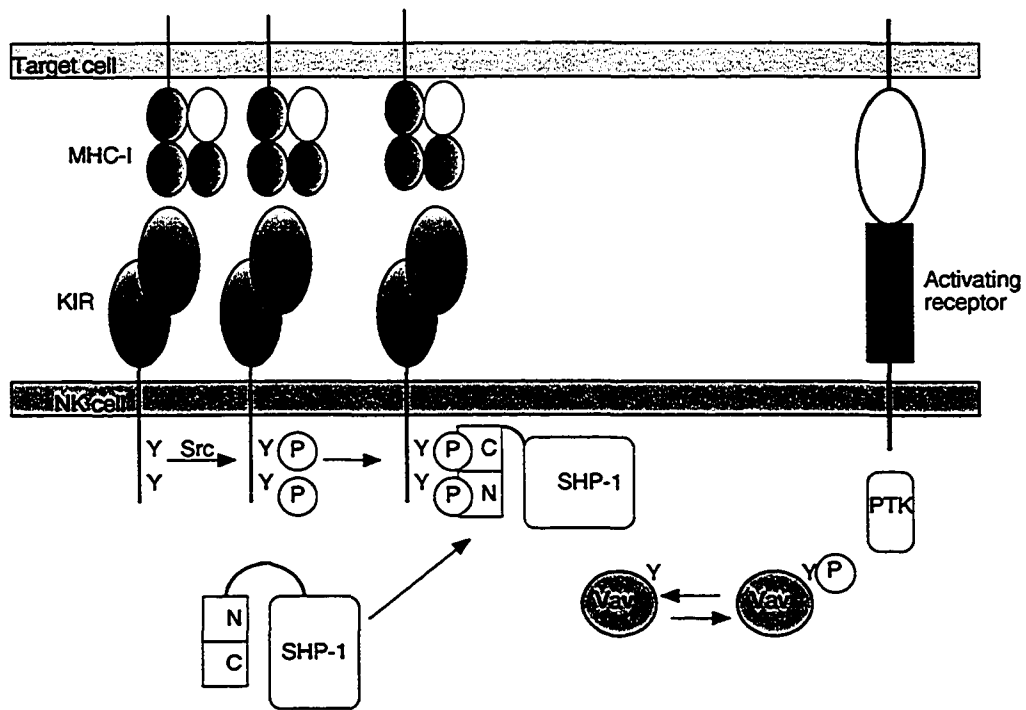


Figure 9: Mechanism of KIR-mediated inhibition. Inhibitory receptors are believed to act "*in cis*" meaning that they must be in close proximity to activating receptors in order to block activating signals. MHC-I engagement of KIR is accompanied by phosphorylation of the conserved tyrosine residues in the ITIMs by Src family kinases. The cytoplasmic protein tyrosine phosphatase SHP-1 is then recruited and activated. Activated SHP-1 dephosphorylates substrates involved in activating signaling cascades, such as the guanine nucleotide exchange factor Vav. The net result is a disruption of activating signals necessary for NK cell effector function. PTK stands for protein tyrosine kinase.

activated following engagement of NK cell activating receptors. In support of this, results from molecular approaches suggest that the Src family kinase Lck is required for KIR phosphorylation but not other Src family kinases, such as Fyn or Lyn (61). Given the involvement of Src family kinases in NK cell activation, this could explain why inhibitory receptors must be in close proximity to activating receptors in order to deliver the inhibitory signal (36). SC2 insect cells transfected with specific ligands of NK cell receptors have been used in an attempt to dissect the minimal requirements for phosphorylation of KIR (62). KIR was rapidly and transiently phosphorylated as a result of interaction with the KIR2DL1 ligand HLA-Cw4 but independently of LFA-1/ICAM-1, CD28/B7.1 interactions (62). KIR phosphorylation was sensitive to inhibitors of Src family kinases and required the presence of zinc, but was not blocked by inhibitors PI3K or actin and tubulin polymerization. However, tyrosine phosphorylation of ITIM-containing KIR following mixing with SC2 target cells bearing HLA-Cw4 was detectable only in the presence of the tyrosine phosphatase inhibitor pervanadate. Therefore, these observations could be the result of using an artificial system and not an adequate or indeed relevant representation of *in vivo* events.

Following ITIM phosphorylation, the cytoplasmic protein tyrosine phosphatase Src homology protein 1 (SHP-1) is recruited to the inhibitory receptor cytoplasmic domain (63) (Figure 9). SHP-1 recruitment releases the catalytic site from auto-inhibition and so allows for the SHP-1-mediated dephosphorylation of substrates that is required for blocking activation signals (64). Perhaps this action of bringing inhibitory receptors in close proximity to activating receptors further serves the purpose of recruiting SHP-1 to the site where activation signals are transmitted and thus also to the

site at which a myriad of potential substrates could be present (36). The point at which SHP-1 blocks NK cell activating signals is only just starting to be elucidated (65). A KIR/SHP-1 chimera with a trapping mutation in the catalytic site selectively bound tyrosine-phosphorylated Vav1 in YTS cells that were incubated with target cells expressing KIR2DL1 ligand (65). In addition, the catalytic site of SHP-1 was required for Vav1 binding. Taken together these data suggest that the dephosphorylation of Vav1 by SHP-1 is a possible mechanism for inhibition by KIR. Vav1 has a number of functions and indeed, activating receptors employ various upstream pathways to stimulate Vav1. Therefore, SHP-1 regulation of Vav1 would enable inhibitory receptors to block signals from a number of different activating receptors regardless of which upstream pathways are involved. However, it is important to keep in mind that even though tyrosine phosphorylated Vav1 was the only molecule detected using the KIR/SHP-1 chimera, this does not preclude the existence of other SHP-1 substrates *in vivo*. Indeed molecules such as LAT and Syk have been identified as potential substrates of SHP-1 (57, 65, 66). In addition, results from a far-Western blot with a trapping mutant of SHP-1 suggest that SLP-76 is a substrate of SHP-1 (65, 67).

1.12 The immunological synapse

In lymphocytes, the intracellular signaling events required for activation of effector function emanate from a stable region of intercellular contact between an effector cell and target cell that I will herein refer to as the immunological synapse. The immunological synapse was first described for helper T cells (helper T cell immunological synapse) but has since been extended to cytotoxic T cells (cytotoxic T

cell immunological synapse) and NK cells (NK cell immunological synapse). Notably, the seminal studies of T cell immunological synapses provided much of the basis for subsequent studies of the NK cell immunological synapse. The application of a multitude of imaging technologies has revealed that receptors and signaling proteins organize into distinct spatial domains known as supramolecular activation clusters (SMACs) during antigen-specific interactions (T cell immunological synapses) or target cell-specific interactions (NK cell immunological synapses) (68). SMACs can be further classified as the central SMAC (c-SMAC) that is surrounded by the peripheral SMAC (p-SMAC) (68).

1.13 The helper T cell immunological synapse

Formation of the helper T cell immunological synapse in living cells is a multi-stage process consisting of junction formation (Stage 1), MHC-peptide transport (Stage 2), and cluster stabilization (Stage3) (Figure 10) (69). During Stage 1, LFA-1 and talin are initially located in the c-SMAC while TCR/CD3 is located in the p-SMAC. Stage 1 is often referred to as the early or immature immunological synapse. During Stage 2, LFA-1 and talin are translocated to the p-SMAC and TCR/CD3 moves into the c-SMAC where they remain during Stage 3. Stage 3 is often referred to as the mature immunological synapse. PKC- θ is also present in the c-SMAC of the mature helper T cell immunological synapse (68).

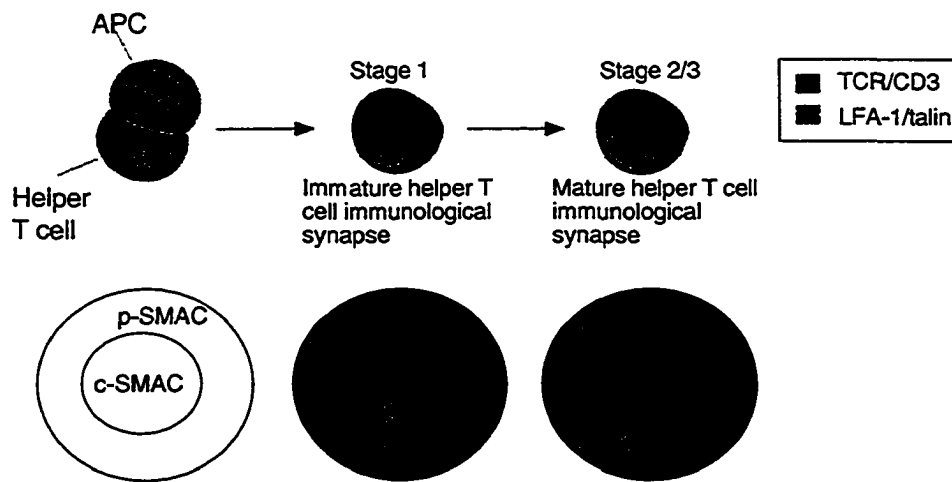


Figure 10: The helper T cell immunological synapse. Formation of the helper T cell immunological synapse in living cells is a multi-stage process consisting of junction formation (Stage 1), MHC-peptide transport (Stage 2), and cluster stabilization (Stage3). The application of a multitude of imaging technologies has revealed that receptors and signaling proteins organize into distinct spatial domains known as SMACs as a result of antigen-specific interactions (see Legend). During Stage 1, LFA-1 and talin are initially located in the c-SMAC while TCR/CD3 is located in the p-SMAC. Stage 1 is often referred to as the early or immature immunological synapse. During Stage 2, LFA-1 and talin are translocated to the p-SMAC and TCR/CD3 moves into the c-SMAC where they remain during Stage 3. Stage 3 is often referred to as the mature immunological synapse. PKC- θ is also present in the c-SMAC of the mature helper T cell immunological synapse. Adapted from Davis *et al.* 2004.

Early studies suggested that the function of the helper T cell immunological synapse was to enhance and sustain the signaling required for T cell proliferation (68, 69). However, it now appears that the initiation of TCR-mediated tyrosine kinase signaling occurs early and precedes the formation of the mature immunological synapse (70). Nevertheless, although the mature immunological synapse is not required for helper T cell activation, the mature synapse could instead be required to regulate T cell proliferation by providing a central platform for regulatory molecules with signal-balancing properties (71, 72). In keeping with this, the mature immunological synapse could be necessary for balancing TCR downregulation and endocytosis (70, 73). Another proposed function for the helper T cell immunological synapse is one of polarized secretion (74, 75).

Formation of the helper T cell immunological synapse requires the active transport of key proteins to a stable region of intercellular contact. Indeed, formation of the immunological synapse results from an active accumulation of surface molecules that is dependent on a directional change in the movement of the actin cytoskeleton that requires costimulation and myosin motor proteins (76, 77). Furthermore, intact and sustained actin dynamics are required for mature immunological synapse formation and for efficient T cell activation (78). The pathways linking TCR stimulation and actin dynamics with mature immunological synapse formation have yet to be fully defined. However, a recent study suggests that relaxation of the cytoskeleton via inactivation of Ezrin-radixin-moesin (ERM) proteins may contribute to increased tight conjugate formation between a T cell and an APC and that this in turn could contribute to mature immunological synapse formation (79).

1.14 The cytotoxic T cell immunological synapse

The cytotoxic T cell immunological synapse consists of a ring of adhesion proteins (namely CD11a, the α subunit of LFA-1) and talin surrounding an inner signaling molecule domain consisting of Lck, PKC θ , and CD3 ζ (Figure 11) (80). Therefore, the cytotoxic T cell immunological synapse also has a c-SMAC that is surrounded by a p-SMAC and is similar in structure to the helper T cell immunological synapse (68, 69). Strikingly, a distinct secretory domain is also present within the c-SMAC. This secretory domain consists of cytolytic granules and is devoid of TCR molecules. Furthermore, cytolytic granules are secreted at a cleft (or membrane bridge) that is formed by indentation of the target cell membrane. These observations suggested that the cytotoxic T cell immunological synapse could play a functional role in directed secretion of cytolytic granules. Interestingly, a recent report suggests that the cytotoxic T cell immunological synapse structure and signaling patterns changes according to the strength of TCR stimulation (81). Strong TCR stimulation resulted in mature (stimulatory) synapse formation that was accompanied by secretion of cytokines and proliferation, whereas weak TCR stimulation resulted in an immature (lytic) synapse formation that was accompanied by polarization of the tubulin cytoskeleton and perforin granules.

The cytotoxic T cell immunological synapse is much more transient in nature than the helper T cell immunological synapse. Indeed, the length of time required for contact with a target cell and for delivery of the lethal hit (polarization and release of cytotoxic granules) is in the order of minutes (72, 80). A final difference between the helper and

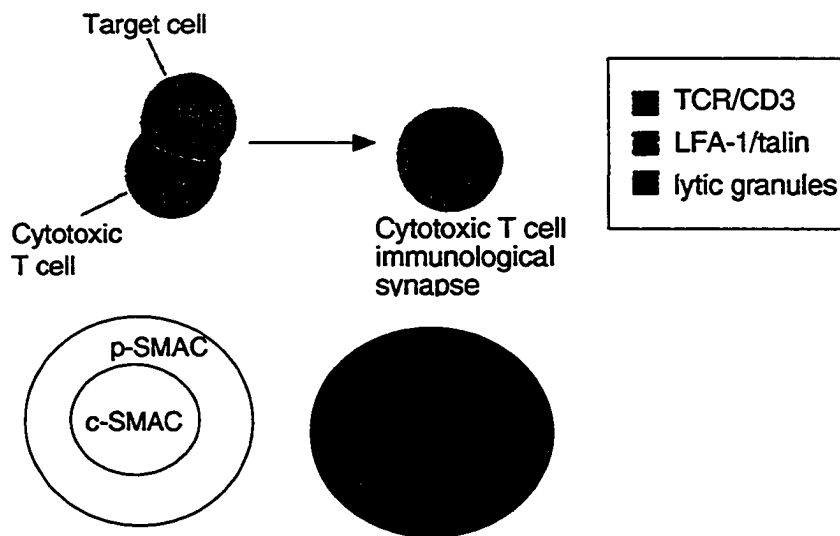


Figure 11: The cytotoxic T cell immunological synapse. The cytotoxic T cell immunological synapse consists of a ring of adhesion proteins (namely CD11a, the α subunit of LFA-1) and talin surrounding an inner signaling molecule domain consisting of Lck, PKC θ , and CD3 ζ (see Legend). Strikingly, a distinct secretory domain is also present within the c-SMAC. Adapted from Davis *et al.* 2004.

cytotoxic T cell immunological synapses is that cytotoxic T cells are able to form multiple synapses with several target cells (76, 82).

1.15 The NK cell immunological synapse

Two distinct NK cell immunological synapses are formed depending on whether the target cells are resistant (inhibitory NK cell immunological synapse) or susceptible (activating NK cell immunological synapse) to NK cell lysis (Figure 12). The inhibitory and activating NK cell immunological synapses differ in their molecular composition and structural organization. Polarization of the MTOC and lysosomes occurs at the activating NK cell immunological synapse, but does not occur after conjugate formation with resistant target cells (inhibitory NK cell immunological synapse) (83). Ezrin, CD43 and CD45 are excluded from the inhibitory NK cell immunological synapse and F-actin accumulates only at the activating NK cell immunological synapse (84). The activating NK cell immunological synapse is further characterized by the presence of WASP, CD2, and a multimolecular signaling complex (consisting of Src family kinases Lck and Fyn, Syk family kinases Syk and ZAP-70, and the adaptor molecule SLP-76) (10, 85) (83). Interestingly, while certain signaling molecules and cell-surface receptors are recruited to both the activating and inhibitory NK cell immunological synapses, their enrichment is maintained only at the activating NK cell immunological synapse. For instance, although nascent lipid rafts appear in the c-SMAC of interfaces with susceptible and resistant target cells, rafts continue to increase in size at the activating NK cell immunological synapse but are quickly dissolved at the inhibitory NK cell immunological synapse (86). Similarly, although LFA-1 is quickly recruited to the p-SMAC of interfaces with

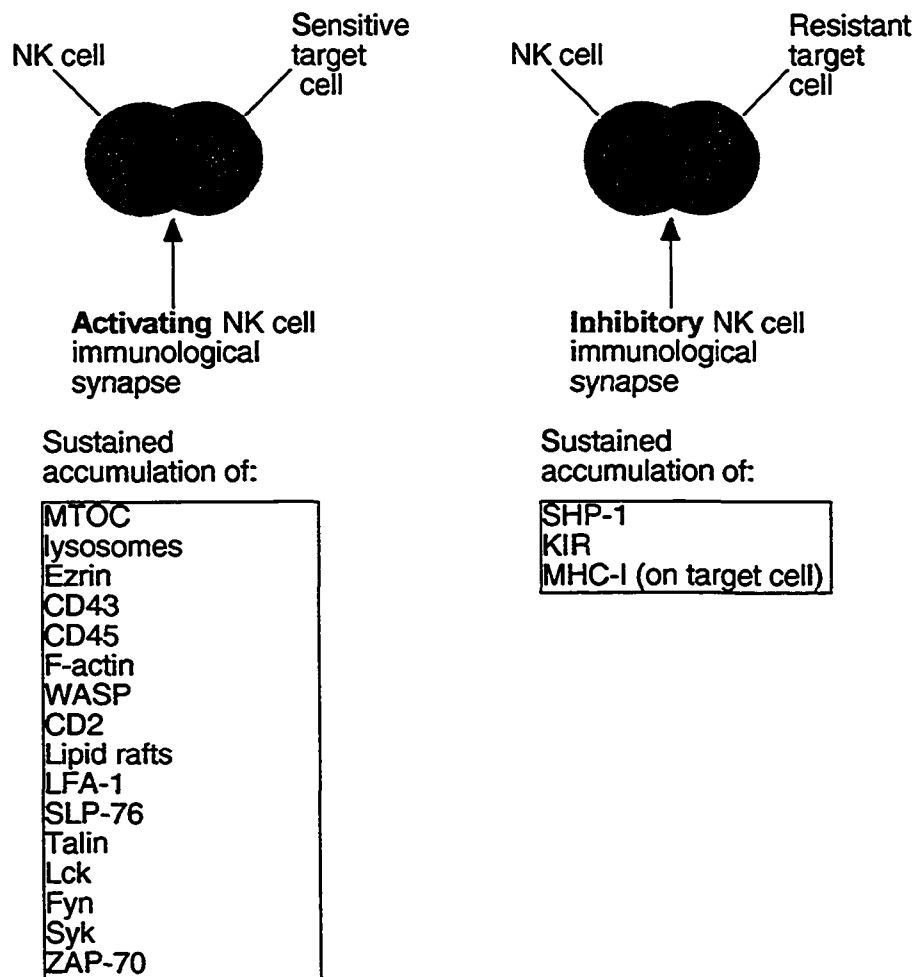


Figure 12: Sustained accumulation of signaling molecules and cell-surface receptors at the inhibitory and activating NK cell immunological synapses. Two distinct NK cell immunological synapses are formed depending on whether the target cells are resistant (inhibitory NK cell immunological synapse) or susceptible (activating NK cell immunological synapse) to NK cell lysis. Studies of the molecular composition and structural organization of both NK cell immunological synapses have revealed that each is characterized by the sustained accumulation of a number of cell surface receptors, adhesion molecules, cytoskeletal components, and signaling molecules (see Legend). Adapted from Davis *et al.* 2004.

susceptible and resistant target cells, LFA-1 recruitment is increased in magnitude only at the activating NK cell immunological synapse (86). In addition, enrichment of talin, Lck, and SHP-1 occurs at both synapses but is maintained only at the activating NK cell immunological synapse. Of note, although SHP-1 accumulates at both the synapses as early as 1 minute after target cell addition, SHP-1 segregates in the c-SMAC of the inhibitory NK cell immunological synapse, but not in the p-SMAC of the activating NK cell immunological synapse (87) (Figure 13). Taken together, these results suggest that although early activation signals occur following interaction with either a resistant or a susceptible target cell, at the inhibitory NK cell immunological synapse these activation signals are rapidly interrupted such that progression of the NK cell cytotoxic response is blocked (86). In addition, it is possible that the removal of SHP-1 is what allows for the activation signals to propagate at the activating NK cell immunological synapse (86).

1.16 KIR at the NK cell immunological synapse

The distribution of inhibitory KIR and its ligand (MHC-I molecules) at the human NK cell immunological synapse has been studied directly using cell lines stably expressing enhanced green fluorescent protein-tagged KIR (KIR-EGFP) (88). Cell lines stably expressing enhanced green fluorescent protein-tagged HLA-C molecules [HLA-C-EGFP] have also been used to indirectly study KIR distribution at the NK cell immunological synapse (84, 89-91). A recent report has also examined the inhibitory NK cell immunological synapse using NK clones retrovirally transduced with EGFP-tagged KIR (86). These studies have demonstrated that both KIR and HLA-C exhibit ligand-

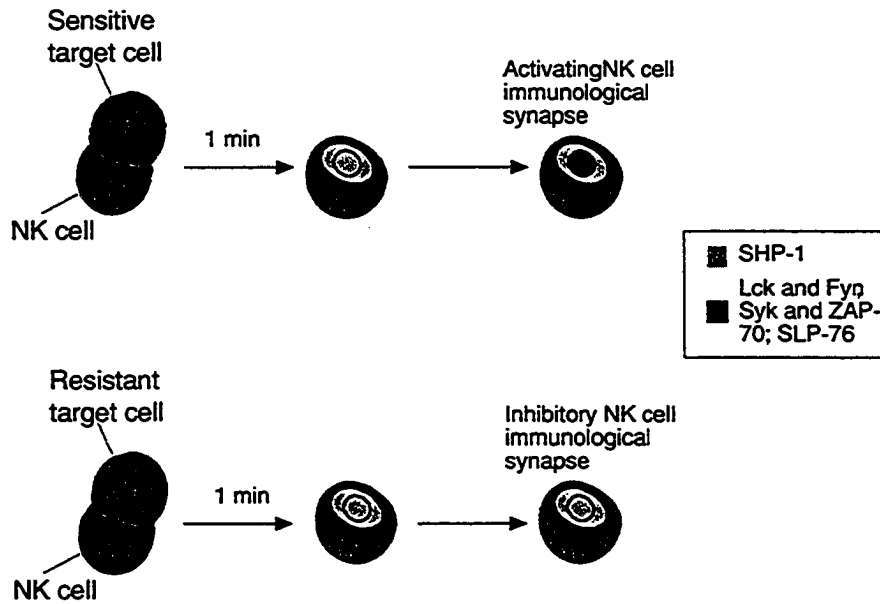


Figure 13: Activating signals are rapidly disrupted at the inhibitory NK cell immunological synapse. Although early activation signals occur following interaction with either a resistant or a susceptible target cell, at the inhibitory NK cell immunological synapse these activation signals are rapidly interrupted such that progression of the NK cell cytotoxic response is blocked. As a result, while certain signaling molecules and cell-surface receptors are recruited to both the activating and inhibitory NK cell immunological synapses, their enrichment is maintained only at the activating NK cell immunological synapse (see Legend). Adapted from Davis *et al.* 2004.

induced enrichment (clustering) at the inhibitory NK cell immunological synapse. We have shown that formation of large areas of KIR enrichment is not essential for inhibition of target cell killing but is correlated with signal strength (88). Studies performed by other laboratories have shown that HLA-C still clusters at the inhibitory NK cell immunological synapse in the presence of drugs that disrupt actin polymerization and independently of the distal portion of the cytoplasmic tail of KIR (90, 91). Zinc is also required for the inhibitory function of KIR2DL1 (but not ligand binding) and for clustering of KIR2DL1 at the inhibitory NK cell immunological synapse (44, 45, 90).

1.17 Investigating the processes that regulate KIR clustering

Given that KIR controls activating receptors in NK cells, and that the activating receptors have the potential to cluster very rapidly through active processes, it is of particular importance to understand how the movement of KIR is regulated. Therefore our aim has been to dissect the process of KIR clustering. To this end we have used confocal laser scanning microscopy to study the distribution of KIR-EGFP at the activating and the inhibitory NK cell immunological synapse. We have investigated the processes that regulate KIR clustering by using a mutant KIR that lacks a cytoplasmic portion, by inhibiting actin polymerization, and by blocking LFA-1-mediated adhesion. We have found that the actin cytoskeleton plays a role in the stability of conjugates with either sensitive or resistant target cells and, importantly, regulates the rate at which KIR clusters. Our results also implicate the cytoplasmic tail of KIR in facilitating efficient clustering. Based on these observations we propose a model for KIR clustering at the inhibitory NK cell immune synapse. There are many remaining unanswered questions

regarding the regulation of KIR clustering at the inhibitory NK cell immune synapse and thus we have outlined strategies for further investigation into the factors regulating KIR enrichment at the inhibitory NK cell immunological synapse.

CHAPTER II

Materials and Methods

2.1 Cell Lines

The cell lines 221-Cw3 and 221-Cw4 were maintained in Iscoves medium containing 10 % FBS, 2 mM L-glutamine (Invitrogen) and 0.5 mg/ml geneticin (Invitrogen) (Table 1) (92). The cell line 221-Cw6-EGFP was maintained in Iscoves medium containing 10 % FBS, 2 mM L-glutamine (Invitrogen), 50 μ M 2-mercaptoethanol, and 0.5 mg/ml geneticin (Invitrogen) (90). The YTS/KIR2DL1, YTS/KIR2DL1-GFP, and YTS/KIR2DL1(K346*) cell lines were maintained in Iscoves medium containing 15% FBS (Hyclone), 50 μ M 2-mercaptoethanol, 2 mM L-glutamine, and 1.0 μ g/ml puromycin (Table 2) (88, 91, 93). The cell line NK92 was purchased from ATCC (CRL-2407) and maintained in Iscoves medium containing 50 % Myelocult (Stem Cell Technologies, Vancouver, Canada), 7.5 % FBS (Hyclone), 25 μ M 2-mercaptoethanol, and 1 mM L-glutamine and supplemented with 100 U/ml of human recombinant IL-2 (Table 3). The NK92/KIR2DL1-GFP cell line was maintained in NK92 medium supplemented with 100 U/ml recombinant IL-2 and 0.5 mg/ml of geneticin (94). The NK92/KIR2DL1 TR-GFP cell line was made by stable transfection of NK92 using the expression vector pBSR α EN (kindly provided by Dr. Kevin Kane, University of Alberta) (94, 95). In particular, NK92 cells (5×10^5) were incubated with 5 μ g of plasmid for 30 minutes at room temperature in a 0.4 cm Gene Pulser Cuvette (BioRad Laboratories) and then pulsed at 0.25 V, 960 μ F using a Gene Pulser Apparatus (BioRad Laboratories). The cells were allowed to recover for 10 minutes at room

Table 1. Properties of the target cell lines used to investigate the processes that regulate KIR2DL1 clustering in YTS and NK92, two human NK-like cell lines.

Name	Description	Notes ^a
721.221	MHC-I deficient EBV transformed B lymphoblastoid cell line	Parental target cell line; lacks KIR2DL1 ligand; <i>sensitive</i> to cytolysis by all of our human NK cell lines regardless of KIR expression
221-Cw3	721.221 transfectant expressing the non-cognate MHC-I protein HLA-Cw3	Lacks KIR2DL1 ligand; <i>sensitive</i> to cytolysis by our human NK cell lines regardless of KIR2DL1 expression
221-Cw3-GFP	721.221 transfectant expressing the non-cognate MHC-I protein HLA-Cw3 with EGFP attached to the C terminus	Lacks KIR2DL1 ligand; <i>sensitive</i> to cytolysis by our human NK cell lines regardless of KIR2DL1 expression
221-Cw4	721.221 transfectant expressing the KIR2DL1 ligand HLA-Cw4	Expresses KIR2DL1 ligand; <i>resistant</i> to cytolysis by our human NK cell lines expressing full-length KIR2DL1
221-Cw4-GFP	721.221 transfectant expressing the KIR2DL1 ligand HLA-Cw4 with EGFP attached to the C terminus	Expresses KIR2DL1 ligand; <i>resistant</i> to cytolysis by our human NK cell lines expressing full-length KIR2DL1
221-Cw6-GFP	721.221 transfectant expressing the KIR2DL1 ligand HLA-Cw6 with EGFP attached to the C terminus	Expressed KIR2DL1 ligand; <i>resistant</i> to cytolysis by our human NK cell lines expressing full-length KIR2DL1
221-Cw15	721.221 transfectant expressing the KIR2DL1 ligand HLA-Cw15	Expresses KIR2DL1 ligand; <i>resistant</i> to cytolysis by our human NK cell lines expressing full-length KIR2DL1 and truncated KIR2DL1

^a Please note that, with the exception of Figure 23 and the Appendix, the 221-Cw3 and 221-Cw4 target cells were used to generate the data presented in this thesis. Target cells mentioned in the text as either data not shown or in reference to studies by other laboratories have also been included in this table.

Table 2. Properties of the immortalized YTS cell lines used to study the processes that regulate KIR2DL1 clustering. Retroviral transduction was used to generate stable lines of YTS.

Name	Description	Notes
YTS	Non-Hodgkin's lymphoma-derived human NK-like cell line; KIR-deficient; IL-2 independent; CD94/NKG2A ⁻ , ILT2 ⁻	Parental NK cell line; lyses MHC-I deficient 721.221 target cells, 721.221 target cells expressing KIR2DL1 ligand, and 721.221 target cells expressing non-cognate MHC-I protein; cytolysis is CD28 and LFA-1 dependent
YTS/KIR2DL1	Stable line of YTS expressing full-length KIR2DL1	Selectively inhibited from killing 721.221 target cells expressing KIR2DL1 ligand
YTS/KIR2DL1-GFP	Stable line of YTS expressing full-length KIR2DL1 with EGFP attached to the C terminus	Selectively inhibited from killing 721.221 target cells expressing KIR2DL1 ligand
YTS/KIR2DL1-GFP/PPSS	Stable line of YTS expressing full-length KIR2DL1 with EGFP attached to the C terminus in which two proline (P) residues between the ITIMs have been mutated to serine residues (S)	Selectively inhibited from killing 721.221 target cells expressing KIR2DL1 ligand
KIR2DL1-GFP/Y2F	Stable line of YTS expressing full-length KIR2DL1 with EGFP attached to the C terminus in which both tyrosine (Y) residues in the ITIMs have been mutated to phenylalanine (F) residues	Lyses MHC-I deficient 721.221 target cells, 721.221 target cells expressing KIR2DL1 ligand, and 721.221 target cells expressing non-cognate MHC-I protein
YTS/KIR2DL1(K346*)	Stable line of YTS expressing KIR2DL1 truncated at residue 246	Lyses MHC-I deficient 721.221 target cells, 721.221 target cells expressing KIR2DL1 ligand, and 721.221 target cells expressing non-cognate MHC-I protein

Table 3. Properties of the immortalized NK92 cell lines used to study the processes that regulate KIR2DL1 clustering. An optimized electroporation protocol was used to generate stable lines of NK92.

Name	Description	Notes
NK92	Non-Hodgkin's lymphoma-derived human NK-like cell line; KIR-deficient; IL-2 dependent, CD94/NKG2A ^{low} , ILT2 ⁺	Parental NK cell line; lyses MHC-I deficient 721.221 target cells, 721.221 target cells expressing KIR2DL1 ligand, and 721.221 target cells expressing non-cognate MHC-I protein
NK92/KIR2DL1-GFP	Stable line of NK92 expressing full-length KIR2DL1 with EGFP attached to the C terminus	Selectively inhibited from killing 721.221 target cells expressing KIR2DL1 ligand
NK92/KIR2DL1 TR-GFP	Stable line of NK92 expressing KIR2DL1 truncated at residue 276 with EGFP attached to the C terminus	Lyses MHC-I deficient 721.221 target cells and 721.221 target cells expressing non-cognate MHC-I protein; inhibited from killing 721.221 target cells expressing high levels of KIR2DL1 ligand

temperature and then gently returned to a flask containing NK92 culture medium supplemented with human recombinant IL-2. Selection was initiated 48 hours later using 1 mg/ml geneticin. Drug resistant lines were propagated, screened for expression by flow cytometry, and then subcloned using limited dilution in order to establish lines with stable levels of expression. The NK92/KIR2DL1 TR-GFP subclone selected for further analysis was maintained in NK92 medium supplemented with 100 U/ml recombinant IL-2 and 0.5 mg/ml of geneticin.

2.2 Antibodies and Reagents

The monoclonal antibody (mAb) EB6 (IgG1) specific for KIR2DL1 that was used to monitor cell surface expression was purchased from Beckman Coulter Immunotech (Mississauga, Canada). The HP-3E4 anti-KIR2DL1 ascites (IgM) that was used to block binding was generated from a hybridoma that was a kind gift from M. Lopez-Botet (Hospital de la Princesa, Universidad Autonoma de Madrid, Spain) (96). The antibody TS1/22.1.1.13 (IgG1) for activated LFA-1 was purified from HB202 (ATCC) culture supernatants by protein A sepharose, filter sterilized and stored in PBS. The control antibody MOPC-21 (IgG1) was purchased from Sigma-Aldrich. PE-conjugated goat anti-mouse was purchased from Cedarlane (Hornby, Canada). Human recombinant IL-2 (TECINTM) was obtained from the Biological Resources Branch of the Division of Cancer Treatment and Diagnosis located at NCI-Frederick Cancer Research and Development Center in Frederick, Maryland. Sodium azide (azide) was purchased from EMD Chemicals Inc. (Gibbstown, NJ) and dissolved in water. PP2 (4-Amino-5-(4-chlorophenyl)-7-(*t*-butyl)pyrazolo(3,4-*d*)pyrimidine was purchased from Calbiochem

(San Diego, CA) and dissolved in dimethyl sulfoxide (DMSO) purchased from Caledon Laboratories Limited (Georgetown, Canada). Cytochalasin D was purchased from Calbiochem (San Diego, CA) and dissolved in DMSO purchased from Caledon Laboratories Limited (Georgetown, Canada).

2.3 Immunofluorescence (cell surface) Staining

Cells (1×10^5 to 5×10^5) were washed in approximately 3 mL of phosphate buffered saline (PBS) containing 2 % FBS (FACs wash buffer) in a 5 mL polystyrene round-bottom tube (VWR International). After decanting to the last drop, cells were resuspended by raking the tube 3 times over a test tube rack. Cells were then incubated with 10 $\mu\text{g}/\text{mL}$ primary antibody for 30 to 60 minutes at 4°C. Following this incubation, cells were washed with 3 mL FACs wash buffer, resuspended by raking, and then incubated with 2 μL of PE-conjugated goat anti-mouse (secondary antibody) for 15 to 30 minutes at 4°C. Cells were then washed with 3 mL FACs wash buffer and resuspended in 300 μL fresh formalin (1:20 dilution of paraformaldehyde in PBS). Flow cytometric analysis was performed using a FACscan (Becton-Dickson). Intensity of staining was compared to background levels obtained when cells (1×10^5 to 5×10^5) were stained with 2 μL of secondary antibody alone.

2.4 Cytolysis Assay

Target cells were labeled with $\text{Na}^{51}\text{CrO}_4$ (PerkinElmer Life and Analytical Sciences, Woodbridge, Canada) for 1 hour at 37°C, 5 % CO_2 and then washed 3 times in

10 mL of Iscoves medium containing 5 % FBS and 2 mM L-glutamine (CTL medium) (spin at 290 x g for 4 minutes). Effector cells (100 μ L) were then incubated with 2.5×10^3 51 Cr-labeled target cells (100 μ L) at various effector:target (E:T) ratios in triplicate for 4 h at 37°C, 5 % CO₂ in V-bottom microtiter plates. After incubation, 50 μ L of top supernatant was transferred to 150 μ L Wallac Optiphase Supermix scintillation cocktail in a 96 well polyethylene terephthalate (PET) sample plate that was then shaken at 750 rpm for approximately 1 hour. Samples were counted using a MicroBeta TriLux liquid scintillation counter (PerkinElmer, Wellesley, MA). Alternatively, target cells were labeled with Delfia[®] bis (acetoxymethyl) 2,2':6',2"- terpyridine- 6,6"- dicarboxylate (BADTA) reagent for 30 minutes at 37°C, 5 % CO₂ and then washed 3 times in 10 mL CTL medium (spin at 1170 rpm for 4 minutes). Effector cells (100 μ L) were then incubated with 3×10^3 BADTA-labeled target cells (100 μ L) at various E:T ratios for 2 h at 37°C, 5% CO₂ in V-bottom microtiter plates. After incubation, 20 μ L of supernatant was transferred to 200 μ L Europium Atomic Absorption Standard Solution (Sigma-Aldrich) in a mirror flat bottom plate that was then shaken on vortex at setting 2 for 10 minutes. Samples were measured by time-resolved fluorescence using a Wallac 1420 VICTOR² plate reader (PerkinElmer, Wellesley, MA). For both assays, percent specific lysis was determined as (mean experimental release – mean spontaneous release)/(mean maximum release – mean spontaneous release) x 100. For experiments with cytochalasin D, PP2 and azide, effector cells were incubated for 30 minutes at 37°C, 5% CO₂ with twice the desired final concentration of drug prior to dilution with the addition of target cells without drug. Assays were done three times unless otherwise indicated.

2.5 Two-Color Flow Cytometry Conjugate Assay

Tight conjugate formation was determined using a two-color flow cytometry assay (23, 94). Effector cells (6×10^6 to 10×10^6 cells in 0.4 mL Diluent C) were stained with PKH67 green fluorescent cell linker ($10 \mu\text{M}$ to $20 \mu\text{M}$ in 0.4 mL Diluent C) (Sigma-Aldrich) for 5 minutes at room temperature. Target cells (6×10^6 to 10×10^6 cells in 0.4 mL Diluent C) were stained with PKH26 red fluorescent cell linker ($10 \mu\text{M}$ to $20 \mu\text{M}$ in 0.4 mL Diluent C) (Sigma-Aldrich) for 5 minutes at room temperature. The labeling reactions were stopped by addition of 2 mL of serum (FBS). The cells were washed twice in 10 mL CTL medium (spin at $290 \times g$ for 4 minutes) and then rested in 10 mL CTL medium for at least 1 hour at $37^\circ\text{C}/5\% \text{CO}_2$. PKH67-labeled effector cells were resuspended at a final concentration 1×10^6 cells/mL and PKH26-labeled target cells were resuspended at a final concentration 2×10^6 cells/mL. 100 μL of effector cells and target cells were combined in a 5 mL polystyrene round-bottom tubes that were spun at 800 rpm for 3 minutes and then placed in a 37°C water bath for various time points. At the end of each time point, samples were subjected to a high-speed vortex for 3 seconds and then fixed with 300 μL ice cold 4% paraformaldehyde solution. A FACscan was promptly used to generate a FL-1 (green) versus FL-2 (red) dot plot for each sample. The red/green double positive cell population in the upper right hand quadrant of the FL-1 versus FL-2 plot was considered to be representative of any heteroconjugates formed between effector cells and target cells. Results were expressed as percentage of effector cells (green) that formed heteroconjugates with target cells (red) as calculated by the ratio of double positive events (red/green) to total effector (green) events. In other words,

percent conjugate formation was determined as (two-color events)/(total effector events) x 100. For the NK92 experiments with cytochalasin D, effector cells were pre-incubated for 30 minutes at 37°C, 5 % CO₂ in the presence of 10 μM cytochalasin D or DMSO alone (no drug) prior to the addition of target cell suspensions containing either 10 μM cytochalasin D or DMSO. For the YTS experiments with cytochalasin D, PP2 or azide, effector cells were pre-incubated for 30 minutes at 37°C, 5 % CO₂ with twice the desired final concentration of drug prior to dilution with the addition of target cells without drug. For the YTS experiments with anti-LFA-1, effector cells were pre-incubated for 5 minutes at room temperature with 10 μg/ml of anti-LFA-1 or MOPC-21 (control IgG1). In order to maintain the correct final antibody concentrations, antibody was also added to the target cells just prior to cell mixing. Assays were done three times unless otherwise indicated.

2.6 Confocal Imaging of Living Cells

Samples were prepared by adding target cells to effector cells and then subjecting the cell mixture to an 800 x g spin for 3 to 4 minutes. For the NK92 experiments, 2×10^4 NK92/KIR2DL1-GFP cells or NK92/KIR2DL1 TR-GFP cells were mixed with 2×10^4 target cells. For the YTS experiments, 4×10^4 YTS/KIR2DL1-GFP cells were mixed with 6×10^4 target cells. A 200 μL aliquot of the cell mixture (including the cell pellet) was then gently transferred onto a 10 x 10 mm cover slip (95) glued over the top of a 14 mm hole drilled into a 35 mm x 10 mm culture dish (Corning). The cover slips were pre-coated with poly-L-lysine (1:5 dilution of a 0.1 % w/v stock solution in sterile water) (Sigma). Optical sections were captured at 0.5 μm intervals in the Z-plane using a laser

scanning confocal microscope (LSM510, Zeiss), a 488 nm Argon laser to excite EGFP, and a temperature-controlled stage. The optimum temperature for maximal KIR clustering was determined to be 37°C for YTS cells and 31°C for NK92 cells. All images were collected at an 8-bit intensity resolution using a 63 x 1.4 oil (differential interference contrast) DIC lens with a pinhole of 1 Airy U. For each experiment, detector sensitivities were set to minimize saturation of detectors while still enabling detection of EGFP-positive cells. All of the confocal images were collected 7 to 30 minutes after cell mixing and centrifugation unless otherwise indicated. Drug and antibody treatments were performed essentially as described for the conjugate assays except that KIR2DL1-GFP clustering was also examined in the presence of HP-3E4 anti-KIR2DL1 ascites (1 μ L ascites added per 200 μ L of sample). As was the case with anti-LFA-1 and MOPC-21, effector cells were pre-incubated for 5 minutes at room temperature with HP3E4 and, in order to maintain the correct final antibody concentrations, it was also added to the target cells prior to cell mixing.

2.7 Determining the Frequency of KIR-EGFP Clustering

Confocal images were processed using the Zeiss LSM Image Browser software. All images collected for a given data set were included in subsequent calculations. Interfaces were counted for conjugates of an EGFP fluorescent effector cell in tight contact with a target cell. Interfaces were scored positive for clustering if enrichment of the EGFP signal was visible in one or more of the sections captured for the conjugate at 0.5 μ m intervals. The percentage clustering (% with cluster) value was determined as (number of interfaces that exhibited clustering)/(total number of interfaces) x 100.

2.8 Generating Snapshots of the Effector:Target Interface

To produce images of the interface regions, snapshots of each interface region were generated using the Imaris® 3-D image software package (Bitplane, Saint Paul, MN). Briefly, the Full 3D Viewer feature of Imaris® was used to rotate a volume rendering of each conjugate at a zoom of 1X. Each conjugate was rotated in order to generate a view of the interface from the perspective of the target cell. A maximum intensity projection (MIP) was subsequently generated for each rotated conjugate and an image of each interface region was collected and then saved as a snapshot.

2.9 Quantifying KIR-EGFP Enrichment at the Effector:Target Interface

The Imaris® 3-D image software package (Bitplane) was also used to quantify the amount of KIR-EGFP enrichment at each interface region. Briefly, the Surpass Viewer feature was used to generate a geometric object for each region of KIR-EGFP enrichment from a volume image of each conjugate regardless of whether KIR-EGFP enrichment was observed. The Isosurface component was then used to compute a surface enclosing all voxels (arbitrary volume unit) with intensities higher than a user-specified threshold value of 120 in the contact region, which corresponds to an approximately 4-fold increase over normal cell surface expression. The values included in each isosurface were then used to calculate a total intensity sum value for each region of KIR-EGFP enrichment.

2.10 Statistics

All statistical analyses were performed using Microsoft Excel[®]98. The total intensity sum values obtained using the Imaris[®] 3-D image software package were used to calculate mean (M) total intensity sum values as well as standard deviation (SD) values for KIR2DL1-GFP and KIR2DL1 TR-GFP. The raw data for KIR2DL1-GFP and KIR2DL1 TR-GFP is shown in Appendix 1. A pooled variance independent *t*-test was used to determine that the mean total intensity sum of KIR2DL1-GFP and KIR2DL1 TR-GFP were statistically different ($p < 0.05$).

CHAPTER III

Results - Part A

3.1 KIR2DL1 chimeras with EGFP

Our lab had previously generated EGFP chimeras with KIR2DL1 in order to study the redistribution of KIR in living cells. These chimeras included EGFP fused to the C terminus of the full-length cytoplasmic tail of KIR2DL1 (KIR2DL1-GFP) and EGFP fused to the C terminus of KIR2DL1 truncated upstream of the membrane proximal ITIM at aspartic acid residue 276 (D276) (KIR2DL1 TR-GFP) (Figure 14) (88, 94). Retroviral transduction had been used to generate stable lines of YTS, a non-Hodgkin's lymphoma-derived human NK-like cell line, expressing KIR2DL1-GFP (YTS/KIR2DL1-GFP) or KIR2DL1 TR-GFP (YTS/KIR2DL1 TR-GFP) (88) (P. Borszcz and D. Burshtyn, unpublished results).

3.2 Generating NK92/KIR2DL1 TR-GFP

Although YTS is considered a valid model, cytolysis by this immortalized line has been shown to rely on the costimulatory molecule CD28, which has not ever been reported for either primary NK cells or other NK-like cell lines (23). We therefore sought to further characterize our KIR-EGFP chimeras in another non-Hodgkin's lymphoma-derived and KIR-deficient NK-like cell line known as NK92 (97). Although

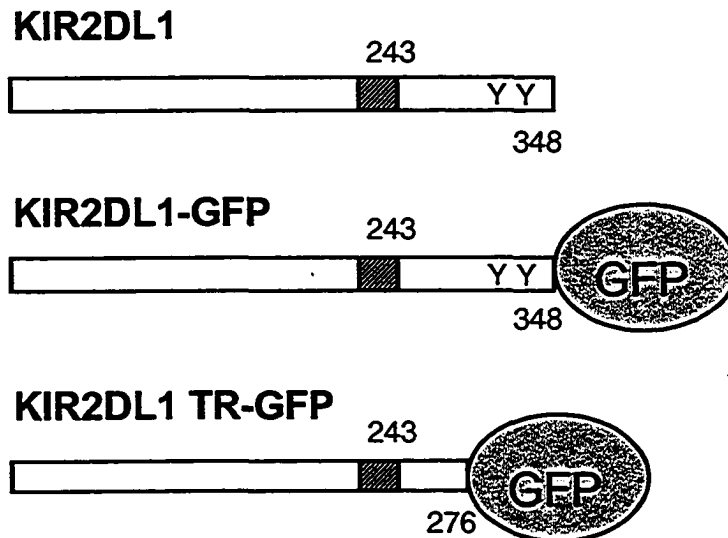


Figure 14: KIR2DL1 chimeras with EGFP. Schematic representation of the non-EGFP-tagged full-length receptor (KIR2DL1) and KIR-EGFP chimera constructs employed throughout this study. Chimeras include EGFP fused to the C terminus of the full-length cytoplasmic tail of KIR2DL1 (KIR2DL1-GFP) and EGFP fused to the C terminus of KIR2DL1 truncated at aspartic acid residue 276 (D276) upstream of the membrane proximal ITIM (KIR2DL1 TR-GFP). The cross-hatched box represents the transmembrane region of KIR2DL1 and Y indicates the location of the ITIMs. The number directly above each construct denotes the final amino acid residue of the transmembrane domain (243). The number directly below each construct denotes the amino acid residue at which either full-length (348) or truncated (276) KIR2DL1 coding sequence was fused to EGFP coding sequence.

our lab had previously generated a stable line of NK92 expressing KIR2DL1-GFP (NK92/KIR2DL1-GFP), a stable line of NK92 expressing the truncated KIR-EGFP chimera had yet to be established. As a result, our first priority was to stably transfect NK92 with KIR2DL1 TR-GFP using the expression vector pBSR α EN (94, 95). The rationale for using this particular vector was that pBSR α EN contains the internal ribosome entry site (IRES) of the encephalomyocarditis virus (ECMV), which permits translation of a gene of interest and a selection marker from the same messenger RNA. The IRES in pBSR α EN therefore increased the likelihood that selection marker resistant NK92 were also expressing KIR2DL1 TR-GFP and thus enhancing transfection. An optimized electroporation protocol was used to transfect NK92 with KIR2DL1 TR-GFP and selection was initiated 48 hours after pulsing the cells (see Materials and Methods for details). Drug resistant lines were propagated, screened for expression by flow cytometry, and then sub-cloned using limited dilution in order to establish lines with stable levels of expression. The cell surface expression profile of the NK92/KIR2DL1 TR-GFP sub-clone selected for further analysis is shown in Figure 15. Figure 15 also shows the cell surface expression profile of the previously generated NK92/KIR2DL1-GFP sub-clone that had yet to be functionally characterized. Although both sub-clones exhibited strong EB6 anti-KIR2DL1 staining, the level of expression of KIR2DL1 TR-GFP was lower than that of the full-length receptor. Nevertheless, given the degree of difficulty and length of time involved in generating stable lines in NK92 and our desire to complement our experiments in YTS in a timely manner, we opted to continue with our functional studies using these two sub-clones.

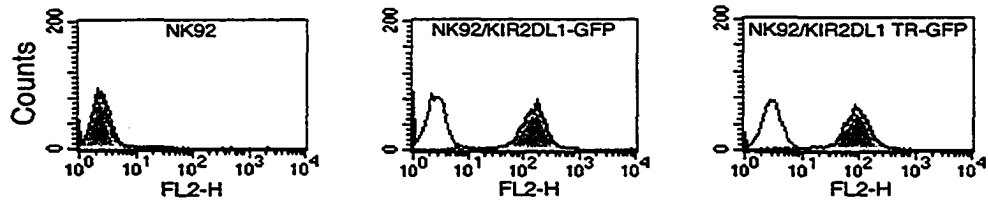


Figure 15: Cell surface expression profiles of NK92/KIR2DL1-GFP and NK92/KIR2DL1 TR-GFP. The human NK-like cell line NK92 was transfected with KIR2DL1-GFP or KIR2DL1 TR-GFP generating NK92/KIR2DL1-GFP and NK92/KIR2DL1 TR-GFP, respectively. The KIR-EGFP cell surface expression profiles of the two sub-clones selected for further analysis are shown, as is the profile of the parental NK92 cell line. Expression profiles were determined using anti-KIR2DL1 mAb EB6 and PE-conjugated goat anti-mouse (shaded histograms) or PE-conjugated goat anti-mouse alone (empty histograms). These expression levels are similar to EB6 anti-KIR staining on primary human NK cells (D.Burshtyn, unpublished observations).

3.3 KIR2DL1-GFP and not KIR2DL1 TR-GFP is capable of mediating inhibition

To assess the function of our KIR-EGFP chimeras in NK92 we performed cytotoxicity assays with 721.221 target cells expressing either the KIR2DL1 ligand HLA-Cw4 (221-Cw4) or the non-cognate MHC-I protein HLA-Cw3 (221-Cw3) (Figure 16) (92). The parental 721.221 target cell line is a MHC class I-deficient Epstein Barr virus (EBV) transformed B lymphoblastoid cell line that is susceptible to NK cell-mediated lysis, including NK92-mediated lysis (S. Kirwan and D. Burshtyn, unpublished results). The 221-Cw4 target cells are considered resistant to cytotoxicity by virtue of the fact that they express KIR2DL1 ligand and can therefore engage this inhibitory receptor. Conversely, the 221-Cw3 target cells are considered sensitive to cytotoxicity since the non-cognate MHC-I protein that they express is unable to engage KIR2DL1. Expression of KIR2DL1-GFP in NK92 cells strongly inhibited cytotoxicity of the 221-Cw4 target cells (Figure 16). Consistent with previous studies in YTS, this result shows that the presence of EGFP at the cytoplasmic tail of KIR2DL1 did not abrogate the ability of this receptor to transduce an inhibitory signal upon contact with the resistant 221-Cw4 target cells (88). In addition, expression of the truncated receptor chimera KIR2DL1 TR-GFP in NK92 cells did not inhibit cytotoxicity of 221-Cw4 target cells. Of note, inhibition by the truncated receptor is seen when 221-Cw15 target cells, which express higher levels of MHC-I molecules, are used (S. Kirwan and D. Burshtyn, unpublished results). We have reason to believe that this inhibition is due to the presence of low levels of the ILT2 inhibitory receptor.

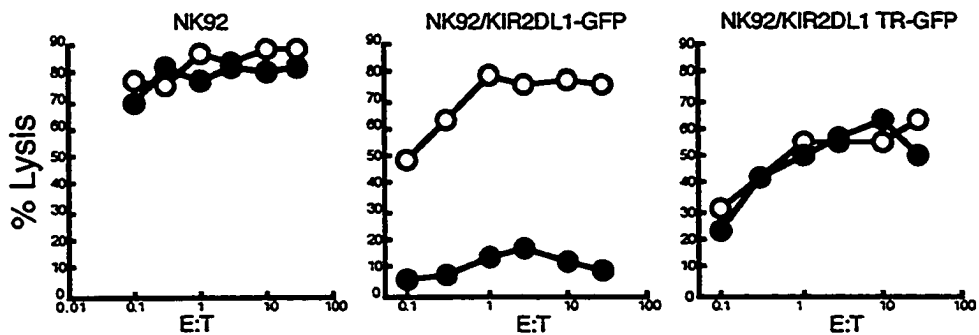


Figure 16: KIR2DL1-GFP inhibits NK92 cytotoxicity of 221-Cw4 target cells. Cytotoxicity of ^{51}Cr -labelled target cells was measured for NK92, NK92/KIR2DL1-GFP, and NK92/KIR2DL1 TR-GFP. The open symbols indicate cytotoxicity of 221-Cw3 target cells and the closed symbols indicate cytotoxicity of 221-Cw4 target cells. Percent specific cytotoxicity (% cytotoxicity) was determined as $(\text{mean experimental release} - \text{mean spontaneous release}) / (\text{mean maximum release} - \text{mean spontaneous release}) \times 100$.

3.4 KIR2DL1-GFP and KIR2DL1 TR-GFP exhibit ligand-induced clustering

To examine receptor enrichment at the immune synapse in living cells, we imaged NK92/KIR2DL1-GFP and NK92/KIR2DL1 TR-GFP cells conjugated with 221-Cw4 or 221-Cw3 target cells by confocal microscopy (see Materials and Methods for details) (94). Briefly, effector and target cells were subjected to a low speed spin and the cell pellet was then transferred to a small culture dish for imaging on a temperature-controlled stage. Differential interference contrast (DIC) and EGFP fluorescence images were then collected for NK92/KIR2DL1-GFP or NK92/KIR2DL1 TR-GFP conjugated with 221-Cw3 or 221-Cw4 target cells. Optical sections were captured at 0.5 μm intervals in the Z-plane using laser scanning confocal microscopy. Confocal images were collected 7 to 30 minutes after cell mixing by centrifugation. Representative DIC and EGFP fluorescence images of a single optical section for all possible effector and target cell combinations are shown in Figure 17. Both full-length and truncated KIR-EGFP chimeras exhibited clustering at the interface with 221-Cw4 target cells. Neither KIR2DL1-GFP nor KIR2DL1 TR-GFP clustered at the interface with 221-Cw3 target cells.

3.5 KIR2DL1 TR-GFP exhibits a defective clustering phenotype

Having established that KIR2DL1-GFP and KIR2DL1 TR-GFP exhibit ligand-induced clustering, we next determined the frequency of clustering for each construct at the inhibitory NK cell immune synapse (see Materials and Methods for details) (94). Briefly, interfaces were counted for heteroconjugates of an EGFP fluorescent effector cell

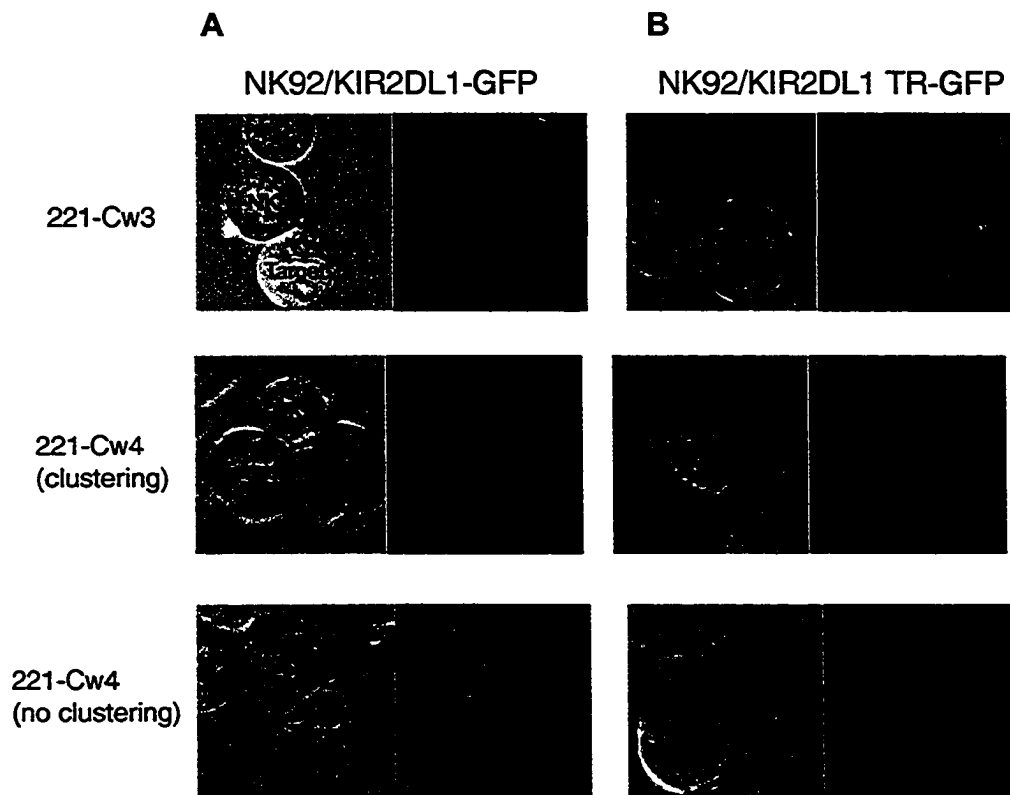


Figure 17: Ligand-induced KIR-EGFP recruitment to the NK cell immune synapse. Representative DIC and EGFP fluorescent images are shown for NK92/KIR2DL1-GFP (A) or NK92/KIR2DL1 TR-GFP (B) conjugated to 221-Cw3 target cells (*upper panels*) or 221-Cw4 target cells (*middle and lower panels*). Please note that the bottom panels show representative images of conjugates with 221-Cw4 target that did not exhibit KIR-EGFP enrichment at the inhibitory NK cell immune synapse. Confocal images (optical sections at captured at 0.5 μm intervals in the Z-plane) were captured 7-30 minutes after cell mixing using a temperature-controlled stage.

in tight contact with a target cell. These interfaces were scored positive for clustering if enrichment of the EGFP signal was visible in one or more of the optical sections captured for the conjugate at 0.5 μm intervals. The percentage clustering (% with cluster) value was then calculated as (number of interfaces that exhibited clustering)/(total number of interfaces) x 100. Of note, all images collected for a given data set were included in frequency of clustering calculations. The frequency of the truncated KIR2DL1 clustering at the inhibitory NK cell immune synapse was consistently less than half that of the full-length receptor chimera (Figure 18). The defect in truncated KIR-EGFP clustering is also apparent in the YTS human NK cell line (98) (Borszcz and Burshtyn, unpublished observations). We next considered the possibility that KIR2DL1 TR-GFP was able to cluster with comparable frequency to full-length receptor but did so at a reduced rate. To verify this notion we examined KIR2DL1 TR-GFP clustering at later time points after cell mixing by centrifugation. In particular, we examined KIR2DL1 TR-GFP clustering at 30 to 60 minutes and 60 to 90 minutes, both of which are outside the standard 7 to 30 minutes time window we had used up to this point (Figure 19). We found that KIR2DL1 TR-GFP clustering did not increase at later time points after cells mixing and indeed appeared to decrease slightly. Please note that although NK92/KIR2DL1 GFP clustering was examined in both of the independent experiments as a quick check to ensure that the experimental conditions were favorable for clustering, for one of the experiments we did not collect sufficient data to calculate the frequency of full-length receptor clustering. For the experiment in which sufficient data was collected, 13 of 30 interfaces exhibited KIR2DL1-GFP clustering, thereby resulting in a % with cluster value of 43%. In one of the two experiments we also examined KIR2DL1 TR-GFP clustering 90-120 minutes

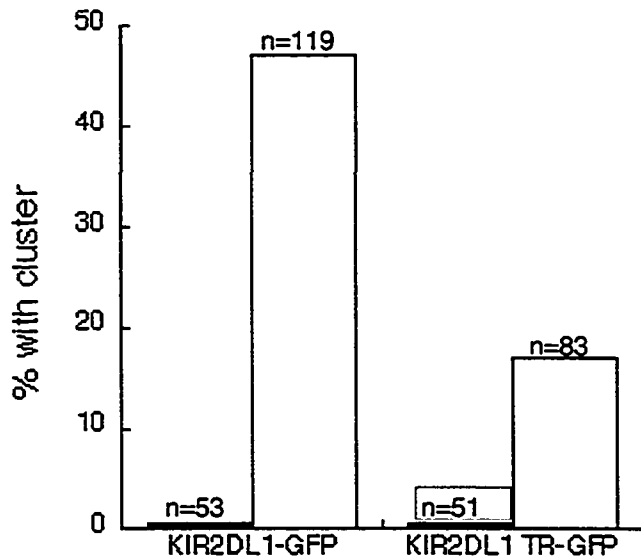


Figure 18: KIR2DL1 TR-EGFP is impaired in its ability to cluster. Bar graph showing the % of interfaces that scored positive for clustering following mixing with 221-Cw3 targets (black bars) or 221-Cw4 targets (white bars). Confocal images (optical sections captured at 0.5 μm intervals in the Z-plane) were captured 7-30 minutes after cell mixing. Interfaces were scored as positive for clustering if enrichment of the EGFP signal was apparent in any section of the Z-series captured for each conjugate. Results were tabulated from four independent experiments using NK92/KIR2DL1-GFP (left) or NK92/KIR2DL1 TR-GFP (right) as effector cells. The "% with cluster" value was determined as (number of interfaces that exhibited clustering)/(total number of interfaces) x 100. The n values indicate the total number of interfaces imaged.

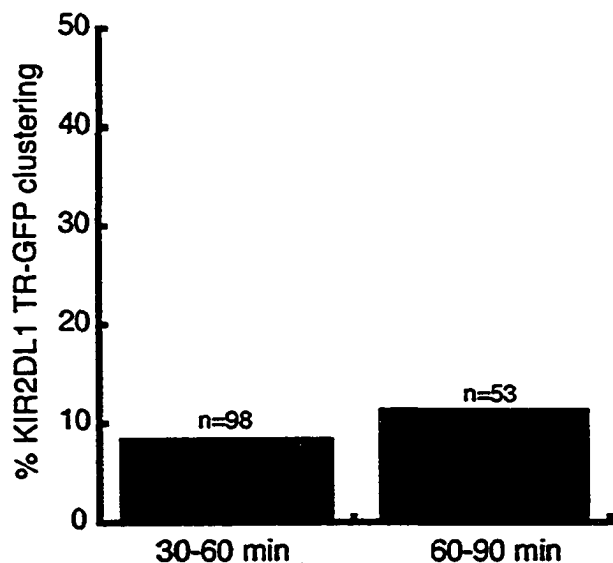


Figure 19: The defect in KIR2DL1 TR-GFP clustering is apparent at later time points after cell mixing. Bar graph showing the % of interfaces that scored positive for clustering following mixing with 221-Cw4 target cells. Confocal images (optical sections captured at 0.5 μm intervals in the Z-plane) were collected 30 - 60 minutes (left) or 60 -90 minutes (right) after mixing NK92/KIR2DL1 TR-GFP effector cells with 221-Cw4 target cells. Interfaces were scored as positive for clustering if enrichment of the EGFP signal was apparent in any 0.5 μm section of the Z-series captured for each conjugate. Results were tabulated from 2 independent experiments. The "% with cluster" value was determined as (number of interfaces that exhibited clustering)/(total number of interfaces) x 100. The n values indicate the total number of interfaces imaged.

after cell mixing. Very few conjugates remained at these time points presumably because KIR2DL1 TR-GFP is not capable of mediating inhibition and therefore the NK92/KIR2DL1 TR-GFP effector cells were capable of killing the 221-Cw4 target cells. None of the 8 interfaces we imaged at 90-120 minutes after cell mixing exhibited clustering. Taken together our results suggest that a reduction in the rate of clustering is not responsible for the defect in KIR2DL1 TR-GFP.

3.6 KIR2DL1-GFP and KIR2DL1 TR-GFP exhibit varying intensities of enrichment at the inhibitory NK cell immune synapse

While collecting our confocal microscopy data, we noticed a varying intensity of enrichment for both full-length and truncated receptor at the inhibitory NK cell immune synapse (Figure 20) (94). A cluster was subjectively categorized as having low, medium, or high degree of enrichment on the basis of its appearance in the Z-series captured for each of the conjugates. Please note that this is not a quantitative measurement of the actual size of the area of enrichment. The varying degrees of KIR-EGFP enrichment were further evident when we generated snapshots of interface regions (Figure 21) (see Materials and Methods for details) (94). We used three-dimensional image software to generate snapshots of interfaces between 221-Cw4 and NK92/KIR2DL1-GFP or 221-Cw4 and NK92/KIR2DL1 TR-GFP. Snapshots were generated for a subset of the conjugates with 221-Cw4 target cells in which clusters of either the full-length or truncated receptor were evident by visual assessment of the EGFP fluorescence image. Briefly, a volume rendering of each conjugate was rotated in order to generate a view of the interface from the perspective of the target cell. A maximum intensity projection

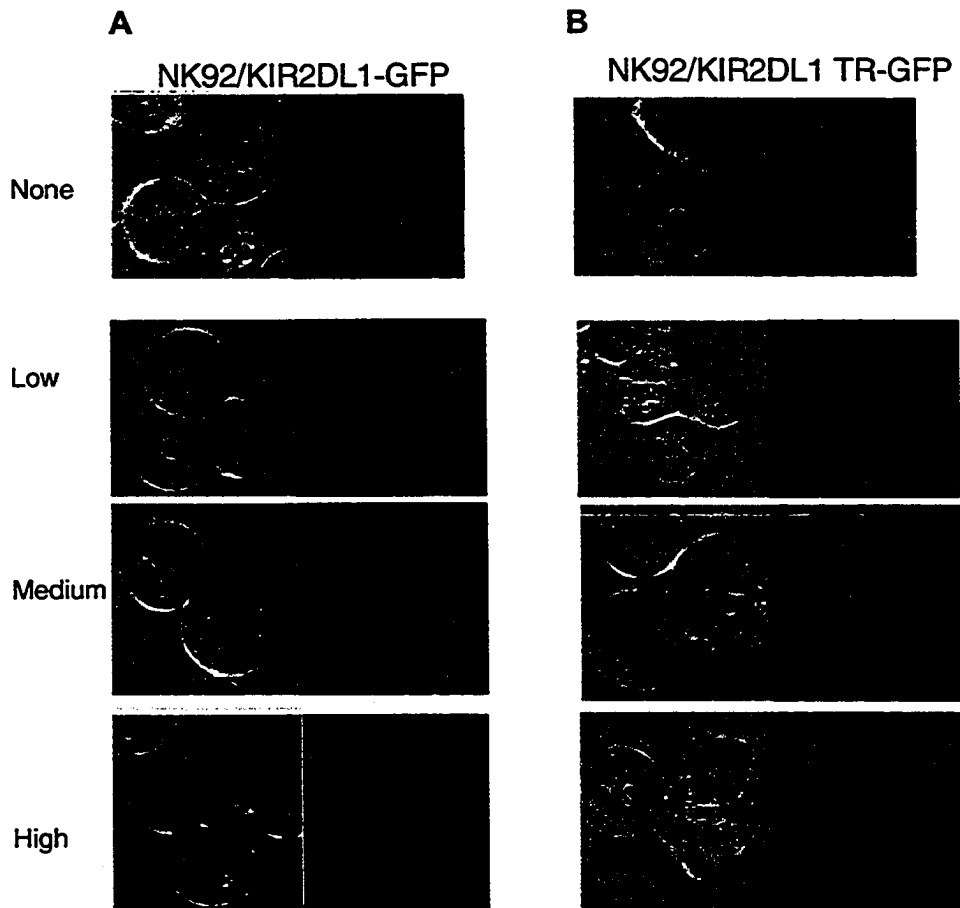


Figure 20: Varying intensities of KIR-EGFP enrichment at the inhibitory NK cell immune synapse. Representative DIC and EGFP fluorescent images of a single 0.5 μm plane are shown for NK92/KIR2DL1-GFP (A) or NK92/KIR2DL1 TR-GFP (B) conjugated to 221-Cw4 target cells. The varying degrees of KIR-GFP recruitment, including no clustering (None) and increasing clustering (Low, Medium, High) are shown.

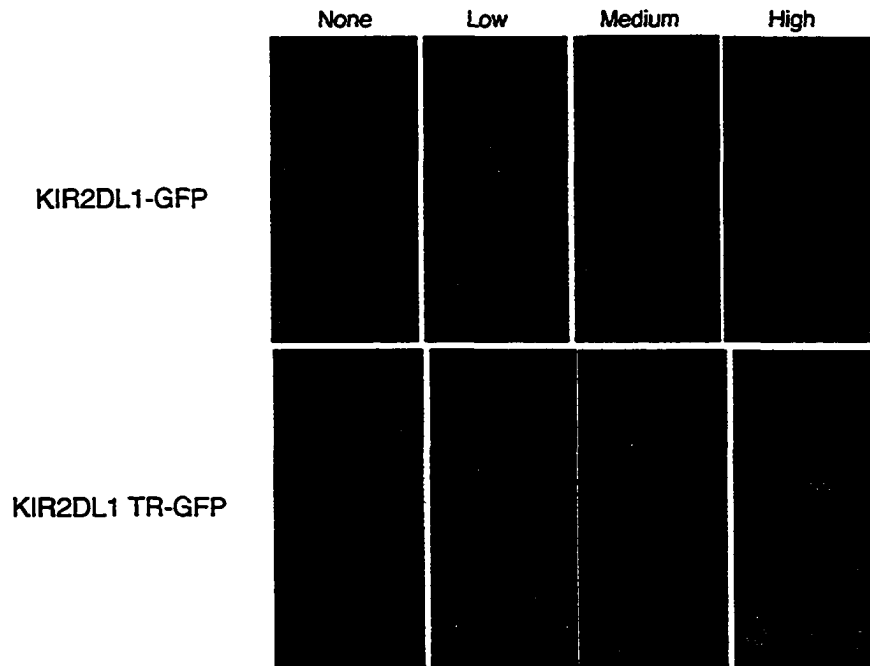


Figure 21: KIR2DL1-GFP and KIR2DL1 TR-GFP exhibit varying patterns of enrichment at the interface with 221-Cw4 target cells. Snapshots of interfaces between 221-Cw4 and NK92/KIR2DL1-GFP (*upper panels*) or 221-Cw4 and NK92/KIR2DL1 TR-GFP (*lower panels*). The interface snapshots are from the same conjugates whose corresponding DIC and EGFP fluorescence images are shown in Figure 3.8.

(MIP) was subsequently generated for each rotated conjugate so that a snapshot of each interface region could be taken. Varying patterns of KIR-EGFP enrichment were evident for both receptors.

3.7 The mean total intensity sum of KIR2DL1-GFP and KIR2DL1 TR-GFP are statistically different

In determining the "% with cluster" values for KIR2DL1-GFP and KIR2DL1 TR-GFP, interfaces were scored as positive for clustering if enrichment of GFP signal was apparent in any 0.5 μ m section of the Z-series captured for each conjugate. Although these values reflect whether or not a cluster was observed at a particular interface, they do not take into account the size of the cluster. In order to perform a comparative quantitative analysis of the KIR-EGFP clustering, we used a three-dimensional image software package to calculate total intensity sum values for each region of KIR-EGFP enrichment (see Materials and Methods) (94). In this instance, the total sum intensity value is a quantification of the total amount of KIR-EGFP enrichment at a particular interface region and therefore these values were used to compare KIR2DL1-GFP and KIR2DL1 TR-GFP clustering. Values were calculated for 30 interface regions with 221-Cw4 target cells irrespective of whether they were scored positive for KIR-EGFP clustering. The raw data used to calculate the mean total intensity sum values are shown in Appendix 1. The mean total intensity sum values as well as the deviation from the mean values were calculated for KIR2DL1-GFP (Mean=101289; SD=141997) and KIR2DL1 TR-GFP (Mean=16957; SD=33609) using images collected on a given day (Table 4). Application of a pooled-variance t-test indicated that there was a significant

Table 4. The mean total intensity sum of KIR2DL1-GFP and KIR2DL1 TR-GFP are significantly different ($p < 0.05$). Application of a pooled-variance independent t -test

Construct	Mean ^a (M)	Standard Deviation (SD)	Number of interface regions ^b (n)
KIR2DL1-GFP	101289	141997	30
KIR2DL1 TR-GFP	16957	33609	30

statistical t -value (t) = 3.165, degrees of freedom (df) = 58, two-tailed p -value (p) = 0.002

^a The mean total intensity sum values (as well as the deviation from the mean values) were calculated from images collected for one experiment on a given day. The raw data used to calculate the mean total intensity sum values for KIR2DL1-TG and KIR2DL1 TR-GFP is shown in Appendix 1.

^b Values were calculated for 30 interface regions with target cells irrespective of whether or not they were scored positive for KIR-EGFP clustering

difference ($p < 0.05$) between the mean total intensity sum of KIR2DL1-GFP and KIR2DL1 TR-GFP (calculated two-tailed p value of 0.002) (see Materials and Methods for details).

3.8 KIR2DL1(K346*) is impaired in its ability to drive 221-Cw6-GFP clustering

A previous report using a more radically truncated KIR did not demonstrate a defect in clustering (91). In their study Fassett *et al.* added a stop codon to the start of the cytoplasmic tail to generate KIR2DL1(K346*) and then used retroviral transduction to express the construct in YTS cells. Although this construct was published as being at amino acid residue 346, according to other parts of their manuscript and to correspondence with Dr. Strominger the truncation was at amino acid residue 246 (Figure 22). For the sake of clarity and in order to be consistent we will refer to this construct as KIR2DL1(K346*) as was done in their original paper. In their study, Fassett *et al.* used EGFP-tagged human HLA-C to monitor movement of their non-EGFP-tagged KIR2DL1 constructs at the NK cell immune synapse. These target cells included 721.221 cells expressing EGFP-tagged HLA-Cw4 (221-Cw4-GFP) or EGFP-tagged HLA-Cw3 (221-Cw3-GFP). Fassett *et al.* reported that KIR2DL1(K346*) was able to drive 221-Cw4-GFP clustering as well as full-length receptor. To address the discrepancy, we obtained the YTS/KIR2DL1(K346*) effector cells and examined receptor clustering upon incubation with 721.221 cells expressing EGFP-tagged KIR2DL1 ligand HLA-Cw6 (221-Cw6-GFP) (23). The 221-Cw6-GFP target cells were obtained from Dr. D. Davis. In our hands, KIR2DL1(K346*) was impaired in its ability to drive HLA-Cw6-GFP clustering, although we did observe a wider variation day to day in the frequency with

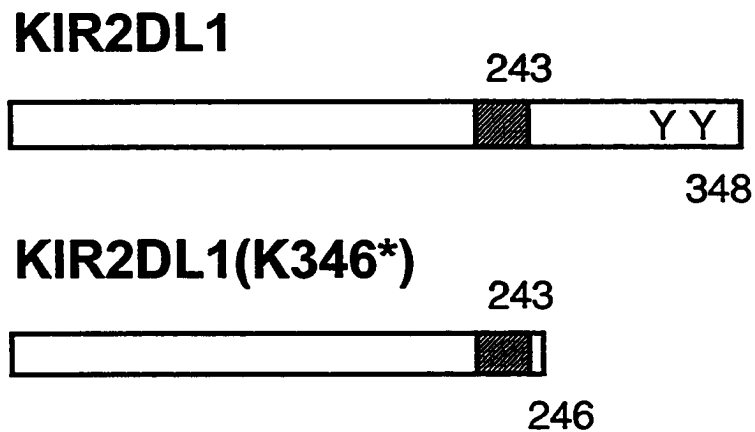


Figure 22: KIR2DL1(K346*) is another KIR2DL1 truncation mutant. Schematic representation of the full-length (KIR2DL1) and truncated (KIR2DL1(K346*)) non-EGFP-tagged KIR2DL1 constructs. The KIR2DL1(K346*) coding sequence contains a stop codon directly after the transmembrane domain. The cross-hatched box represents the transmembrane region of KIR2DL1 and Y indicates the location of the ITIMs. The number directly above each construct denotes the final amino acid residue of the transmembrane domain (243). The number directly below each construct denotes the final amino acid residue in the cytoplasmic tail of full-length (348) or truncated (276) KIR.

KIR2DL1. KIR2DL1(K346*) (Figure 23). Of note, the 221-Cw6-GFP cells seemed to exhibit a higher clustering background than did the YTS/KIR TR-GFP. The reason for the discrepancy between our findings using KIR2DL1(K346*) and those of another study is also not obvious. At first we speculated that the discrepancy was due to a difference in sample preparation, given that our images were collected at early time points following cell mixing, whereas in the other study images were collected following a 45-60 minute incubation of the conjugates. However, the fact that KIR2DL1 TR-GFP clustering did not increase to wild type KIR2DL1-GFP levels at later time points after cell mixing suggests that this difference in methodology is not the cause. Perhaps we were more stringent when scoring interfaces as positive for clustering as a result of noticing the higher background of clustering for the 221-Cw6-GFP target cells. It is also possible that the Strominger lab performed their experiments exclusively on days when the frequency of KIR2DL1(K346*) clustering was high, although no mention of variation in clustering frequency is made (91). Finally, it is possible that there is a connection between KIR clustering and the cell cycle and therefore differences in length of time between tissue culture passages could result in day to day variation. Indeed, a study is currently underway to investigate the possible connection between cell cycle and HLA-C-GFP clustering (personal communication with Dr. D. Davis, Imperial College, London, United Kingdom). It is worth noting that our system uses EGFP-tagged KIR to directly monitor movement of inhibitory receptors in living cells, whereas in the other study EGFP-tagged HLA-C is used to indirectly monitor inhibitory receptor movement in fixed cells.

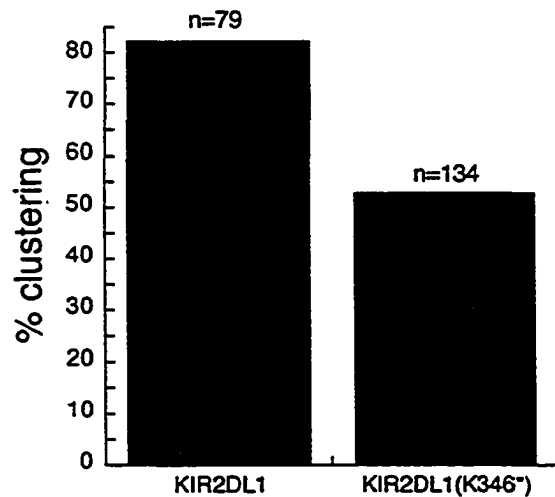


Figure 23: KIR2DL1(K346*) is impaired in its ability to drive 221-Cw6-GFP clustering. Bar graph showing the % of interfaces that scored positive for clustering following mixing with 221-Cw6-GFP target cells. Confocal images (optical sections captured at 0.5 μm intervals in the Z-plane) were captured 5-30 minutes after cell mixing. Interfaces were scored as positive for clustering if enrichment of the EGFP signal was apparent in any section of the Z-series captured for each conjugate. Results were tabulated from four independent experiments using YTS/KIR2DL1-GFP (left) or YTS/KIR2DL1(K346*) (right) as effector cells. The "% with cluster" value was determined as (number of interfaces that exhibited clustering)/(total number of interfaces) x 100. The n values indicate the total number of interfaces imaged.

CHAPTER IV

Results - Part B

4.1 YTS /KIR2DL1-GFP cytolysis of target cells is inhibited by azide

Having established that both full-length and truncated KIR-EGFP exhibit ligand-induced clustering, but that the truncated receptor exhibits a defective clustering phenotype, we next sought to dissect the cellular requirements for KIR enrichment at the inhibitory immune synapse. With this aim in mind we examined KIR2DL1-GFP clustering in the presence of a panel of pharmacological inhibitors, the first of which was sodium azide (azide). Azide was used to study the impacts of ATP depletion on KIR-EGFP clustering. A previous published study of EGFP-tagged HLA-C enrichment used azide as an inhibitor of intracellular ATP generation (90). We were conscious of the fact that azide is a potent metabolic inhibitor with the potential to interfere with a broad-spectrum of cellular processes. Thus we viewed the experiments with azide as a starting point for determining whether KIR clustering could be blocked using pharmacological inhibitors. To begin, we examined the impacts of ATP depletion on YTS cytolysis of target cells (Figure 24). We chose to use YTS because this valid model system has been used in previous studies of KIR enrichment using pharmacological inhibitors and because YTS was more amenable to these types of experiments, owing to higher KIR2DL1-GFP cell surface expression. YTS/KIR2DL1-GFP lysis of sensitive and resistant target cells was measured in the presence of 0, 25, or 50 mM azide using a ⁵¹Cr cytolysis assay (see Materials and Methods for details) (94). For these experiments, effector cells were incubated for 30 minutes at 37°C, 5% CO₂ with twice the desired final concentration of

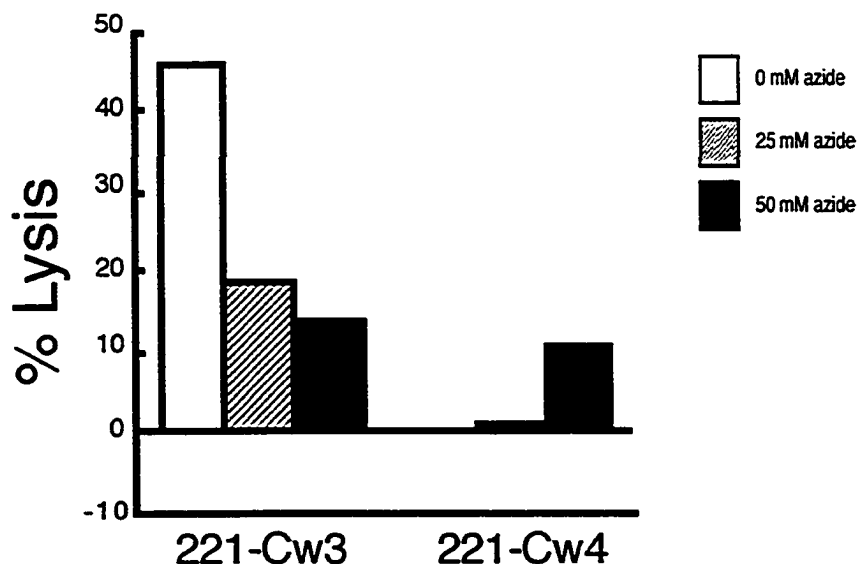


Figure 24: YTS cytolysis of sensitive target cells is inhibited by azide in a dose-dependent manner. Lysis of ^{51}Cr -labeled 221-Cw3 target cells (left) or 221-Cw4 target cells (right) was measured in the presence of azide at an E:T of 30:1. Azide was used at a final concentration of 0 mM, 25 mM, and 50 mM as depicted by white bars, crosshatched bars, and black bars, respectively (see Legend). Percent specific lysis (% Lysis) was determined as $(\text{mean experimental release} - \text{mean spontaneous release}) / (\text{mean maximum release} - \text{mean spontaneous release}) \times 100$. Spontaneous values were determined for each target in the presence of each indicated concentration of azide. Although percent specific lysis values were determined for all indicated cell combinations in the presence of all indicated drug inhibitor concentrations, bars representing values between 0-1 % are not visible. This figure represents results from one of two independent experiments.

drug prior to dilution with the addition of target cells without drug. This was done to ensure full saturation of effector cells with azide while minimizing target cell contact with the pharmacological inhibitor. We found that azide inhibited lysis of sensitive target cells in a dose-dependent manner. This result was not unexpected given that cytolysis is an active process and therefore should require intracellular ATP. Unfortunately, doses that fully blocked cytolysis were accompanied by gross morphological changes of the target cells, as well as high spontaneous release by targets. This could perhaps explain why cytolysis of 221-Cw4 target cells appears to increase in the presence of the highest dose of azide.

4.2 YTS/KIR2DL1-GFP conjugate formation with target cells is inhibited by azide

We next examined YTS/KIR2DL1-GFP conjugate formation with target cells in the presence of azide (Figure 25). A two-color flow cytometry conjugate assay was used to measure YTS/KIR2DL1-GFP conjugate formation with 221-Cw3 or 221-Cw4 target cells in the presence of 0, 25, or 50 mM azide (see Materials and Methods for details) (23) (94). In this assay cells are stained with a red or green fluorescent dye, incubated at 37°C for various lengths of time, and then subjected to a high-speed vortex. Therefore, in this instance, the term conjugate refers to tight, sustained conjugates that are resistant to the vortex step in the flow cytometry assay. Flow cytometry is then used to quantify the number of two-color events (indicative of heteroconjugates) and a percent conjugate formation value is calculated as $(\text{two-color events})/(\text{total effector events}) \times 100$. Using this assay, we found that azide inhibited conjugate formation with sensitive target cells in

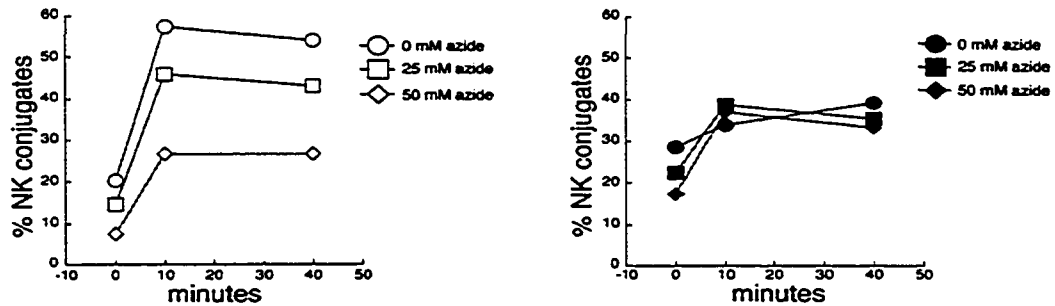


Figure 25: YTS conjugate formation with sensitive target cells is inhibited by azide in a dose-dependent manner. A two-color flow cytometry conjugate assay was used to determine tight conjugate formation of YTS/KIR2DL1-GFP with 221-Cw3 target cells (left) or 221-Cw4 target cells (right) in the presence of azide. The open symbols indicate conjugates with 221-Cw3 target cells and the closed symbols indicate conjugates with 221-Cw4 target cells. Azide was used at a final concentration of 0 mM, 25 mM, and 50 mM as depicted by circles, squares and diamonds, respectively (see Legends). Percent conjugate formation (% NK conjugates) was determined as (two-color events)/(total effector events) x 100.

a dose-dependent manner. This effect was apparent not only at early time points, but also at later time points after cell mixing, at 10 minutes or 40 minutes, respectively. Once again this result was not unexpected given that conjugate formation with target cells is an active rather than passive process. In addition, consistent with our previous study of NK cell adhesion to target cells, in the absence of pharmacological inhibitor, the engagement of KIR2DL1-GFP disrupted conjugate formation with resistant 221-Cw4 target cells (23). We maintain that such disruption of NK cell conjugate formation with resistant target cells could serve to increase the availability of NK cells for the detection of sensitive target cells that trigger a cytotoxicity (23). Interestingly, the reduced conjugate formation due to inhibition by KIR2DL1-TG was not further reduced in the presence of any of the doses of azide tested. It may be of interest to include a blocking anti-KIR antibody to determine whether the interaction of KIR2DL1-TG with HLA-Cw4 on target cells itself contributes some level of adhesion as occurs with inhibition of Src family kinases (23).

4.3 KIR2DL1-GFP clustering in YTS is decreased in the presence of azide

Having determined that cytotoxicity and conjugate formation by YTS are inhibited by azide in a dose-dependent manner, we next examined KIR2DL-GFP clustering in the presence of 50 mM azide, the highest dose tested in the cytotoxicity and conjugate assays (Figure 26). In particular, we calculated the frequency of KIR2DL1-GFP clustering at the inhibitory immune synapse in the presence of 50 mM azide. Interfaces were scored as positive for clustering if enrichment of the EGFP signal was apparent in any optical section of the Z-series captured for each conjugate. Effector cells were incubated with

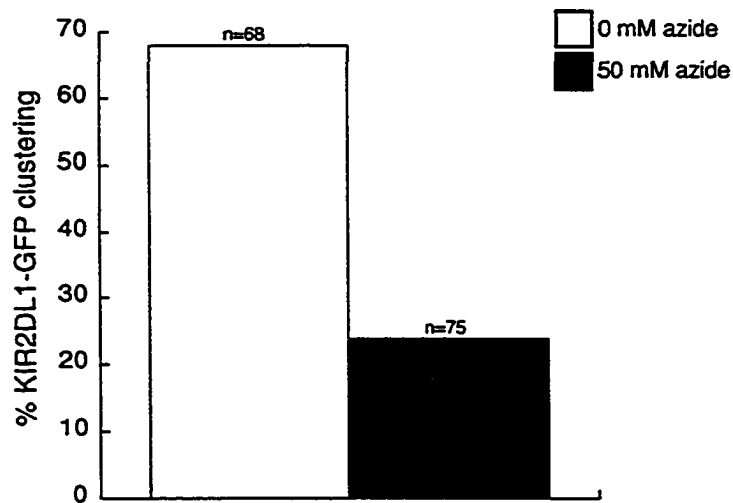


Figure 26: KIR2DL1-GFP clustering is decreased in the presence of 50mM azide. Bar graph showing tabulated results from three independent experiments in which using 50 mM azide (black bars) or aqueous solution alone (white bars) (see Legend). YTS/KIR2DL1-GFP effector cells were pre-incubated for 30 minutes prior to addition of 221-Cw4 target cells. Confocal images (optical sections captured at 0.5 μm intervals in the Z-plane) were captured 5 - 15 minutes after cell mixing. Interfaces were scored as positive for clustering if enrichment of the EGFP signal was apparent in any section of the Z-series captured for each conjugate. The n values indicate the total number of interfaces imaged. At least three samples were examined per treatment per experiment. The "% with cluster" value was determined as (number of interfaces that exhibited clustering)/(total number of interfaces) x 100.

50 mM azide for 30 minutes prior to mixing with target cells and confocal images were collected 5 to 15 minutes after cell mixing (see Materials and Methods and Chapter III). A final concentration of 50 mM azide was maintained in the drug-treated samples at all times. For the no-drug controls, effector cells were preincubated with aqueous solution, the solvent used to dissolve the sodium azide compound. We found that KIR2DL1-GFP clustering was decreased in the presence of 50 mM azide. Although it is tempting to speculate from this result that KIR clustering is an ATP-dependent process, we are unable to rule out any non-specific effects of this potent pharmacological inhibitor.

4.4 YTS /KIR2DL1 -GFP cytolysis of target cells is Src family kinase dependent

Our work with azide suggested that KIR-EGFP clustering is an active process and therefore could be dependent on any number of signaling pathways, including pathways mediated by signaling kinases. To begin, we used the pharmacological inhibitor PP2 to examine the requirement of Src family kinases for YTS cytolysis of target cells (Figure 27) (see Materials and Methods for details). PP2 inhibited YTS/KIR2DL1-GFP cytolysis of sensitive cells in a dose-dependent manner. This result was not unexpected given that we had previously found that PP1, a related pharmacological inhibitor, inhibited lysis of sensitive target cells (23). This result is also consistent with the work of a previous graduate student in our lab (98). In addition, replicate experiments using the NK92 cell line have been done by an undergraduate project student (Karen Chu) in our laboratory.

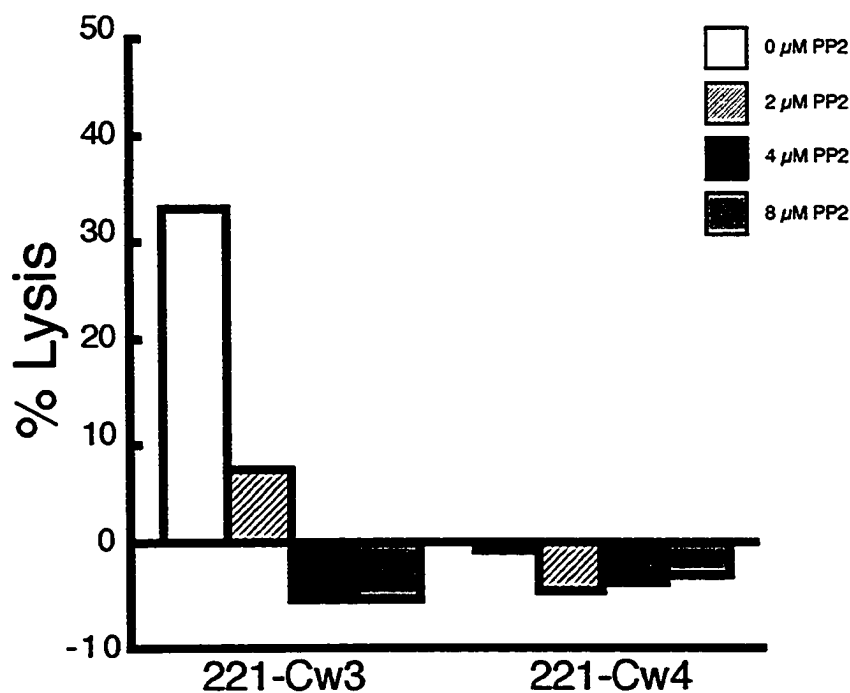


Figure 27: YTS cytolysis of sensitive target cells is dependent on Src family kinases. Lysis of ^{51}Cr -labeled 221-Cw3 target cells (left) or 221-Cw4 target cells (right) was measured at an E:T of 10:1. PP2 was present at a final concentration of 0 μM , 2 μM , 4 μM , and 8 μM as depicted by white bars, crosshatched bars, black bars, and gray bars respectively (see Legend). Percent specific lysis (% Lysis) was determined as (mean experimental release – mean spontaneous release)/(mean maximum release – mean spontaneous release) x 100. This figure represents results from one experiment; however, replicate experiments have been performed by Karen Chu.

4.5 YTS/KIR2DL1-GFP conjugate formation with target cells is Src family kinase dependent

We next examined YTS/KIR2DL1-GFP conjugate formation with target cells in the presence of PP2 (Figure 28). A two-color flow cytometry conjugate assay was used to measure YTS/KIR2DL1-GFP conjugate formation with 221-Cw3 or 221-Cw4 target cells in the presence of 0, 2, 4, or 8 μ M PP2 (see Materials and Methods for details) (94). In this instance, the term conjugate refers to tight conjugates that are resistant to the vortex step in the flow cytometry conjugate assay. We found that PP2 inhibited conjugate formation with sensitive target cells in a dose-dependent manner. This effect was apparent not only at early time points, but also at later time points after cell mixing, at 10 minutes or 40 minutes, respectively. These results are consistent with those of a previous graduate student in our lab (98). The reduced conjugate formation due to inhibition by KIR2DL1-TG was not further reduced in the presence of any of the doses of PP2 tested. This is consistent with results from a previous study by our laboratory. Of note, in that study, a blocking anti-KIR antibody was used to show that the interaction of KIR2DL1-TG with HLA-Cw4 on target cells itself contributes some level of adhesion (23).

4.6 KIR2DL1-GFP clustering in YTS is independent of Src family kinase signaling

Having determined that cytolysis and conjugate formation by YTS are inhibited by PP2 in a dose-dependent manner, we next examined KIR2DL1-GFP clustering in the presence of 8 μ M PP2 (Figure 29). We found that KIR2DL1-GFP clustering was

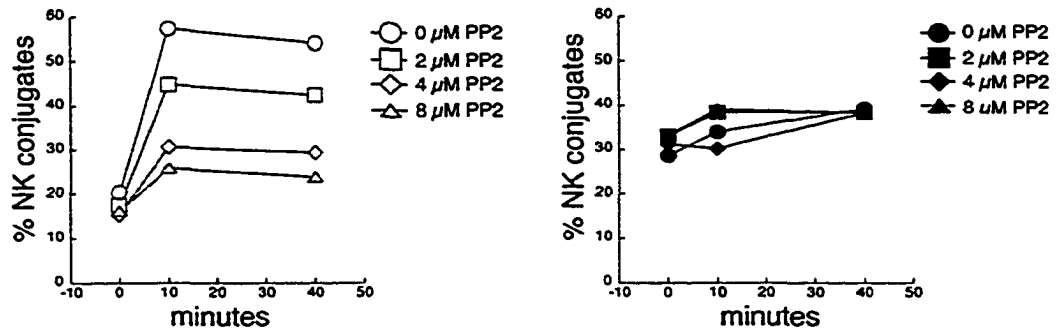


Figure 28: YTS conjugate formation with sensitive target cells is dependent on Src family kinases. A two-color flow cytometry conjugate assay was used to determine tight conjugate formation with 221-Cw3 target cells (left) or 221-Cw4 target cells (right) in the presence of PP2. The open symbols indicate conjugates with 221-Cw3 target cells and the closed symbols indicate conjugates with 221-Cw4 target cells. PP2 was present at a final concentration of 0 μ M, 2 μ M, 4 μ M, and 8 μ M as depicted by circles, squares, diamonds, and triangles, respectively (see Legends). Percent conjugate formation (% NK conjugates) was determined as (two-color events)/(total effector events) x 100.

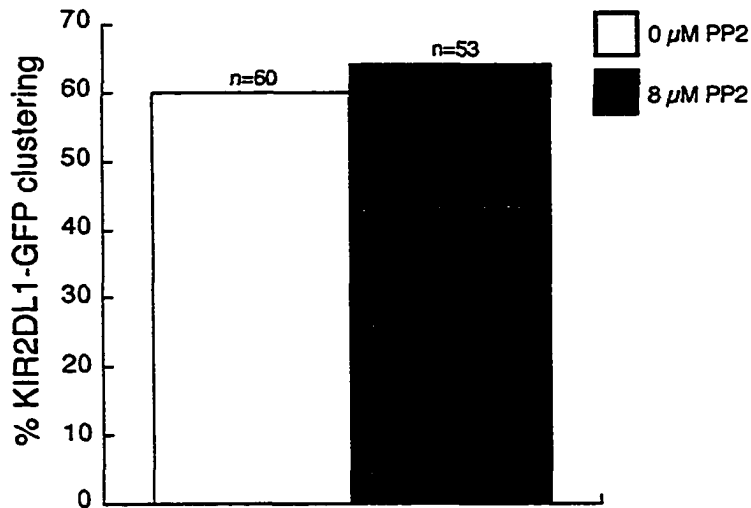


Figure 29: KIR2DL1-GFP clustering is independent of Src family kinase signaling.

Tabulated results from two independent experiments in which YTS/KIR2DL1-GFP cells were pre-treated with 0 μM PP2 (black bars) or 0 μM PP2 (white bars) (see Legend). Effector cells were preincubated for 30 minutes prior to addition of target cells. Confocal images (optical sections captured at 0.5 μm intervals in the Z-plane) were captured 5 - 15 minutes after mixing with 221-Cw4 target cells. Interfaces were scored as positive for clustering if enrichment of the EGFP signal was apparent in any 0.5 μm section of the Z-series captured for each conjugate. The n values indicate the total number of interfaces imaged. At least three samples were examined per treatment per experiment. The "% with cluster" value was determined as (number of interfaces that exhibited clustering)/(total number of interfaces) x 100.

unchanged in the presence of 8 μ M PP2. Of note, the 8 μ M dose of PP2 had pronounced effect on both cytolysis and conjugate formation. This result suggests that KIR2DL1-GFP clustering is independent of Src family kinase signaling and is consistent with the findings of a previous graduate student (98). Although this result had been previously observed, in this particular study I collected a much larger set of data for KIR2DL1-GFP clustering in the presence of PP2 and tabulated the results from two independent experiments.

4.7 NK92/KIR2DL1-GFP cytolysis of target cells requires an intact actin cytoskeleton

In general, the actin cytoskeleton plays an important role in activation of NK cell cytolysis of target cells (11, 99). To determine if the cytoskeleton plays a role in NK92 cytolysis, we examined the effect of cytochalasin D, an inhibitor of actin polymerization, on this process (Figure 30). Due to the reversibility of cytochalasin D it was maintained throughout the experiments. NK92 and NK92/KIR2DL1-GFP cytolysis of target cells was completely inhibited in the presence of 10 μ M cytochalasin D. Replicate experiments using NK92 have been done by Karen Chu, an undergraduate project student in our laboratory. This result is also consistent with a data generated by a previous graduate student showing that 10 μ M cytochalasin D inhibited YTS cytolysis of target cells (98).

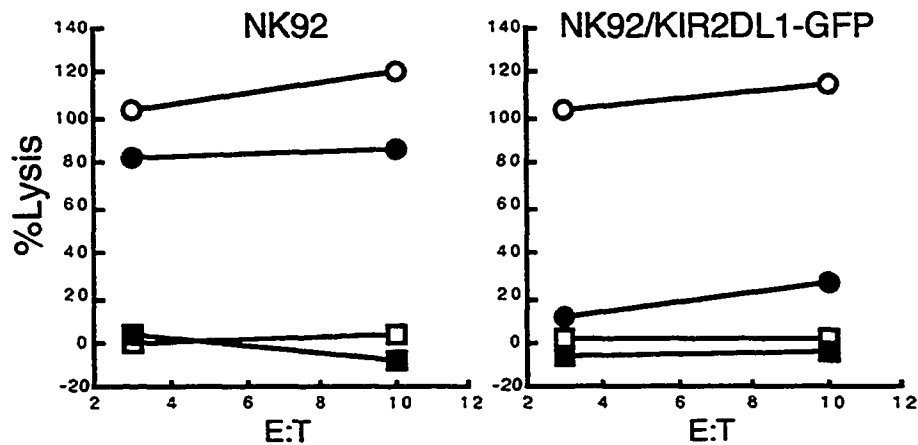


Figure 30: NK92 cytolysis of sensitive target cells requires an intact cytoskeleton. Lysis of BADTA-labeled target cells was determined for NK92 and NK92/KIR2DL1-GFP in the presence of 10 μ M cytochalasin D (squares) or DMSO alone (circles). The open symbols indicate lysis of 221-Cw3 target cells and the closed symbols indicate lysis of 221-Cw4 target cells. Effector cells were incubated for 30 minutes at 37°C, 5% CO₂ with twice the desired final concentration of drug prior to dilution with the addition of target cells without drug. Percent specific lysis (% Lysis) was determined as (mean experimental release – mean spontaneous release)/(mean maximum release – mean spontaneous release) x 100. This experiment was performed once by Leah Standeven; however replicates have been done by Karen Chu.

4.8 NK92/KIR2DL1 conjugate formation requires an intact cytoskeleton

In addition to facilitating cytolysis, the actin cytoskeleton also plays an important role in NK cell conjugate formation with target cells (11, 99). To determine if the cytoskeleton plays a role in NK92 conjugate formation, we examined the effect of cytochalasin D, an inhibitor of actin polymerization, on this process (Figure 31). Similar to cytolysis, NK92 conjugate formation was completely inhibited in the presence of 10 μ M cytochalasin D. Notably, the engagement of KIR in NK92 did not reduce the amount of conjugates as much as has been observed in YTS cells and with a primary NK clone (23, 83). Given that previously we found that engagement of KIR2DL1 expressed at low levels in YTS resulted in only a modest but reproducible inhibition of adhesion, it is possible that the moderate reduction in NK92 is the result of relatively low receptor level expression or more potent activation (88).

4.9 KIR2DL1-GFP clustering in NK92 and YTS requires an intact cytoskeleton

To assess the effect of cytochalasin D on inhibitory receptor enrichment in living cells, we performed confocal microscopy analysis of KIR-GFP clustering in the presence of 10 μ M cytochalasin D or DMSO alone (Figure 32). Images were collected between 7-30 minutes following mixing of effector cells with 221-Cw4 target cells. Of note, samples for confocal microscopy were not subjected to the vortex step used in the flow cytometry conjugate assay so as to allow loose conjugates to remain intact for imaging. The clustering of full-length receptor expressed in NK92 decreased by approximately 50% in the presence of cytochalasin D. In contrast, cytochalasin D did not have a

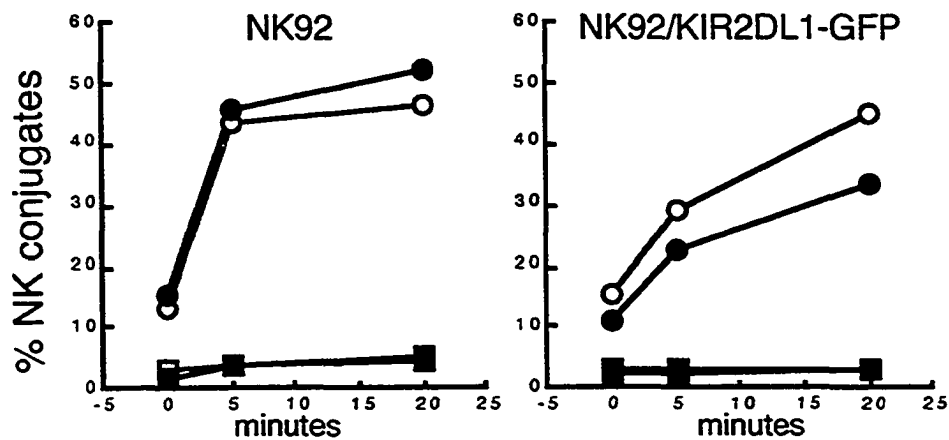


Figure 31: NK92 conjugate formation with target cells requires an intact cytoskeleton. A two-color flow cytometry was used to measure tight conjugate formation between NK92 or NK92/KIR2DL1-GFP and 221-Cw3 target cells (open symbols) or 221-Cw4 target cells. Conjugate formation was measured in the presence of 10 μ M cytochalasin D (squares) or DMSO alone (circles). Effector cells were pre-incubated for 30 minutes at 37°C, 5 % CO₂ in the presence of 10 μ M cytochalasin D or DMSO alone (no drug) prior to the addition of target cell suspensions containing either 10 μ M cytochalasin D or DMSO alone. Representative results from one of two independent experiments are shown. Percent conjugate formation (% NK conjugates) was determined as (two-color events)/(total effector events) x 100.

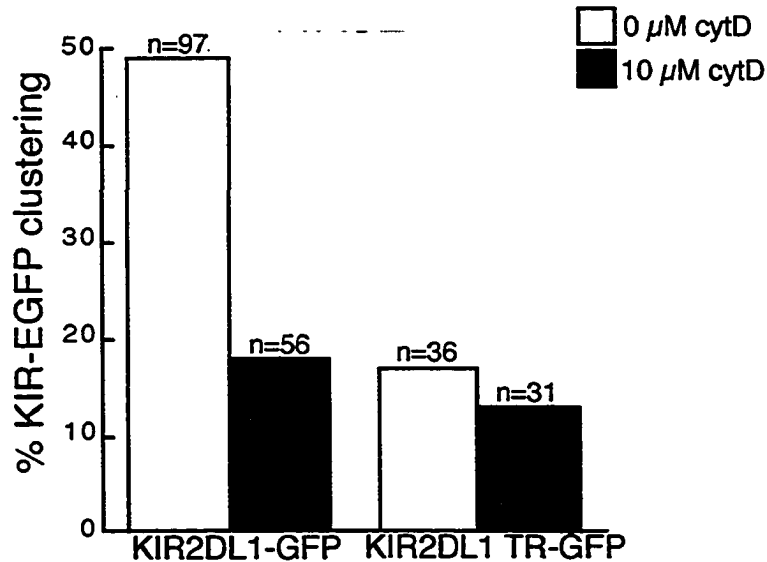


Figure 32: KIR2DL1-GFP clustering in NK92 requires an intact cytoskeleton. Tabulated results from four independent experiments in which KIR-EGFP clustering was scored in the presence of 10 μM cytochalasin D (black bars) or 0 μM cytochalasin D (DMSO alone; white bars) (see Legend). NK92/KIR2DL1-GFP (left) or NK92/KIR2DL1 TR-GFP effector cells were pre-incubated for 30 minutes prior to addition of 221-Cw4 target cells. Indicated cytochalasin D concentrations were maintained in the samples at all times. Confocal images (optical sections captured at 0.5 μm intervals in the Z-plane) were captured 5 - 15 minutes after cell mixing. Interfaces were scored as positive for clustering if enrichment of the EGFP signal was apparent in any 0.5 μm section of the Z-series captured for each conjugate. The n values indicate the total number of interfaces imaged. At least three samples were examined per treatment per experiment. The "% with cluster" value was determined as (number of interfaces that exhibited clustering)/(total number of interfaces) x 100.

significant effect on the clustering of KIR2DL1 TR-GFP expressed in NK92. Similar to NK92, the frequency of KIR2DL1-GFP clustering was reduced by approximately 50% in YTS cells in the presence of cytochalasin D (Figure 33). Taken together our data suggests that a dynamic actin cytoskeleton is required for full-length KIR clustering.

4.10 The actin cytoskeleton regulates the rate at which KIR2DL1-GFP and Cw6-GFP cluster

Our results using cytochalasin D were surprising given a previous study by the Davis lab in which 10 μ M cytochalasin D was found to have no effect on KIR induced HLA-C-GFP clustering (90). Based on their results, Davis *et al.* concluded that KIR induced HLA-C-GFP clustering independently of actin polymerization. Thus, in collaboration with the Davis lab, we decided to address this discrepancy. We sent our YTS/KIR2DL1-GFP cells to the Davis lab so that experiments using EGFP-tagged KIR2DL1 and EGFP-tagged HLA-C could be performed side by side. A comparison of our protocols revealed that the Davis lab was collecting confocal images following a 45 - 60 minute incubation after cell mixing, whereas we were collecting confocal images within 30 minutes of cell mixing (90, 94). We therefore hypothesized that the effect of cytochalasin D was a question of kinetics. In order to test this, Leo Carlin, a graduate student in the Davis lab, performed a time course analysis of KIR-GFP clustering in YTS effector cells or HLA-C-GFP clustering in 721.221 target cells (Appendix 2) (94). For these particular experiments, the target cells expressed the KIR2DL1 ligand HLA-Cw6 (221-Cw6) or HLA-Cw6 fused to GFP (221-Cw6-GFP) as well as the non-cognate MHC-I protein HLA-Cw3 (221-Cw3) or HLA-Cw3 fused to EGFP (221-Cw3-GFP). To

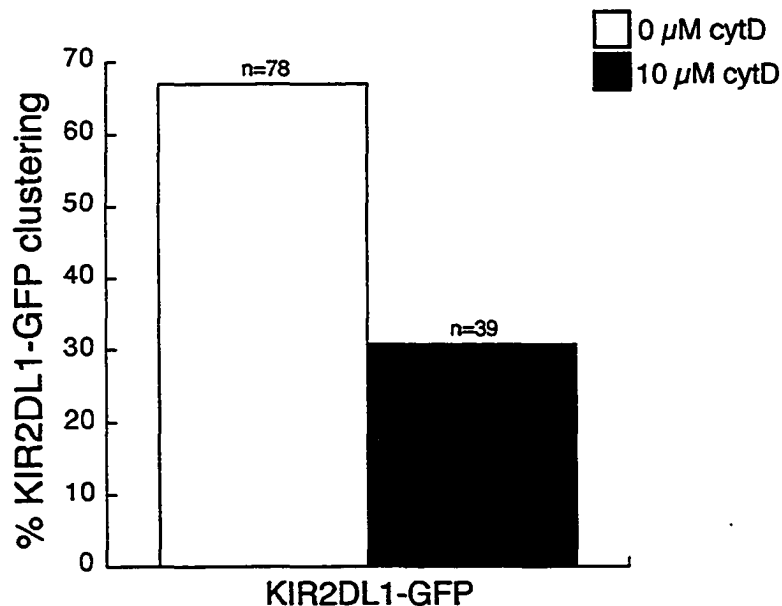


Figure 33: KIR2DL1-GFP clustering in YTS requires an intact cytoskeleton. Tabulated results from three independent experiments in which KIR2DL1-GFP clustering was scored in the presence of 10 μM cytochalasin D (black bars) or 0 μM cytochalasin D (DMSO alone; white bars) (see Legend). YTS/KIR2DL1-GFP effector cells were preincubated for 30 minutes prior to addition of 221-Cw4 target cells. Indicated cytochalasin D concentrations were maintained in the samples at all times. Confocal images (optical sections captured at 0.5 μm intervals in the Z-plane) were captured 5 - 30 minutes after cell mixing. Interfaces were scored as positive for clustering if enrichment of the EGFP signal was apparent in any 0.5 μm section of the Z-series captured for each conjugate. The n values indicate the total number of interfaces imaged. At least three samples were examined per treatment per experiment. The "% with cluster" value was determined as (number of interfaces that exhibited clustering)/(total number of interfaces) x 100.

facilitate these experiments, the conjugates were fixed at discrete time points as well as permeabilized to verify the effect of cytochalasin D by using phalloidin-Alexafluor633[®] to stain F-actin. Remarkably, time-course analysis of Cw6-GFP and KIR2DL1-GFP clustering revealed that 10 μ M cytochalasin D had a pronounced effect at earlier time points after cell mixing but not by 40 minutes after cell mixing. In the absence of cytochalasin D, the clustering of Cw6-GFP and KIR2DL1-GFP at the inhibitory NK cell immune synapse reaches 60-70 % by the 10 minute time point. In contrast, when the cells were treated with cytochalasin D, the clustering of Cw6-GFP and KIR2DL1-GFP was substantially lower than that of the controls until the time point of 40 minutes. In the case of the activating NK cell immune synapse, neither Cw3-GFP nor KIR2DL1-GFP clustered at any of the time points. Staining with phalloidin-Alexafluor633[®] showed an increase in F-actin over time at activating NK cell immune synapses and that this increase was blocked in the presence of cytochalasin D. By comparison, there was no increase in accumulation of F-actin at inhibitory NK cell immune synapses at any of the time points examined. Taken together these results suggest that the actin cytoskeleton regulates the rate of KIR clustering.

4.11 The dose response to actin disruption for cytolysis by YTS cells

Given the dramatic effect of 10 μ M cytochalasin D on cytolysis, we further examined the impacts of actin disruption of YTS cytolysis with a dose response (94). YTS/KIR2SL1-GFP cytolysis was measured in the presence of 0 μ M, 2 μ M, 5 μ M, and 10 μ M cytochalasin D (Figure 34). We found that cytolysis of sensitive 221/Cw3 target cells was completely inhibited even at 2 μ M cytochalasin D. In separate experiments we

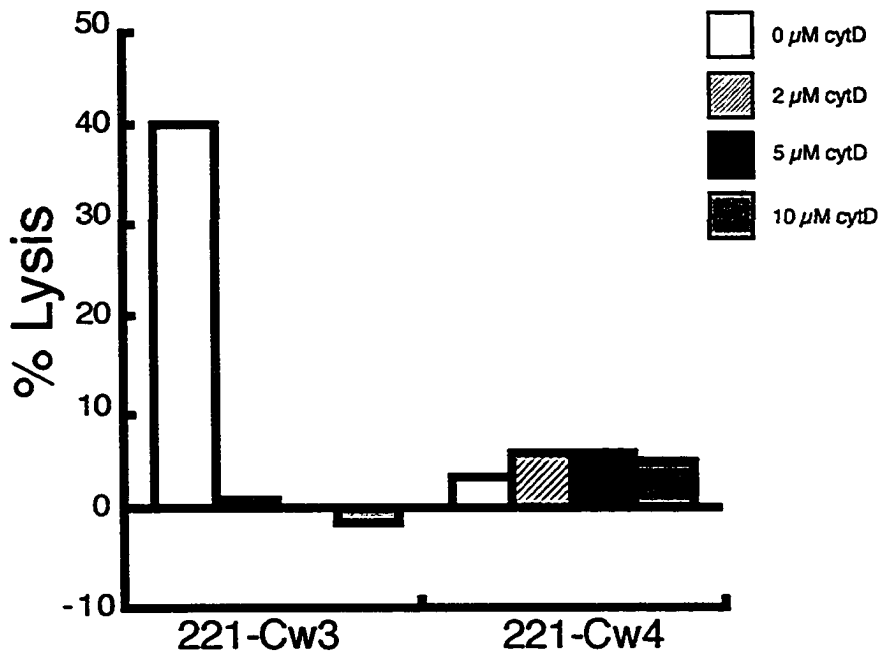


Figure 34: The dose response to actin disruption for cytolysis by YTS cells. Lysis of ^{51}Cr -labeled 221-Cw3 target cells (left) or 221-Cw4 target cells (right) was measured at an E:T of 30:1. Cytochalasin D was present at a final concentration of 0 μM , 2 μM , 5 μM , and 10 μM as depicted by white bars, crosshatched bars, black bars, and gray bars respectively (see Legend). Percent specific lysis (% Lysis) was determined as (mean experimental release – mean spontaneous release)/(mean maximum release – mean spontaneous release) x 100. This figure is representative of results from two independent experiments.

determined that the effect on cytolysis was lessened at 1 μM cytochalasin D and no longer apparent at 0.1 μM cytochalasin D (Figure 35). Therefore the effects of actin disruption on cytolysis as a result of treatment with cytochalasin D could be titrated.

4.12 The dose response to actin disruption for conjugate formation by YTS cells

We next examined YTS/KIR2DL1-GFP conjugate formation with target cells in the presence of various doses of cytochalasin D (Figure 36). A two-color flow cytometry conjugate assay was used to measure YTS/KIR2DL1-GFP conjugate formation with 221-Cw3 or 221-Cw4 target cells in the presence of 0 μM , 2 μM , 5 μM , or 10 μM cytochalasin D (see Materials and Methods for details) (94). We found that cytochalasin D completely inhibited tight conjugate formation with sensitive target cells even in the presence of the lowest dose of 2 μM . Furthermore, this effect was apparent not only at early time points, but also at later time points after cell mixing, at 10 minutes and 40 minutes, respectively.

4.13 The dose response to actin disruption for clustering by KIR-EGFP in YTS cells

To further assess the effect of cytochalasin D on inhibitory receptor enrichment in living cells, we performed confocal microscopy analysis of KIR-GFP clustering in the presence of 0 μM , 2 μM , 5 μM , and 10 μM cytochalasin D (Figure 37). Images were collected between 7-30 minutes following mixing of effector cells with 221-Cw4 target cells. Of note, samples for confocal microscopy were not subjected to the vortex step

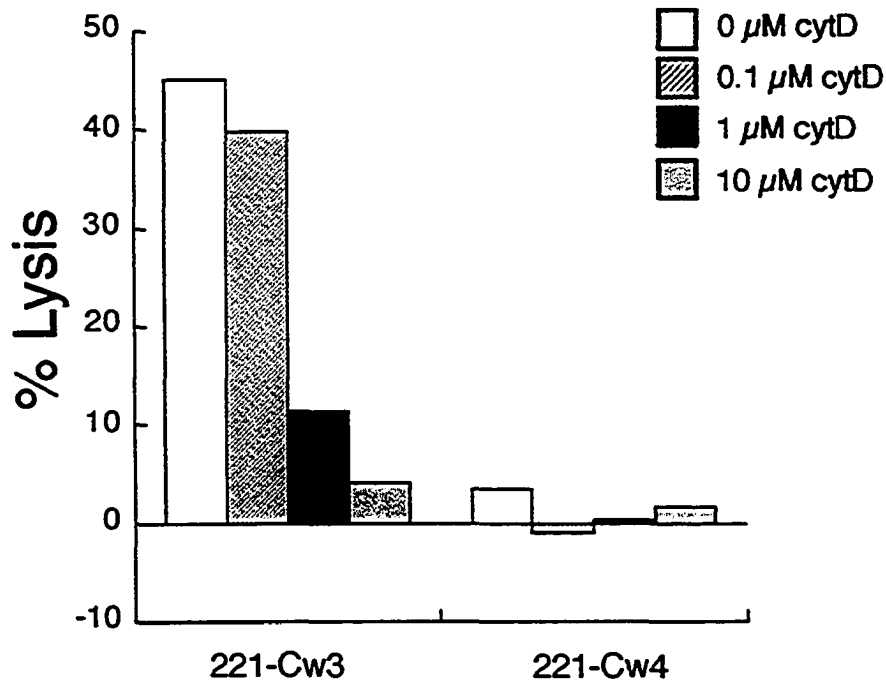


Figure 35: The dose response to actin disruption for cytolysis by YTS cells can be titrated. Lysis of ^{51}Cr -labeled 221-Cw3 target cells (left) or 221-Cw4 target cells (right) was measured at an E:T of 30:1. Cytochalasin D was present at a final concentration of 0 μM , 0.1 μM , 1 μM , and 10 μM as depicted by white bars, crosshatched bars, black bars, and gray bars respectively (see Legend). Percent specific lysis (% Lysis) was determined as (mean experimental release – mean spontaneous release)/(mean maximum release – mean spontaneous release) x 100. This figure is representative of results from two independent experiments.

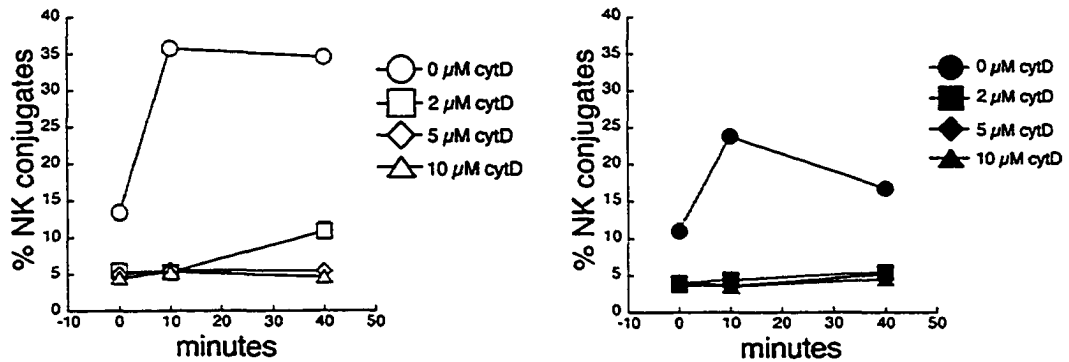


Figure 36: The dose response to actin disruption for conjugate formation by YTS cells. A two-color flow cytometry conjugate assay was used to determine tight conjugate formation of YTS/KIR2DL1-GFP with 221-Cw3 target cells (left) or 221-Cw4 target cells (right) in the presence of the indicated doses of cytochalasin D. The open symbols indicate conjugates with 221-Cw3 target cells and the closed symbols indicate conjugates with 221-Cw4 target cells. Cytochalasin D was present at a final concentration of 0 mM, 2 μM, 5 μM, and 10 μM as depicted by circles, squares and diamonds, respectively (see Legends). Percent conjugate formation (% NK conjugates) was determined as (two-color events)/(total effector events) x 100. Results show are representative of four independent experiments.

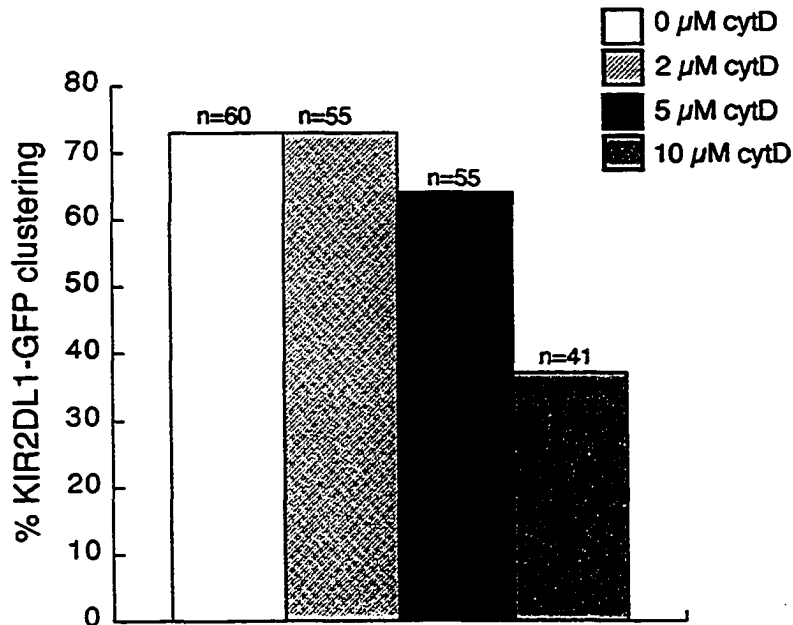


Figure 37: The dose response to actin disruption for clustering by KIR-EGFP in YTS cells. Tabulated results from three independent experiments in which cytochalasin D was present at a final concentration of 0 μM, 2 μM, 5 μM, and 10 μM as depicted by open bars, cross-hatched bars, black bars, and grey bars, respectively (see Legend). YTS/KIR2DL1-GFP effector cells were preincubated for 30 minutes with the indicated drug concentration prior to addition of 221-Cw4 target cells. Confocal images (optical sections captured at 0.5 μm intervals in the Z-plane) were captured 5 - 15 minutes after cell mixing. Interfaces were scored as positive for clustering if enrichment of the EGFP signal was apparent in any 0.5 μm section of the Z-series captured for each conjugate. The n values indicate the total number of interfaces imaged. At least three samples were examined per treatment per experiment. The "% with cluster" value was determined as (number of interfaces that exhibited clustering)/(total number of interfaces) x 100.

used in the flow cytometry conjugate assay so as to allow loose conjugates to remain intact for imaging. We found that the effect of cytochalasin D on KIR2DL1-GFP clustering was lessened at 5 μM and no longer apparent at 2 μM even though clustering was reduced by approximately 50% in the presence of the standard 10 μM dose. In other words, the low doses of cytochalasin D used in our study had little to no effect on KIR clustering. Taken together, this data suggests that KIR2DL1-GFP clustering in YTS is not as sensitive as cytolysis or conjugate formation to minor interference with cytoskeletal dynamics.

4.14 The effect of cytochalasin D on KIR clustering is not through inhibition of LFA-1 mediated adhesion

The actin cytoskeleton is involved in several processes relevant to immune synapse formation including integrin-mediated adhesion and transport of molecules to the synapse. LFA-1 is the principle integrin that mediates YTS cell binding to 721.221 target cells and requires actin polymerization to cluster at the activating NK cell immune synapse in *ex vivo* cells (23, 85). To address the possibility that the effect of cytochalasin D on KIR clustering was through inhibition of LFA-1 mediated adhesion, we determined the effect of an anti-LFA-1 antibody on adhesion and KIR clustering for YTS cells. The antibody TS1/22.1.1.13 reacts with the activated form of LFA-1 and thus recognizes a change in LFA-1 conformation but not a change in LFA-1 avidity, which is regulated through clustering. The anti-LFA-1 antibody TS1/22.1.1.13 constitutively stains YTS cells (Figure 38). Although some staining was observed for the 221-Cw3 and 221-Cw4 target cells, the intensity of staining for both target cell lines was much lower than that of

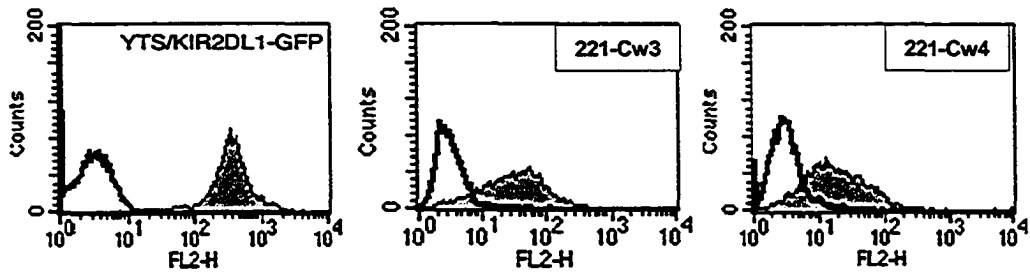


Figure 38: The TS1/22.1.1.13 anti-LFA-1 antibody constitutively stains YTS/KIR2DL1-GFP. Representative activated LFA-1 cell surface expression profiles for YTS/KIR2DL1 effector cells as well as 221-Cw3 and 221-Cw4 target cells. Expression profiles were determined using anti-LFA-1 antibody TS1/22.1.1.13 and PE-conjugated goat anti-mouse (shaded histograms) or PE-conjugated goat anti-mouse alone (empty histograms).

YTS/KIR2DL1-GFP. We next determined the effect of anti-LFA-1 on YTS tight conjugate formation with sensitive and resistant target cells. A two-color flow cytometry assay was used to measure YTS/KIR2DL1-GFP adhesion to 221-Cw3 or 221-Cw4 cells in the presence of 10 μ g/mL anti-LFA-1 or control antibody (Figure 39) (see Materials and Methods) (94). In the presence of anti-LFA-1, the number of effector cells able to adhere to 221-CW3 and 221-Cw4 target cells was reduced to about 10 %. Although the lower level of conjugation due to KIR2DL1-GFP engagement by HLA-Cw4 is evident, the number of conjugates decreased in the presence of anti-LFA-1 to a similar level regardless of whether or not KIR was engaged. We next determined the effect of anti-LFA-1 on inhibitory receptor enrichment in living cells. To do this we performed confocal microscopy analysis of KIR2DL1-GFP clustering in the presence of anti-LFA-1 or control antibody (Figure 40) (94) (see Materials and Methods). Although we did not quantify the difference, the frequency of conjugates appeared lower under the conditions used for live cell imaging. However, within the population of conjugates that did form in the presence of anti-LFA-1, the frequency of KIR clustering was unchanged. In a separate experiment we determined that KIR2DL1-GFP clustering was blocked in the presence of anti-KIR but not in the presence of anti-LFA-1 (Figure 41). Taken together, these data suggest that although LFA-1 mediated adhesion is key to forming stable conjugates and therefore is likely often engaged upstream of KIR clustering, LFA-1 mediated adhesion is not essential for KIR clustering.

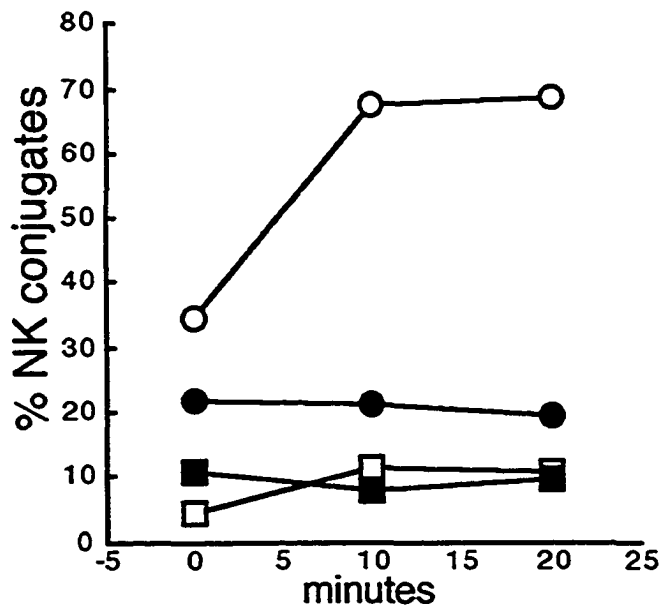


Figure 39: YTS adhesion to target cells is dependent on activated LFA-1. Tight conjugate formation between YTS/KIR2DL1-GFP and 221-Cw3 (open symbols) or 221-Cw4 (closed symbols) was measured in the presence of 10 $\mu\text{g/ml}$ anti-LFA-1 (squares) or MOPC-21 control IgM (circles). Percent conjugate formation (% NK conjugates) was determined as (two-color events)/(total effector events) x 100.

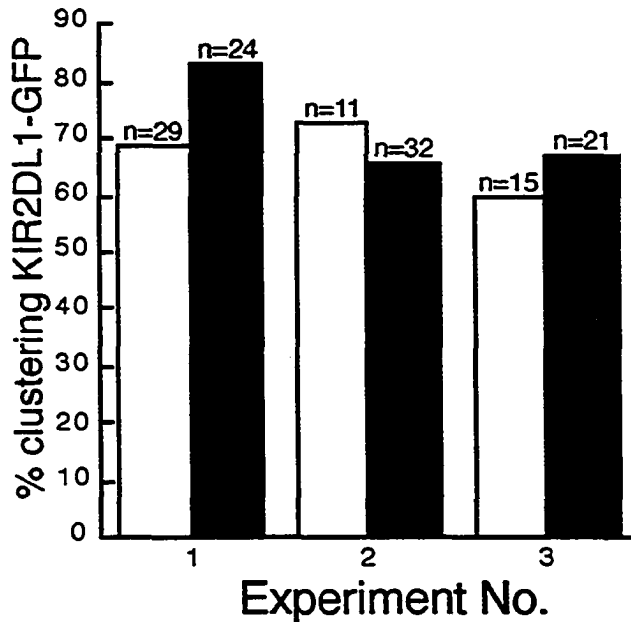


Figure 40: KIR2DL1-GFP clustering is independent of activated LFA-1. Bar graph showing tabulated results from three independent experiments using 10 $\mu\text{g}/\text{mL}$ anti-LFA-1 (black bars) or MOPC-21 control antibody (white bars). YTS/KIR2DL1-GFP effector cells were pre-incubated for 5 minutes at room temperature prior to addition of 221-Cw4 target cells. Confocal images (optical sections captured at 0.5 μm intervals in the Z-plane) were captured 5 - 15 minutes after cell mixing. Interfaces were scored as positive for clustering if enrichment of the EGFP signal was apparent in any 0.5 μm section of the Z-series captured for each conjugate. The n values indicate the total number of interfaces imaged. At least three samples were examined per treatment per experiment. The "% with cluster" value was determined as (number of interfaces that exhibited clustering)/(total number of interfaces) x 100.

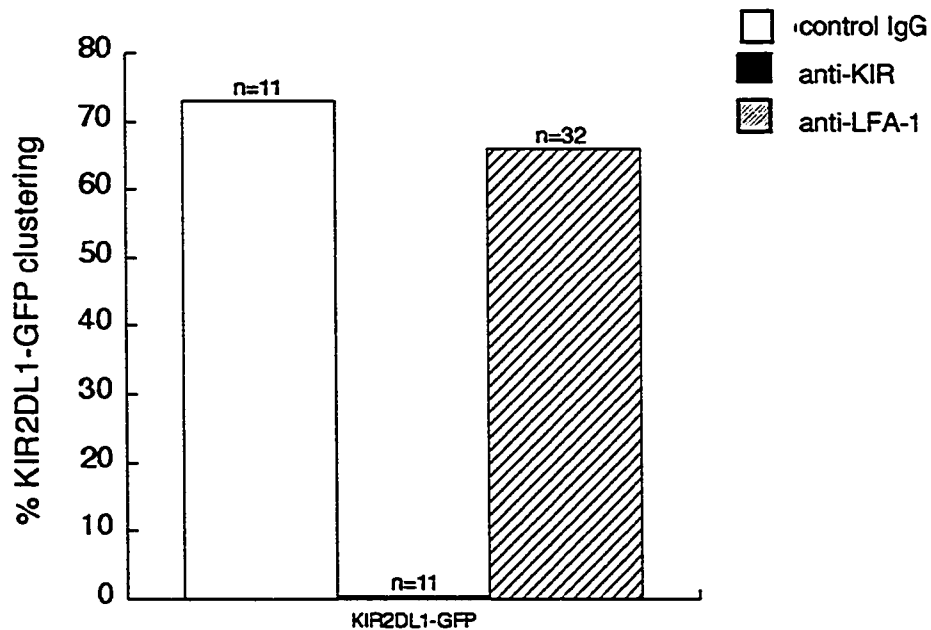


Figure 41: The anti-KIR antibody HP3E4 blocks KIR2DL1-GFP clustering in YTS. Bar graph showing results tabulated from a single experiment in which YTS/KIR2DL1-GFP effector cells were pre-incubated for 5 minutes at room temperature with 10 $\mu\text{g}/\text{mL}$ control antibody (open bar), HP3E4 anti-KIR2DL1 ascites (black bar), or 10 $\mu\text{g}/\text{mL}$ HB202 anti-LFA-1 (cross-hatched bar). In order to maintain the correct final concentration, antibody was added to the target cells just prior to cell mixing. Confocal images (optical sections captured at 0.5 μm intervals in the Z-plane) were captured 7 - 30 minutes after mixing with 221-Cw4 target cells. Interfaces were scored as positive for clustering if enrichment of the EGFP signal was apparent in any 0.5 μm section of the Z-series captured for each conjugate. The n values indicate the total number of interfaces imaged. At least three samples were examined per treatment per experiment. The "% with cluster" value was determined as (number of interfaces that exhibited clustering)/(total number of interfaces) x 100.

CHAPTER V

Discussion

We have found that our truncated KIR-EGFP chimera has a defective clustering phenotype. The frequency of KIR2DL1 TR-GFP enrichment was not only lower, but also the mean total intensity sum values of KIR2DL1-GFP and KIR2DL1 TR-GFP were significantly different. Our data suggests that the distal portion of the cytoplasmic tail is required for efficient KIR clustering at the inhibitory NK cell immunological synapse. Given that KIR2DL1 TR-GFP is incapable of mediating inhibition, perhaps the missing inhibitory receptor signaling is what is required for efficient KIR clustering.

Alternatively, the events involved in formation of an activating synapse, which would occur in spite of engagement of the truncated receptor, would also disrupt KIR accumulation (84). For example, the coalescence of lipid rafts, recruitment of many cell surface proteins and fusion of cytoplasmic granules at the interface might diminish the amount of KIR accumulation by competition for space. Treatment with cytochalasin D would then be expected to completely mimic the situation of the truncated receptor because cytochalasin D prevents activation pathways a well.

To address this, we have already constructed a KIR-EGFP chimera called KIR2DL1-GFP/Y2F in which both tyrosine (Y) residues of the ITIMs in KIR2DL1-GFP have been mutated to phenylalanine (F) residues (Figure 42). We have generated a YTS cell line with stable expression of KIR2DL1-GFP/Y2F and results from a standard ^{51}Cr release killing assay indicate that this construct is signaling incompetent. Preliminary experiments indicate that the frequency and the mean total intensity sum value of the

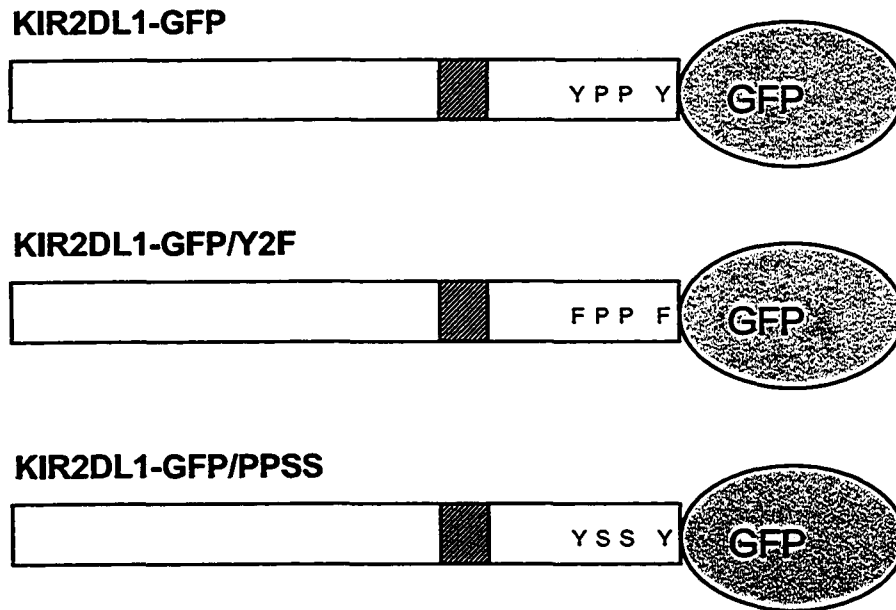


Figure 42: KIR2DL1-GFP mutants. Schematic representation of the KIR-EGFP chimera constructs. Chimeras include KIR2DL1-GFP in which both tyrosine residues in the ITIMs have been mutated to phenylalanine residues (KIR2DL1-GFP/Y2F) and KIR2DL1-GFP in which two proline residues between the ITIMs have been mutated to serine residues (KIR2DL1-GFP/PPSS). The cross-hatched box represents the transmembrane region of KIR2DL1 and Y indicates the location of the ITIMs.

signaling-deficient KIR2DL1-GFP/Y2F chimera were comparable to those of the wild type KIR2DL1-GFP signaling-competent mutant. Although this suggests that the inability of the truncated KIR-EGFP chimera to cluster efficiently is not due to a lack of inhibitory receptor signaling, these results must be repeated before any firm conclusions can be made. In addition, it would be of interest to verify the inability of KIR2DL1-GFP/Y2F to signal for inhibition by examining its phosphorylation. This could be accomplished by anti-GFP immunoprecipitation in the presence of pervanadate and then using western blot analysis to examine tyrosine phosphorylation. The anti-GFP has been kindly provided by Dr. Luc Berthiaume, Department of Cell Biology, Edmonton, AB. Based on our killing assay results we would predict that the signaling deficient KIR2DL1-GFP/Y2F mutant that is lacking the crucial tyrosine residues in the ITIMs would not be tyrosine phosphorylated.

An alternative (and not mutually exclusive) explanation for the defective clustering phenotype of KIR2DL1 TR-GFP is that the distal portion of the cytoplasmic interacts with another protein in order to cluster efficiently at the inhibitory NK cell immunological synapse. Such an interaction could also be required to sustain KIR clustering. In addition, the observation that cytochalasin D did not further decrease clustering of KIR2DL1 TR-GFP also suggests the possibility of an interaction (either direct or indirect) of full-length receptor with the actin cytoskeleton. One possibility is that an adaptor protein such as talin might be required directly for KIR clustering. Talin tethers the integrin LFA-1 (via the β -subunit) to the actin cytoskeleton. Perhaps talin is also required for KIR tethering to the actin cytoskeleton. In support of this, talin is initially recruited to the interface whether or not the NK cell will become activated or

inhibited by KIR (87). Talin is subsequently released from inhibitory synapses but maintained in activating synapses. Perhaps the initial colocalisation of talin and KIR results from an interaction between the two proteins.

There are no obvious sequence motifs in KIR2DL1 that could facilitate an interaction with adaptor proteins or the actin cytoskeleton. This is based on results from queries using the Pfam protein domain and conserved region database, the PRINTS motif database, and the Eukaryotic Linear Motif (ELM) server database (100, 101). However, results from our query using the PRINTS database did identify a proline rich extensin signature (PSQRPKTPPTDIIVYTELPNAESRSK) in the cytoplasmic tail of KIR2DL1. Interestingly, results from our query using the ELM server database also highlighted this region by identifying two motifs recognized by Src homology 3 (SH3) domains with a non-canonical class I recognition specificity (SQRPKTP and SKVVSCP, respectively). SH3 domains bind proline-rich sequences to facilitate the formation of complicated networks of proteins involved in signal transduction, cytoskeleton organization, membrane traffic, and organelle assembly. Although proline-rich sequences usually contain classical PxxP motif, some proline-rich sequences have novel SH3 domain-binding motifs. For example, the deubiquitinating enzyme UBPY contains a novel motif that binds to the SH3 domain of mouse STAM2 (102). Perhaps the proline-rich sequence located between the two ITIMs in the cytoplasmic tail KIR2DL1 mediates protein-protein interactions necessary for KIR enrichment at the inhibitory NK cell immunological synapse. And indeed, there is evidence for the contribution of a proline-rich motif to cellular localization of an intracellular protein kinase known as Akt (103). According to a recent study, a proline-rich motif in the C-terminus of Akt contributes to its localization

during the early stages of T cell activation. Mutation of two prolines to alanine in the C-terminus of Akt resulted in an altered pattern of recruitment to the plasma membrane T cells forming an interface with antigen-loaded B cells.

To address this we have already constructed KIR2DL1-GFP/PPSS in which two proline (P) residues in the KIR2DL1-GFP cytoplasmic tail with the potential to mediate protein-protein interactions have been mutated to serine (S) residues (Figure 42). We have stably expressed KIR2DL1-GFP/PPSS in YTS and results from a standard cytolysis assay indicate that this construct is signaling competent. The use of confocal microscopy to determine the frequency of clustering of the KIR2DL1-GFP/PPSS mutant should provide some insight into whether the proline-rich sequence is important for KIR clustering. Preliminary experiments indicate that the frequency and the mean total intensity sum value of KIR2DL1-GFP/PPSS chimera were comparable to those of the wild type KIR2DL1-GFP signaling-competent mutant, suggesting that the proline-rich region is not essential for KIR-EGFP clustering. However, these results must be repeated before any firm conclusions can be made. Construction of a series of KIR2DL1 truncation mutants (with progressively shorter cytoplasmic tails) and stable expression of these panels of truncated constructs in YTS will also aid in determination of the minimal requirement for efficient KIR clustering. Immunoprecipitation studies could be used to identify KIR2DL1 protein-protein interactions. Anti-GFP would be used to pull-down KIR-GFP in lysates. Alternatively, recombinant KIR could be used as a bait protein in a far-Western blot (104). Bands representing putative KIR2DL1-interacting proteins could be identified either by mass spectroscopy and/or by Western blot.

Full-length receptor clustering was inhibited in the presence of azide, suggesting that intracellular ATP is required for KIR clustering. Although we did not measure ATP depletion following treatment with azide, a study published by another laboratory has already verified the effect of 50 mM azide on ATP concentrations in the YTS and 721.221 cell lines by assaying luciferase activity in the presence of cell lysates (90). Our results suggest that KIR clustering is an active process. However, azide is a potent metabolic inhibitor with the potential to interfere with a broad-spectrum of cellular processes and thus we cannot rule out any effects unrelated to actin polymerization. Our results contradict those of a previous study of HLA-C-GFP clustering (90). Perhaps these data are reconciled by the demonstration that actin polymerization effects the early accumulation of KIR but not the accumulation of KIR following long periods of co-incubation with target cells. Confocal microscopy could be used to examine KIR clustering in the presence of azide at later time points after cell mixing; however, longer incubation times with azide may exacerbate the toxic effects which are already apparent at much earlier time points. Other pharmacological inhibitors, including cyanide, dinitrophenol, antimycin A, and rotenone, could be used to further examine the requirement of intracellular ATP for KIR clustering. However, as was the case with azide, the specificity and cellular toxicity of these other pharmacological inhibitors would be an issue.

The absence of an effect of the pharmacological inhibitor PP2 suggests that KIR clustering is not a Src family kinase-dependent process. The lack of a requirement for Src family kinases could be the result of redundancy by other protein kinases. It would, therefore, be of interest to continue to delineate the upstream signaling pathways

involved in KIR clustering. To accomplish this, KIR2DL1-GFP clustering would be examined in the presence of pharmacological inhibitors of other signaling kinases expressed in NK cells. To begin, herbimycin A and genistein, which are potent and cell-permeable protein tyrosine kinase inhibitors, could be used to confirm that protein tyrosine kinase activation is necessary for KIR clustering. KIR2DL1-GFP clustering would then be examined in the presence of wortmannin or LY294002 (inhibitors of PI3K), piceatannol (an inhibitor of Syk family kinases), and rotterlin and GF109203X (inhibitors of PKC). As with all experiments using pharmacological inhibitors, factors such as inhibitor specificity and cell permeability would have to be considered.

We have investigated the role of the actin cytoskeleton in KIR clustering at the inhibitory NK cell immunological synapse in living cells. Cytolysis, conjugate formation, and KIR-EGFP clustering were examined in the presence of cytochalasin D, a reversible inhibitor of actin polymerization. Contrary to a previously published study, in our hands, full-length receptor clustering was inhibited in the presence of a standard dose (10 μ M) of cytochalasin D. This discrepancy was reconciled when, in collaboration with Dan Davis' lab, the kinetics of KIR clustering were examined at the inhibitory and activating NK cell immunological synapse in the presence or absence of 10 μ M (the standard dose) of cytochalasin D. Our kinetic analysis of KIR clustering indicates KIR clustering is a relatively rapid process reaching its maximum by 10 minutes. We have further shown that formation of new actin filaments was required for efficient clustering of KIR, since KIR enrichment took much longer in the presence of a standard dose of cytochalasin D. Although KIR was seen to accumulate at the 40 minutes time point in untreated conjugates, the rapid KIR clustering driven by remodeling of the cytoskeleton

is most likely key (relevant) to the function of KIR since taking 20–40 minutes to accumulate would often be too late to counteract activating signals.

Rapid clustering of KIR driven by remodeling of the cytoskeleton similar to how receptors are translocated in other cell types is an appealing idea because activation of cytotoxicity can occur within a few minutes (77, 80, 105-107). In other words, given that activation of cytotoxicity is a rapid process, the rate of KIR accumulation must be sufficient to block activating receptors that presumably are rapidly recruited to the synapse during activation of effector function. Indeed, we have previously shown that the degree of clustering correlates with the strength of the inhibitory signal (88). Another consideration is that the actin filament formation that is relevant for rapid KIR clustering need not be stimulated by interaction with the target cell but instead could be part of the normal turnover of F-actin in NK cells or even in the target cells. Of note, the actin cytoskeleton of cytotoxic cells that are migrating is in constant flux with new polymerization being favored at the leading edge and depolymerization at the trailing edge (uropod) (reviewed in (9)). Interestingly, the actin-based motility machinery of migrating cells is also common to neuronal processes (108). The migration of neurons and the extension of neurites require the organized polymerization of F-actin filaments at a membrane extension (the leading edge) (108). Of note, a study by Star *et al.* of dendritic spines suggests that virtually all actin in the spine is in a dynamic state (109). Dendritic spines, which are tree-like extensions of neurons, are the contact sites for most excitatory synapses in the human brain (110). Perhaps the actin cytoskeleton in NK cells is in a dynamic state, similar to what has been observed in neuronal cells.

Further investigation into the requirement of the actin cytoskeleton for efficient KIR clustering will require the determination of which (if any) F-actin regulatory mechanisms are also involved in inhibitory receptor enrichment. F-actin can be regulated by different mechanisms including those that stimulate formation of filaments such as Vav-1/Rac1 (reviewed in (111)) and WASP/Arp2/3 (reviewed in (112)), and those that prevent actin disassembly such as RhoA/ROCK/LIMK/cofilin (113, 114). Vav1, Vav2, Rac1, WASP and RhoA have all been implicated in activation of cytotoxicity in NK cells (115, 116) (15, 85). Furthermore, it has been suggested that the LFA-1/Vav1 pathway may act upstream of KIR (117). Gene specific silencing by RNA interference (RNAi) could be used to determine whether these F-actin regulatory signaling pathways are required for KIR-EGFP clustering. For our purpose, this would involve preparing and then introducing double stranded RNA into an NK cell in order to cause degradation of the complementary mRNA and thus silencing of a specific (targeted) gene of interest. Confocal microscopy would be used determine the frequency of clustering of the KIR-EGFP in our stable human NK cell lines following gene silencing by RNAi. A decrease in mRNA expression could be confirmed by semi-quantitative RT-PCR and reduction in protein expression could be detected by Western blot. A standard ⁵¹Cr cytotoxicity assay could also be used to monitor for loss of function, assuming that redundancy between signaling molecules is not an issue. There is precedence for the use of gene specific silencing by RNAi in NK cells. Antisense oligodeoxynucleotide treatments has been used in human NK cell populations and siRNA has been used in both primary human NK cells and a human NK cell line (118, 119).

The role of actin polymerization in KIR clustering must be reconciled with the observation that F-actin does not increase at an inhibitory NK cell immunological synapse (84, 120). It is possible that initial actin polymerization is required for KIR tracking to the immunological synapse. However, once KIR is engaged and maintained at the immunological synapse, the inhibitory receptor may mediate actin depolymerization as a means to disrupt activation signals, thereby resulting in no detectable net effect on actin polymerization. In helper T cells, Vav is an important regulator of the cell surface rearrangements during productive T cell activation (121). Work with vav *-/-* mice has led to the suggestion that the protooncogene vav is an important mediator of the actin cytoskeleton-driven process that drives receptor accumulation at the helper T cell immunological synapse (121). It has been shown in YTS cells that KIR associated SHP-1 targets Vav1, for dephosphorylation (65). Thus, in NK cells, it is possible that the early dephosphorylation of Vav1 by SHP-1 blocks the Vav1 induced actin polymerization essential for activation of NK cell effector function (65).

Cytochalasin D disrupts the actin cytoskeleton by binding to the barbed ends of rapidly growing microfilaments but does not interfere with basal levels of depolymerization leading to a net reduction in F-actin. The block of lysis at low doses of cytochalasin D is consistent with recent findings by Wulfing *et al.* that NK cell killing is particularly sensitive to interference with cytoskeletal dynamics (122). In their study, Wulfing *et al.* report that NK cell cytoskeletal polarization occurred in a stepwise fashion and a moderate interference with cytoskeletal dynamics using Jasplakinolide was sufficient to block NK cell lysis but not cytotoxic T cell lysis. Interestingly, the low

doses of cytochalasin D used in our study had little to no effect on KIR clustering. At present we are unable to explain why receptor clustering is not as sensitive to minor interference with cytoskeletal dynamics. There is precedence for differential effects of cytochalasin D doses in lymphocytes. Low doses of cytochalasin D are thought to stimulate adhesion by the release of LFA-1 from cytoskeletal restraints, whereas high doses are thought to dramatically reduce adhesion by blocking establishment of new connections to the cytoskeleton (123, 124). A similar dichotomy could explain why, in our study, low doses are sufficient to block cytolysis while high doses are required to block KIR clustering. Moreover, it has previously been shown that although subtle changes in the actin cytoskeleton are detectable at nanomolar concentrations, which correlates with disruption of mitosis in adherent cells, the changes in actin are much more dramatic at micromolar concentrations (125). Perhaps KIR clustering relies solely on the basal levels F-actin, and so the levels present after brief treatment with the low doses of cytochalasin D used in our study may be sufficient to facilitate inhibitory receptor enrichment. Alternatively, cytochalasin D may act by disrupting attachments of barbed ends to membranes or other cellular structures (126). If this were true, then perhaps at the higher doses of cytochalasin D used in our study, a greater proportion of filaments would be displaced and retracted thereby exceeding the threshold level necessary for inhibition of KIR clustering. We cannot preclude the possibility that the standard 10 μ M dose of cytochalasin D is having effects on processes other than actin cytoskeleton remodeling and that these processes are key to KIR clustering. It is also possible that lower doses of cytochalasin D are having effects on processes dependent or independent

of the actin cytoskeleton and that these processes are key to lysis and adhesion, but not to inhibitory receptor clustering.

Preliminary work suggests that probing a Western blot of these lysates with anti-phosphotyrosine (4G10) and anti-KIR (LIG1) allows us to visualize the phosphorylation status of the KIR2DL1-GFP receptor following stimulation with resistant or sensitive target cells at 0, 30, 60, 90 and 120 seconds after cell mixing. Indeed it appears that we are able to detect KIR2DL1-GFP phosphorylation as early as 90 seconds following stimulation with resistant target cells. In addition, it appears that this phosphorylation of KIR2DL1-GFP is blocked in the presence of 20 μ M cytochalasin D although this experiment must be repeated using the standard 10 μ M dose. In light of the dose-dependent effects of cytochalasin D on KIR-EGFP clustering, it may be of interest to examine KIR phosphorylation with a cytochalasin D dose response. Given that 10 μ M cytochalasin D did not have a pronounced effect on KIR clustering at 40 minutes after cell mixing, it may also be of interest to examine the effect of this standard dose on KIR2DL1-GFP phosphorylation at later time points after cell mixing.

Further investigation of the proposed dose-dependent effects of cytochalasin D on KIR clustering could also be accomplished using confocal microscopy. Staining with phalloidin-Alexafluor633[®] could be used to visualize F-actin in the presence of decreasing concentrations of cytochalasin D. Given that KIR clustering and phalloidin-Alexafluor633[®] staining appears to reach their maximums by 10 minutes and 20 minutes, respectively, images of activating and inhibitory NK cell immune synapses in the presence of decreasing concentrations of cytochalasin D would be collected 0 to 20 minutes after cell mixing. Close examination at early time points (0 to 10 minutes) at

short (1 minute) intervals would also be necessary given that as early as 1 minute after cell mixing, the location of SHP-1 distinguishes the activating NK cell immune synapse from the inhibitory NK cell immune synapse (87). Another strategy would be to use of beads to monitor the movement of the cortical actin cytoskeleton in the presence of standard (high) and low doses of cytochalasin D (77). NK cells would be surface biotinylated with an amine-reactive form of biotin in order to facilitate attachment of large streptavidin beads (77). Alternatively, a lipid that is biotinylated at its head could be exchanged into the cell surface of NK cells from liposomes in order to facilitate attachment to streptavidin beads (77) (127). Bead movement would be visualized using confocal microscopy in resting (unstimulated) NK cells, in NK cells conjugated with sensitive target cells (activating NK cell immunological synapse) and in NK cells conjugated to resistant target cells (inhibitory NK cell immunological synapse). The effects of cytochalasin D on bead and/or KIR-EGFP movement with dose response would also be evaluated. We have found that KIR clustering is not as sensitive to minor interference with cytoskeletal dynamics. To address the issue, it may be of interest to determine the requirement of sustained actin dynamics for KIR clustering using a novel approach developed by Tskvitaria-Fuller *et al.* (78). Briefly, a membrane-permeable version of the C-terminal effector domain of the WASP (tat WASP VCA) was used as a tool to selectively block cytoskeletal dynamics associated with optimal, but not limiting, primary helper T cell activation (78). While early T cell actin cytoskeleton accumulation at the immunological synapse was observed, its lamellopodial pattern, the extent of sustained actin accumulation, and the central pattern of F-actin accumulation were partially yet significantly blocked following introduction of tat WASP VCA into T cells

(78). Confocal microscopy could be used to monitor KIR-EGFP enrichment in our NK cell lines following the introduction of tat WASP VCA (to block sustained, but not early, actin accumulation).

We have also determined that blocking the activated form of LFA-1 inhibited tight conjugate formation but that KIR clustering is normal in conjugates that form in the absence of activated LFA-1 mediated interactions. Since the results with anti-LFA-1 did not mimic treatment with cytochalasin D, it suggests that cytochalasin D exerts a more complete block on adhesion or another process that is involved in KIR clustering. Similarly, a recent report using insect cells to express KIR ligands indicated KIR clustered and was phosphorylated independently of LFA-1/ICAM-1 interactions (62). Another cell surface molecule that promotes adhesion to a target cell and provides costimulation for cytotoxic effector function in NK cells is CD2, a transmembrane protein belonging to the Immunoglobulin receptor superfamily (24, 128, 129). In T cells, CD2 is thought to mediate the redistribution of cell surface molecules required for SMAC formation and CD2 itself is found in the SMAC (130). At present, CD2 is thought to mediate cell surface molecule rearrangement by coupling to the actin cytoskeleton via an interaction with an intracellular adaptor (CD2AP) (131). Intact WASP is required for CD2 clustering in T cells (132). CD2 accumulation has also been reported for the activating NK cell immunological synapse of the human NK cell line YTS (10). However, unlike T cells, CD2 clustering at the NK cell requires both actin polymerization (as evidenced by treatment with cytochalasin D) and WASP function (10). Examination the distribution of CD2 and KIR-EGFP at the activating NK cell immunological synapse and the inhibitory NK cell immunological synapse may provide

some insight into the role (if any) CD2 plays in KIR clustering. It would also be of interest to examine KIR-EGFP clustering in the presence of anti-CD2 antibodies to establish whether there is a complete block (as seen in the presence of cytochalasin D) or there is no change in KIR clustering (as seen in the presence of anti-LFA-1). Similarly, KIR-EGFP could also be examined in the presence of anti-CD2 and anti-LFA-1.

In summary, the observations presented in this study demonstrate that the actin cytoskeleton and the cytoplasmic tail of KIR play an important role in the efficiency of KIR accumulation at the inhibitory NK cell immunological synapse. Based on these results we propose a mechanism whereby KIR associates (directly or indirectly via an adaptor protein) via the distal portion of its cytoplasmic tail with F-actin in order to actively track towards the inhibitory NK cell immunological synapse (Figure 43). Enrichment of KIR would then facilitate the phosphorylation of the ITIMs that in turn is necessary for recruitment and activation of SHP-1. Activated SHP-1 dephosphorylates Vav1 and thus inactivates this GEF. Vav1 would no longer activate Rac1 thereby blocking the actin polymerization necessary for activation of NK cell effector function, including receptor movement, granule mobilization, and signaling cascades. Although KIR accumulates at the interface with a target cell provided there is sufficient amount of contact time, we propose that the rapid KIR redistribution of KIR mediated by a dynamic actin cytoskeleton is what is relevant to the inhibitory function of KIR. Our findings suggest that KIR clustering cannot be explained solely on the basis of simple diffusion towards the interface with the target cell but rather is a complex process (90). There are many unanswered questions regarding the regulation of KIR clustering at the inhibitory

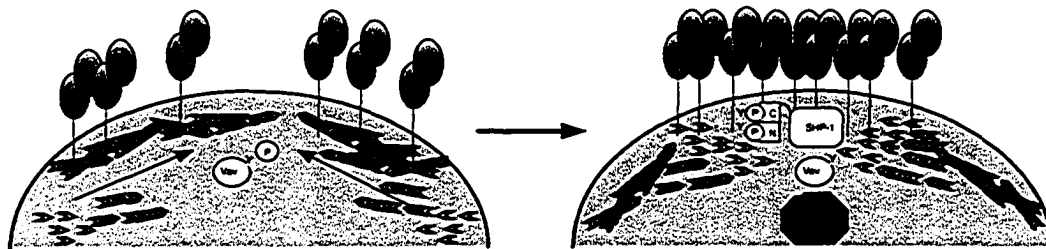


Figure 43 : Proposed model for KIR clustering at the inhibitory NK cell immunological synapse. According to this model, the transport of KIR is modulated by the actin cytoskeleton. Enrichment of KIR then facilitates the phosphorylation of the ITIMs in the cytoplasmic tail that is in turn necessary for recruitment and activation of SHP-1. Activated SHP-1 desphosphorylates Vav thereby blocking the actin polymerization at the immunological synapse necessary for activation of NK cell effector function, including receptor movement, granule mobilization, and signaling cascades. For example, dephosphorylated Vav1 would no longer serve as an activator for Rac1 thereby disrupting a pathway that drives cytotoxic function in NK cells through granule mobilization.

NK cell immune synapse and we have herein outlined strategies for further investigation into the factors regulating KIR enrichment at the inhibitory NK cell immunological synapse. It will be interesting to dissect the underlying mechanisms and determine if there are implications for other inhibitory receptors.

Referenced Literature

1. Trinchieri, G. 1989. Biology of natural killer cells. *Adv Immunol* 47:187.
2. Trinchieri, G. 1995. Natural killer cells wear different hats: effector cells of innate resistance and regulatory cells of adaptive immunity and of hematopoiesis. *Semin Immunol* 7:83.
3. Ljunggren, H. G., and K. Karre. 1990. In search of the 'missing self': MHC molecules and NK cell recognition. *Immunol Today* 11:237.
4. Shawar, S. M., J. M. Vyas, J. R. Rodgers, and R. R. Rich. 1994. Antigen presentation by major histocompatibility complex class I-B molecules. *Annu Rev Immunol* 12:839.
5. Borrego, F., M. Ulbrecht, E. H. Weiss, J. E. Coligan, and A. G. Brooks. 1998. Recognition of human histocompatibility leukocyte antigen (HLA)-E complexed with HLA class I signal sequence-derived peptides by CD94/NKG2 confers protection from natural killer cell-mediated lysis. *J Exp Med* 187:813.
6. Braud, V. M., D. S. Allan, C. A. O'Callaghan, K. Soderstrom, A. D'Andrea, G. S. Ogg, S. Lazetic, N. T. Young, J. I. Bell, J. H. Phillips, L. L. Lanier, and A. J. McMichael. 1998. HLA-E binds to natural killer cell receptors CD94/NKG2A, B and C. *Nature* 391:795.

7. Karre, K., H. G. Ljunggren, G. Piontek, and R. Kiessling. 1986. Selective rejection of H-2-deficient lymphoma variants suggests alternative immune defence strategy. *Nature* 319:675.
8. Schmidt, A., and M. N. Hall. 1998. Signaling to the actin cytoskeleton. *Annu Rev Cell Dev Biol* 14:305.
9. Samstag, Y., S. M. Eibert, M. Klemke, and G. H. Wabnitz. 2003. Actin cytoskeletal dynamics in T lymphocyte activation and migration. *J Leukoc Biol* 73:30.
10. Orange, J. S., K. E. Harris, M. M. Andzelm, M. M. Valter, R. S. Geha, and J. L. Strominger. 2003. The mature activating natural killer cell immunologic synapse is formed in distinct stages. *Proc Natl Acad Sci U S A* 100:14151.
11. Katz, P., A. M. Zaytoun, and J. H. Lee, Jr. 1982. Mechanisms of human cell-mediated cytotoxicity. III. Dependence of natural killing on microtubule and microfilament integrity. *J Immunol* 129:2816.
12. Stinchcombe, J. C., D. C. Barral, E. H. Mules, S. Booth, A. N. Hume, L. M. Machesky, M. C. Seabra, and G. M. Griffiths. 2001. Rab27a is required for regulated secretion in cytotoxic T lymphocytes. *J Cell Biol* 152:825.
13. Khurana, D., and P. J. Leibson. 2003. Regulation of lymphocyte-mediated killing by GTP-binding proteins. *J Leukoc Biol* 73:333.

14. Jiang, K., B. Zhong, D. L. Gilvary, B. C. Corliss, E. Hong-Geller, S. Wei, and J. Y. Djeu. 2000. Pivotal role of phosphoinositide-3 kinase in regulation of cytotoxicity in natural killer cells. *Nat Immunol* 1:419.
15. Lou, Z., D. D. Billadeau, D. N. Savoy, R. A. Schoon, and P. J. Leibson. 2001. A role for a RhoA/ROCK/LIM-kinase pathway in the regulation of cytotoxic lymphocytes. *J Immunol* 167:5749.
16. Constantin, G., M. Majeed, C. Giagulli, L. Piccio, J. Y. Kim, E. C. Butcher, and C. Laudanna. 2000. Chemokines trigger immediate beta2 integrin affinity and mobility changes: differential regulation and roles in lymphocyte arrest under flow. *Immunity* 13:759.
17. Beals, C. R., A. C. Edwards, R. J. Gottschalk, T. W. Kuijpers, and D. E. Staunton. 2001. CD18 activation epitopes induced by leukocyte activation. *J Immunol* 167:6113.
18. Stewart, M. P., C. Cabanas, and N. Hogg. 1996. T cell adhesion to intercellular adhesion molecule-1 (ICAM-1) is controlled by cell spreading and the activation of integrin LFA-1. *J Immunol* 156:1810.
19. Dustin, M. L., and T. A. Springer. 1989. T-cell receptor cross-linking transiently stimulates adhesiveness through LFA-1. *Nature* 341:619.
20. van Kooyk, Y., S. J. van Vliet, and C. G. Figdor. 1999. The actin cytoskeleton regulates LFA-1 ligand binding through avidity rather than affinity changes. *J Biol Chem* 274:26869.

21. Stewart, M. P., A. McDowall, and N. Hogg. 1998. LFA-1-mediated adhesion is regulated by cytoskeletal restraint and by a Ca²⁺-dependent protease, calpain. *J Cell Biol* 140:699.
22. Pardi, R., L. Inverardi, and J. R. Bender. 1992. Regulatory mechanisms in leukocyte adhesion: flexible receptors for sophisticated travelers. *Immunol Today* 13:224.
23. Burshtyn, D. N., J. Shin, C. Stebbins, and E. O. Long. 2000. Adhesion to target cells is disrupted by the killer cell inhibitory receptor. *Curr Biol* 10:777.
24. Barber, D. F., and E. O. Long. 2003. Coexpression of CD58 or CD48 with intercellular adhesion molecule 1 on target cells enhances adhesion of resting NK cells. *J Immunol* 170:294.
25. Barber, D. F., M. Faure, and E. O. Long. 2004. LFA-1 contributes an early signal for NK cell cytotoxicity. *J Immunol* 173:3653.
26. Mocsai, A., M. Zhou, F. Meng, V. L. Tybulewicz, and C. A. Lowell. 2002. Syk is required for integrin signaling in neutrophils. *Immunity* 16:547.
27. Sivori, S., M. Vitale, L. Morelli, L. Sanseverino, R. Augugliaro, C. Bottino, L. Moretta, and A. Moretta. 1997. p46, a novel natural killer cell-specific surface molecule that mediates cell activation. *J Exp Med* 186:1129.
28. Pessino, A., S. Sivori, C. Bottino, A. Malaspina, L. Morelli, L. Moretta, R. Biassoni, and A. Moretta. 1998. Molecular cloning of NKp46: a novel member of

the immunoglobulin superfamily involved in triggering of natural cytotoxicity. *J Exp Med* 188:953.

29. Pende, D., S. Parolini, A. Pessino, S. Sivori, R. Augugliaro, L. Morelli, E. Marcenaro, L. Accame, A. Malaspina, R. Biassoni, C. Bottino, L. Moretta, and A. Moretta. 1999. Identification and molecular characterization of NKp30, a novel triggering receptor involved in natural cytotoxicity mediated by human natural killer cells. *J Exp Med* 190:1505.
30. Vitale, M., C. Bottino, S. Sivori, L. Sanseverino, R. Castriconi, E. Marcenaro, R. Augugliaro, L. Moretta, and A. Moretta. 1998. NKp44, a novel triggering surface molecule specifically expressed by activated natural killer cells, is involved in non-major histocompatibility complex-restricted tumor cell lysis. *J Exp Med* 187:2065.
31. Wu, J., Y. Song, A. B. Bakker, S. Bauer, T. Spies, L. L. Lanier, and J. H. Phillips. 1999. An activating immunoreceptor complex formed by NKG2D and DAP10. *Science* 285:730.
32. Chang, C., J. Dietrich, A. G. Harpur, J. A. Lindquist, A. Haude, Y. W. Loke, A. King, M. Colonna, J. Trowsdale, and M. J. Wilson. 1999. Cutting edge: KAP10, a novel transmembrane adapter protein genetically linked to DAP12 but with unique signaling properties. *J Immunol* 163:4651.
33. Reth, M. 1989. Antigen receptor tail clue. *Nature* 338:383.

34. Cambier, J. C. 1995. New nomenclature for the Reth motif (or ARH1/TAM/ARAM/YXXL). *Immunol Today* 16:110.
35. Lanier, L. L., B. C. Corliss, J. Wu, C. Leong, and J. H. Phillips. 1998. Immunoreceptor DAP12 bearing a tyrosine-based activation motif is involved in activating NK cells. *Nature* 391:703.
36. Long, E. O., D. F. Barber, D. N. Burshtyn, M. Faure, M. Peterson, S. Rajagopalan, V. Renard, M. Sandusky, C. C. Stebbins, N. Wagtmann, and C. Watzl. 2001. Inhibition of natural killer cell activation signals by killer cell immunoglobulin-like receptors (CD158). *Immunol Rev* 181:223.
37. Brooks, A. G., P. E. Posch, C. J. Scorzelli, F. Borrego, and J. E. Coligan. 1997. NKG2A complexed with CD94 defines a novel inhibitory natural killer cell receptor. *J Exp Med* 185:795.
38. Burshtyn, D. N., A. M. Scharenberg, N. Wagtmann, S. Rajagopalan, K. Berrada, T. Yi, J. P. Kinet, and E. O. Long. 1996. Recruitment of tyrosine phosphatase HCP by the killer cell inhibitor receptor. *Immunity* 4:77.
39. Carretero, M., G. Palmieri, M. Llano, V. Tullio, A. Santoni, D. E. Geraghty, and M. Lopez-Botet. 1998. Specific engagement of the CD94/NKG2-A killer inhibitory receptor by the HLA-E class Ib molecule induces SHP-1 phosphatase recruitment to tyrosine-phosphorylated NKG2-A: evidence for receptor function in heterologous transfectants. *Eur J Immunol* 28:1280.

40. Marsh, S. G., P. Parham, B. Dupont, D. E. Geraghty, J. Trowsdale, D. Middleton, C. Vilches, M. Carrington, C. Witt, L. A. Guethlein, H. Shilling, C. A. Garcia, K. C. Hsu, and H. Wain. 2003. Killer-cell immunoglobulin-like receptor (KIR) nomenclature report, 2002. *Tissue Antigens* 62:79.
41. Vilches, C., and P. Parham. 2002. KIR: diverse, rapidly evolving receptors of innate and adaptive immunity. *Annu Rev Immunol* 20:217.
42. Burshtyn, D. N., A. S. Lam, M. Weston, N. Gupta, P. A. Warmerdam, and E. O. Long. 1999. Conserved residues amino-terminal of cytoplasmic tyrosines contribute to the SHP-1-mediated inhibitory function of killer cell Ig-like receptors. *J Immunol* 162:897.
43. Fan, Q. R., E. O. Long, and D. C. Wiley. 2001. Crystal structure of the human natural killer cell inhibitory receptor KIR2DL1-HLA-Cw4 complex. *Nat Immunol* 2:452.
44. Rajagopalan, S., and E. O. Long. 1998. Zinc bound to the killer cell-inhibitory receptor modulates the negative signal in human NK cells. *J Immunol* 161:1299.
45. Rajagopalan, S., C. C. Winter, N. Wagtmann, and E. O. Long. 1995. The Ig-related killer cell inhibitory receptor binds zinc and requires zinc for recognition of HLA-C on target cells. *J Immunol* 155:4143.
46. Jongeneel, C. V., J. Bouvier, and A. Bairoch. 1989. A unique signature identifies a family of zinc-dependent metallopeptidases. *FEBS Lett* 242:211.

47. Vales-Gomez, M., R. A. Erskine, M. P. Deacon, J. L. Strominger, and H. T. Reyburn. 2001. The role of zinc in the binding of killer cell Ig-like receptors to class I MHC proteins. *Proc Natl Acad Sci U S A* 98:1734.
48. Cosman, D., N. Fanger, L. Borges, M. Kubin, W. Chin, L. Peterson, and M. L. Hsu. 1997. A novel immunoglobulin superfamily receptor for cellular and viral MHC class I molecules. *Immunity* 7:273.
49. Colonna, M., F. Navarro, T. Bellon, M. Llano, P. Garcia, J. Samaridis, L. Angman, M. Cella, and M. Lopez-Botet. 1997. A common inhibitory receptor for major histocompatibility complex class I molecules on human lymphoid and myelomonocytic cells. *J Exp Med* 186:1809.
50. Chapman, T. L., A. P. Heikeman, and P. J. Bjorkman. 1999. The inhibitory receptor LIR-1 uses a common binding interaction to recognize class I MHC molecules and the viral homolog UL18. *Immunity* 11:603.
51. Chapman, T. L., A. P. Heikema, A. P. West, Jr., and P. J. Bjorkman. 2000. Crystal structure and ligand binding properties of the D1D2 region of the inhibitory receptor LIR-1 (ILT2). *Immunity* 13:727.
52. Windebank, K. P., R. T. Abraham, G. Powis, R. A. Olsen, T. J. Barna, and P. J. Leibson. 1988. Signal transduction during human natural killer cell activation: inositol phosphate generation and regulation by cyclic AMP. *J Immunol* 141:3951.

53. Binstadt, B. A., K. M. Brumbaugh, and P. J. Leibson. 1997. Signal transduction by human NK cell MHC-recognizing receptors. *Immunol Rev* 155:197.
54. Vyas, Y. M., H. Maniar, and B. Dupont. 2002. Visualization of signaling pathways and cortical cytoskeleton in cytolytic and noncytolytic natural killer cell immune synapses. *Immunol Rev* 189:161.
55. Jiang, K., B. Zhong, D. L. Gilvary, B. C. Corliss, E. Vivier, E. Hong-Geller, S. Wei, and J. Y. Djeu. 2002. Syk regulation of phosphoinositide 3-kinase-dependent NK cell function. *J Immunol* 168:3155.
56. Lanier, L. L. 2003. Natural killer cell receptor signaling. *Curr Opin Immunol* 15:308.
57. Brumbaugh, K. M., B. A. Binstadt, D. D. Billadeau, R. A. Schoon, C. J. Dick, R. M. Ten, and P. J. Leibson. 1997. Functional role for Syk tyrosine kinase in natural killer cell-mediated natural cytotoxicity. *J Exp Med* 186:1965.
58. Lou, Z., D. Jevremovic, D. D. Billadeau, and P. J. Leibson. 2000. A balance between positive and negative signals in cytotoxic lymphocytes regulates the polarization of lipid rafts during the development of cell-mediated killing. *J Exp Med* 191:347.
59. Ravetch, J. V., and L. L. Lanier. 2000. Immune inhibitory receptors. *Science* 290:84.

60. Kaufman, D. S., R. A. Schoon, M. J. Robertson, and P. J. Leibson. 1995. Inhibition of selective signaling events in natural killer cells recognizing major histocompatibility complex class I. *Proc Natl Acad Sci U S A* 92:6484.
61. Binstadt, B. A., K. M. Brumbaugh, C. J. Dick, A. M. Scharenberg, B. L. Williams, M. Colonna, L. L. Lanier, J. P. Kinet, R. T. Abraham, and P. J. Leibson. 1996. Sequential involvement of Lck and SHP-1 with MHC-recognizing receptors on NK cells inhibits FcR-initiated tyrosine kinase activation. *Immunity* 5:629.
62. Faure, M., D. F. Barber, S. M. Takahashi, T. Jin, and E. O. Long. 2003. Spontaneous clustering and tyrosine phosphorylation of NK cell inhibitory receptor induced by ligand binding. *J Immunol* 170:6107.
63. Long, E. O., D. N. Burshtyn, W. P. Clark, M. Peruzzi, S. Rajagopalan, S. Rojo, N. Wagtmann, and C. C. Winter. 1997. Killer cell inhibitory receptors: diversity, specificity, and function. *Immunol Rev* 155:135.
64. Barford, D., and B. G. Neel. 1998. Revealing mechanisms for SH2 domain mediated regulation of the protein tyrosine phosphatase SHP-2. *Structure* 6:249.
65. Stebbins, C. C., C. Watzl, D. D. Billadeau, P. J. Leibson, D. N. Burshtyn, and E. O. Long. 2003. Vav1 dephosphorylation by the tyrosine phosphatase SHP-1 as a mechanism for inhibition of cellular cytotoxicity. *Mol Cell Biol* 23:6291.
66. Valiante, N. M., J. H. Phillips, L. L. Lanier, and P. Parham. 1996. Killer cell inhibitory receptor recognition of human leukocyte antigen (HLA) class I blocks

formation of a pp36/PLC-gamma signaling complex in human natural killer (NK) cells. *J Exp Med* 184:2243.

67. Binstadt, B. A., D. D. Billadeau, D. Jevremovic, B. L. Williams, N. Fang, T. Yi, G. A. Koretzky, R. T. Abraham, and P. J. Leibson. 1998. SLP-76 is a direct substrate of SHP-1 recruited to killer cell inhibitory receptors. *J Biol Chem* 273:27518.
68. Monks, C. R., B. A. Freiberg, H. Kupfer, N. Sciaky, and A. Kupfer. 1998. Three-dimensional segregation of supramolecular activation clusters in T cells. *Nature* 395:82.
69. Grakoui, A., S. K. Bromley, C. Sumen, M. M. Davis, A. S. Shaw, P. M. Allen, and M. L. Dustin. 1999. The immunological synapse: a molecular machine controlling T cell activation. *Science* 285:221.
70. Lee, K. H., A. D. Holdorf, M. L. Dustin, A. C. Chan, P. M. Allen, and A. S. Shaw. 2002. T cell receptor signaling precedes immunological synapse formation. *Science* 295:1539.
71. Huppa, J. B., M. Gleimer, C. Sumen, and M. M. Davis. 2003. Continuous T cell receptor signaling required for synapse maintenance and full effector potential. *Nat Immunol* 4:749.
72. Huppa, J. B., and M. M. Davis. 2003. T-cell-antigen recognition and the immunological synapse. *Nat Rev Immunol* 3:973.

73. Lee, K. H., A. R. Dinner, C. Tu, G. Campi, S. Raychaudhuri, R. Varma, T. N. Sims, W. R. Burack, H. Wu, J. Wang, O. Kanagawa, M. Markiewicz, P. M. Allen, M. L. Dustin, A. K. Chakraborty, and A. S. Shaw. 2003. The immunological synapse balances T cell receptor signaling and degradation. *Science* 302:1218.
74. Davis, S. J., and P. A. van der Merwe. 2001. The immunological synapse: required for T cell receptor signalling or directing T cell effector function? *Curr Biol* 11:R289.
75. Poo, W. J., L. Conrad, and C. A. Janeway, Jr. 1988. Receptor-directed focusing of lymphokine release by helper T cells. *Nature* 332:378.
76. Wulfing, C., M. D. Sjaastad, and M. M. Davis. 1998. Visualizing the dynamics of T cell activation: intracellular adhesion molecule 1 migrates rapidly to the T cell/B cell interface and acts to sustain calcium levels. *Proc Natl Acad Sci U S A* 95:6302.
77. Wulfing, C., and M. M. Davis. 1998. A receptor/cytoskeletal movement triggered by costimulation during T cell activation. *Science* 282:2266.
78. Tskvitaria-Fuller, I., A. L. Rozelle, H. L. Yin, and C. Wulfing. 2003. Regulation of sustained actin dynamics by the TCR and costimulation as a mechanism of receptor localization. *J Immunol* 171:2287.
79. Faure, S., L. I. Salazar-Fontana, M. Semichon, V. L. Tybulewicz, G. Bismuth, A. Trautmann, R. N. Germain, and J. Delon. 2004. ERM proteins regulate cytoskeleton relaxation promoting T cell-APC conjugation. *Nat Immunol* 5:272.

80. Stinchcombe, J. C., G. Bossi, S. Booth, and G. M. Griffiths. 2001. The immunological synapse of CTL contains a secretory domain and membrane bridges. *Immunity* 15:751.
81. Faroudi, M., C. Utzny, M. Salio, V. Cerundolo, M. Guiraud, S. Muller, and S. Valitutti. 2003. Lytic versus stimulatory synapse in cytotoxic T lymphocyte/target cell interaction: manifestation of a dual activation threshold. *Proc Natl Acad Sci USA* 100:14145.
82. McGavern, D. B., U. Christen, and M. B. Oldstone. 2002. Molecular anatomy of antigen-specific CD8(+) T cell engagement and synapse formation in vivo. *Nat Immunol* 3:918.
83. Vyas, Y. M., K. M. Mehta, M. Morgan, H. Maniar, L. Butros, S. Jung, J. K. Burkhardt, and B. Dupont. 2001. Spatial organization of signal transduction molecules in the NK cell immune synapses during MHC class I-regulated noncytolytic and cytolytic interactions. *J Immunol* 167:4358.
84. McCann, F. E., B. Vanherberghen, K. Eleme, L. M. Carlin, R. J. Newsam, D. Goulding, and D. M. Davis. 2003. The size of the synaptic cleft and distinct distributions of filamentous actin, ezrin, CD43, and CD45 at activating and inhibitory human NK cell immune synapses. *J Immunol* 170:2862.
85. Orange, J. S., N. Ramesh, E. Remold-O'Donnell, Y. Sasahara, L. Koopman, M. Byrne, F. A. Bonilla, F. S. Rosen, R. S. Geha, and J. L. Strominger. 2002. Wiskott-Aldrich syndrome protein is required for NK cell cytotoxicity and

- colocalizes with actin to NK cell-activating immunologic synapses. *Proc Natl Acad Sci U S A* 99:11351.
86. Vyas, Y. M., H. Maniar, C. E. Lyddane, M. Sadelain, and B. Dupont. 2004. Ligand binding to inhibitory killer cell Ig-like receptors induce colocalization with SRC homology domain 2-containing protein tyrosine phosphatase 1 and interruption of ongoing activation signals. *J Immunol* 173:1571.
87. Vyas, Y. M., H. Maniar, and B. Dupont. 2002. Cutting edge: differential segregation of the SRC homology 2-containing protein tyrosine phosphatase-1 within the early NK cell immune synapse distinguishes noncytolytic from cytolytic interactions. *J Immunol* 168:3150.
88. Borszcz, P. D., M. Peterson, L. Standeven, S. Kirwan, M. Sandusky, A. Shaw, E. O. Long, and D. N. Burshtyn. 2003. KIR enrichment at the effector-target cell interface is more sensitive than signaling to the strength of ligand binding. *Eur J Immunol* 33:1084.
89. Carlin, L. M., K. Eleme, F. E. McCann, and D. M. Davis. 2001. Intercellular transfer and supramolecular organization of human leukocyte antigen C at inhibitory natural killer cell immune synapses. *J Exp Med* 194:1507.
90. Davis, D. M., I. Chiu, M. Fassett, G. B. Cohen, O. Mandelboim, and J. L. Strominger. 1999. The human natural killer cell immune synapse. *Proc Natl Acad Sci U S A* 96:15062.

91. Fassett, M. S., D. M. Davis, M. M. Valter, G. B. Cohen, and J. L. Strominger. 2001. Signaling at the inhibitory natural killer cell immune synapse regulates lipid raft polarization but not class I MHC clustering. *Proc Natl Acad Sci U S A* 98:14547.
92. Litwin, V., J. Gumperz, P. Parham, J. H. Phillips, and L. L. Lanier. 1993. Specificity of HLA class I antigen recognition by human NK clones: evidence for clonal heterogeneity, protection by self and non-self alleles, and influence of the target cell type. *J Exp Med* 178:1321.
93. Cohen, G. B., R. T. Gandhi, D. M. Davis, O. Mandelboim, B. K. Chen, J. L. Strominger, and D. Baltimore. 1999. The selective downregulation of class I major histocompatibility complex proteins by HIV-1 protects HIV-infected cells from NK cells. *Immunity* 10:661.
94. Standeven, L. J., L. M. Carlin, P. Borszcz, D. M. Davis, and D. N. Burshtyn. 2004. The actin cytoskeleton controls the efficiency of killer Ig-like receptor accumulation at inhibitory NK cell immune synapses. *J Immunol* 173:5617.
95. Nakamura, M. C., E. C. Niemi, M. J. Fisher, L. D. Shultz, W. E. Seaman, and J. C. Ryan. 1997. Mouse Ly-49A interrupts early signaling events in natural killer cell cytotoxicity and functionally associates with the SHP-1 tyrosine phosphatase. *J Exp Med* 185:673.
96. Melero, I., A. Salmeron, M. A. Balboa, J. Aramburu, and M. Lopez-Botet. 1994. Tyrosine kinase-dependent activation of human NK cell functions upon

- stimulation through a 58-kDa surface antigen selectively expressed on discrete subsets of NK cells and T lymphocytes. *J Immunol* 152:1662.
97. Gong, J. H., G. Maki, and H. G. Klingemann. 1994. Characterization of a human cell line (NK-92) with phenotypical and functional characteristics of activated natural killer cells. *Leukemia* 8:652.
 98. Borszcz, P. 2001. Clustering of inhibitory killer Ig-like receptors. A thesis submitted for the degree of Master of Science from the Department of Medical Microbiology & Immunology. University of Alberta, Edmonton.
 99. Quan, P. C., T. Ishizaka, and B. R. Bloom. 1982. Studies on the mechanism of NK cell lysis. *J Immunol* 128:1786.
 100. Attwood, T. K. 2002. The PRINTS database: a resource for identification of protein families. *Brief Bioinform* 3:252.
 101. Puntervoll, P., R. Linding, C. Gemund, S. Chabanis-Davidson, M. Mattingsdal, S. Cameron, D. M. Martin, G. Ausiello, B. Brannetti, A. Costantini, F. Ferre, V. Maselli, A. Via, G. Cesareni, F. Diella, G. Superti-Furga, L. Wyrwicz, C. Ramu, C. McGuigan, R. Gudavalli, I. Letunic, P. Bork, L. Rychlewski, B. Kuster, M. Helmer-Citterich, W. N. Hunter, R. Aasland, and T. J. Gibson. 2003. ELM server: A new resource for investigating short functional sites in modular eukaryotic proteins. *Nucleic Acids Res* 31:3625.
 102. Kaneko, T., T. Kumasaka, T. Ganbe, T. Sato, K. Miyazawa, N. Kitamura, and N. Tanaka. 2003. Structural insight into modest binding of a non-PXXP ligand to the

- signal transducing adaptor molecule-2 Src homology 3 domain. *J Biol Chem* 278:48162.
103. Kane, L. P., M. N. Mollenauer, and A. Weiss. 2004. A proline-rich motif in the C terminus of Akt contributes to its localization in the immunological synapse. *J Immunol* 172:5441.
104. Fan, Q. R., D. N. Garboczi, C. C. Winter, N. Wagtmann, E. O. Long, and D. C. Wiley. 1996. Direct binding of a soluble natural killer cell inhibitory receptor to a soluble human leukocyte antigen-Cw4 class I major histocompatibility complex molecule. *Proc Natl Acad Sci U S A* 93:7178.
105. Matter, A. 1979. Microcinematographic and electron microscopic analysis of target cell lysis induced by cytotoxic T lymphocytes. *Immunology* 36:179.
106. Rothstein, T. L., M. Mage, G. Jones, and L. L. McHugh. 1978. Cytotoxic T lymphocyte sequential killing of immobilized allogeneic tumor target cells measured by time-lapse microcinematography. *J Immunol* 121:1652.
107. Sanderson, C. J. 1976. The mechanism of T cell mediated cytotoxicity. II. Morphological studies of cell death by time-lapse microcinematography. *Proc R Soc Lond B Biol Sci* 192:241.
108. Meyer, G., and E. L. Feldman. 2002. Signaling mechanisms that regulate actin-based motility processes in the nervous system. *J Neurochem* 83:490.

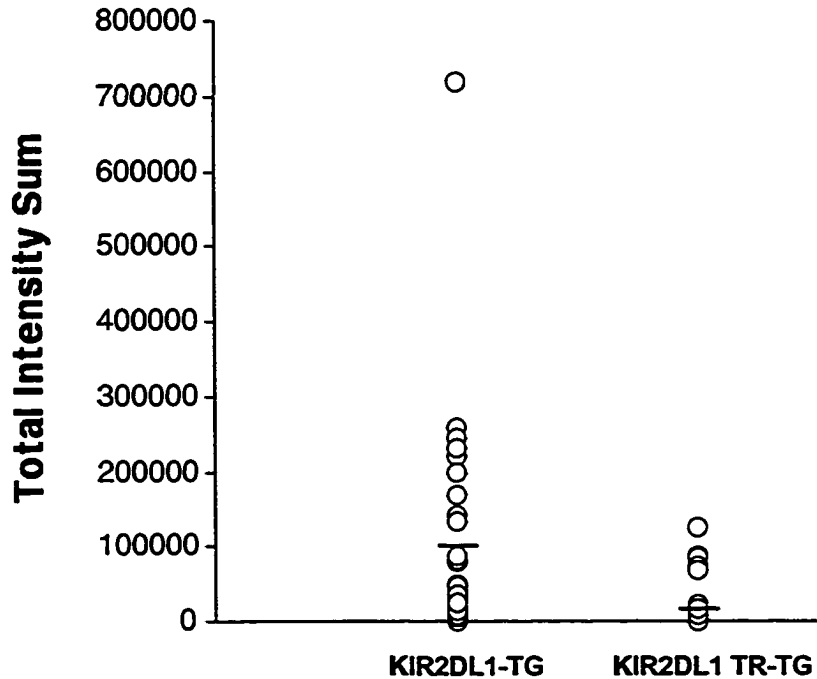
109. Star, E. N., D. J. Kwiatkowski, and V. N. Murthy. 2002. Rapid turnover of actin in dendritic spines and its regulation by activity. *Nat Neurosci* 5:239.
110. Matus, A. 2000. Actin-based plasticity in dendritic spines. *Science* 290:754.
111. Bustelo, X. R. 2000. Regulatory and signaling properties of the Vav family. *Mol Cell Biol* 20:1461.
112. Higgs, H. N., and T. D. Pollard. 2001. Regulation of actin filament network formation through ARP2/3 complex: activation by a diverse array of proteins. *Annu Rev Biochem* 70:649.
113. Maekawa, M., T. Ishizaki, S. Boku, N. Watanabe, A. Fujita, A. Iwamatsu, T. Obinata, K. Ohashi, K. Mizuno, and S. Narumiya. 1999. Signaling from Rho to the actin cytoskeleton through protein kinases ROCK and LIM-kinase. *Science* 285:895.
114. Edwards, D. C., L. C. Sanders, G. M. Bokoch, and G. N. Gill. 1999. Activation of LIM-kinase by Pak1 couples Rac/Cdc42 GTPase signalling to actin cytoskeletal dynamics. *Nat Cell Biol* 1:253.
115. Billadeau, D. D., K. M. Brumbaugh, C. J. Dick, R. A. Schoon, X. R. Bustelo, and P. J. Leibson. 1998. The Vav-Rac1 pathway in cytotoxic lymphocytes regulates the generation of cell-mediated killing. *J Exp Med* 188:549.

116. Billadeau, D. D., S. M. Mackie, R. A. Schoon, and P. J. Leibson. 2000. The Rho family guanine nucleotide exchange factor Vav-2 regulates the development of cell-mediated cytotoxicity. *J Exp Med* 192:381.
117. Riteau, B., D. F. Barber, and E. O. Long. 2003. Vav1 phosphorylation is induced by beta2 integrin engagement on natural killer cells upstream of actin cytoskeleton and lipid raft reorganization. *J Exp Med* 198:469.
118. Galandrini, R., G. Palmieri, M. Piccoli, L. Frati, and A. Santoni. 1999. Role for the Rac1 exchange factor Vav in the signaling pathways leading to NK cell cytotoxicity. *J Immunol* 162:3148.
119. Ma, L. L., C. L. Wang, G. G. Neely, S. Epelman, A. M. Krensky, and C. H. Mody. 2004. NK cells use perforin rather than granulysin for anticryptococcal activity. *J Immunol* 173:3357.
120. Dietrich, J., M. Cella, and M. Colonna. 2001. Ig-like transcript 2 (ILT2)/leukocyte Ig-like receptor 1 (LIR1) inhibits TCR signaling and actin cytoskeleton reorganization. *J Immunol* 166:2514.
121. Wulfing, C., A. Bauch, G. R. Crabtree, and M. M. Davis. 2000. The vav exchange factor is an essential regulator in actin-dependent receptor translocation to the lymphocyte-antigen-presenting cell interface. *Proc Natl Acad Sci U S A* 97:10150.

122. Wulfing, C., B. Purtic, J. Klem, and J. D. Schatzle. 2003. Stepwise cytoskeletal polarization as a series of checkpoints in innate but not adaptive cytolytic killing. *Proc Natl Acad Sci U S A* 100:7767.
123. Kucik, D. F., M. L. Dustin, J. M. Miller, and E. J. Brown. 1996. Adhesion-activating phorbol ester increases the mobility of leukocyte integrin LFA-1 in cultured lymphocytes. *J Clin Invest* 97:2139.
124. Yauch, R. L., D. P. Felsenfeld, S. K. Kraeft, L. B. Chen, M. P. Sheetz, and M. E. Hemler. 1997. Mutational evidence for control of cell adhesion through integrin diffusion/clustering, independent of ligand binding. *J Exp Med* 186:1347.
125. Wakatsuki, T., B. Schwab, N. C. Thompson, and E. L. Elson. 2001. Effects of cytochalasin D and latrunculin B on mechanical properties of cells. *J Cell Sci* 114:1025.
126. Verkhovskiy, A. B., T. M. Svitkina, and G. G. Borisy. 1997. Polarity sorting of actin filaments in cytochalasin-treated fibroblasts. *J Cell Sci* 110 (Pt 15):1693.
127. Ting, A. E., and R. E. Pagano. 1990. Detection of a phosphatidylinositol-specific phospholipase C at the surface of Swiss 3T3 cells and its potential role in the regulation of cell growth. *J Biol Chem* 265:5337.
128. Schmidt, R. E., J. P. Caulfield, J. Michon, A. Hein, M. M. Kamada, R. P. MacDermott, R. L. Stevens, and J. Ritz. 1988. T11/CD2 activation of cloned human natural killer cells results in increased conjugate formation and exocytosis of cytolytic granules. *J Immunol* 140:991.

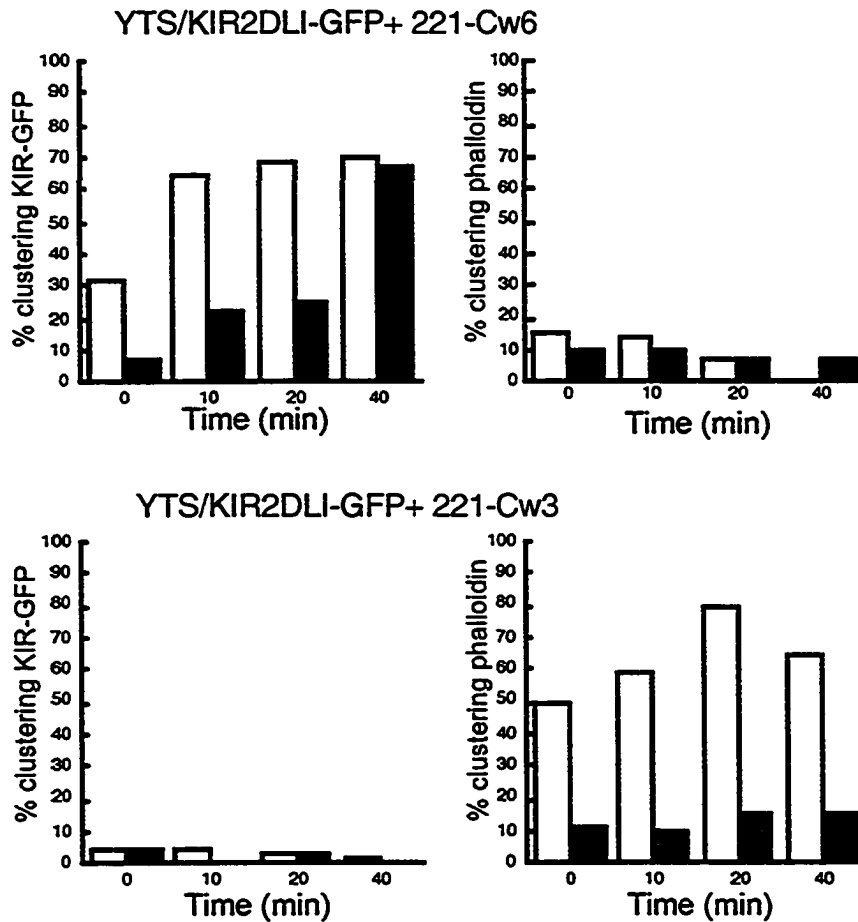
129. Robertson, M. J., M. A. Caligiuri, T. J. Manley, H. Levine, and J. Ritz. 1990. Human natural killer cell adhesion molecules. Differential expression after activation and participation in cytolysis. *J Immunol* 145:3194.
130. Zaru, R., T. O. Cameron, L. J. Stern, S. Muller, and S. Valitutti. 2002. Cutting edge: TCR engagement and triggering in the absence of large-scale molecular segregation at the T cell-APC contact site. *J Immunol* 168:4287.
131. Dustin, M. L., M. W. Olszowy, A. D. Holdorf, J. Li, S. Bromley, N. Desai, P. Widder, F. Rosenberger, P. A. van der Merwe, P. M. Allen, and A. S. Shaw. 1998. A novel adaptor protein orchestrates receptor patterning and cytoskeletal polarity in T-cell contacts. *Cell* 94:667.
132. Badour, K., J. Zhang, F. Shi, M. K. McGavin, V. Rampersad, L. A. Hardy, D. Field, and K. A. Siminovitch. 2003. The Wiskott-Aldrich syndrome protein acts downstream of CD2 and the CD2AP and PSTPIP1 adaptors to promote formation of the immunological synapse. *Immunity* 18:141.

Appendix 1



Appendix 1: Distribution of the total sum intensity values calculated for each region of KIR2DL1-GFP or KIR2DL1 TR-GFP enrichment. Three-dimensional image software was used to generate total sum intensity values for regions between 221-Cw4 and NK92/KIR2DL1-GFP (*left*) or 221-Cw4 and NK92/KIR2DL1 TR-GFP (*right*). The total intensity sum value is a measure of the total amount of KIR-EGFP enrichment at a particular interface region. Total sum intensity values were calculated for 30 interface regions from images collected for one experiment on a given day irrespective of whether or not they were scored positive for KIR-EGFP clustering. Values are indicated by circles. The mean total intensity sum values for KIR2DL1-TG and KIR2DL1 TR-GFP are indicated by horizontal lines.

Appendix 2



Appendix 2: Time-course of KIR2DL1-GFP clustering and F-actin formation in the presence of 10µM cytochalasin D. KIR2DL1-GFP clustering and F-actin formation at the NK immune synapse in fixed conjugates. Confocal images were collected at the indicated time points. Contacts between effector and target cells were scored as demonstrating enrichment of KIR2DL1-EGFP or Alexafluor633® conjugated phalloidin if the intensity at the interface was more than double that of the rest of the cell. The black bars indicate enrichment in the presence of 10 µM cytochalasin D and the white bars indicate enrichment in the presence of 0.1 % DMSO. Although measurements were included for all indicated time points, bars representing values between 0-1 % are not visible. Graphical representations of the confocal data are shown for KIR2DL1-GFP and phalloidin-Alexafluor633® at the inhibitory NK cell immune synapse (*Upper panels*) and the activating NK cell immune synapse (*Lower panels*).